Coordination Chemistry Reviews 475 (2023) 214889

Contents lists available at ScienceDirect

Coordination Chemistry Reviews

journal homepage: www.elsevier.com/locate/ccr

Review

Covalent organic frameworks for photocatalysis: Synthesis, structural features, fundamentals and performance

Yun-Nan Gong [a], Xinyu Guan [b], Hai-Long Jiang [b,*]

[a] Institute for New Energy Materials and Low Carbon Technologies, School of Materials Science and Engineering, School of Chemistry and Chemical Engineering, Tianjin University of Technology, Tianjin 300384, PR China
[b] Department of Chemistry, University of Science and Technology of China, Hefei, Anhui 230026, PR China

ARTICLE INFO

Article history:
Received 30 May 2022
Received in revised form 24 August 2022
Accepted 3 October 2022
Available online 15 October 2022

Keywords:
Covalent organic frameworks
Structural features
Photocatalysis
Structure-property relationship

ABSTRACT

Covalent organic frameworks (COFs) are a new class of crystalline porous materials obtained from covalently attached organic building units. By virtue of the unique characteristics such as periodic and well-defined structures, low-density, high surface area, excellent stability as well as desired semiconductor-like behavior, COFs have gained tremendous attention for functional applications in many fields, especially in photocatalysis. In this review, we summarize the different methods for the synthesis of COFs, such as solvothermal synthesis, microwave synthesis, ionothermal synthesis, room temperature solution synthesis, mechanochemical synthesis and interfacial synthesis firstly. Then, the structural features of COFs including diversity, tailorability, stability and porosity are provided. Afterwards, the fundamentals and advantages of COFs for photocatalysis are briefly introduced. Following this, the photocatalytic applications of COF-based materials toward H_2 production, CO_2 reduction, organic transformation and pollution degradation are discussed. Meanwhile, a series of strategies are highlighted to improve photocatalytic performance for the understanding of the structure-property relationship in this part. Finally, the remaining challenges and prospects on further development of efficient COF-based photocatalysts are indicated.

Contents

* Corresponding author.
E-mail address: jianglab@ustc.edu.cn (H.-L. Jiang).

https://doi.org/10.1016/j.ccr.2022.214889
0010-8545/

Nomenclature

Abbreviations

1D	One-dimensional
2D	Two-dimensional
3D	Three-dimensional
2,3-DHTA	2,3-dihydroxyterephthalaldehyde
2,2'-BPDA	2,2'-bipyridyl-5,5'-dialdehyde
AA	Ascorbic acid
AFM	Atomic force microscope
BD-H_2	Benzidine
BD-$(CH_3)_2$	*o*-tolidine
BD-$(OCH_3)_2$	*o*-dianisidine
BD-$(NO_2)_2$	3,3'-dinitrobenzidine
BDBA	1,4-benzene diboronic acid
BT	1,3,5-triformylbenzene
Bpy	2,2'-bipyridine-5,5'-diamino
BIH	Dimethylphenylbenzimidazoline
BCPy	5,5'-bis(cyanomethyl)-2,2'-bipyridine
BTD	Benzo[*c*][1,2,5]thiadiazole-4,7-dicarbaldehyde
BDCH	Benzene-1,4-dicarboximidamide hydrochloride
BDA	4,4'-(buta-1,3-diyne-1,4-diyl)dibenzaldehyde
BPDA	Biphenyl-4,4'-dicarboxaldehyde
BET	Brunauer-Emmett-Teller
BTCA	1,3,5-benzenetricarbaldehyde
BD-CYANO	4,4'-diamino-[1,1'-biphenyl]-3,3'-dicarbonitrile
BTDA	4,4'-(benzo[c][1,2,5]thiadiazole-4,7-diyl)dianiline
BDF-CHO	4,4'-(benzo[1,2-*b*:4,5-*b*']difuran-4,8-diyl)dibenzaldehyde
BCTB	4,4',4'',4'''-([9,9'-bicarbazole]-3,3',6,6'-tetrayl)tetrabenzaldehyde
PBDT	4,4',4''-(1,4-phenylene)bis([2,2':6',2''-terpyridine]-5,5'-dicarbaldehyde
bdta	2,6-dicarbaldehyde-4,8-dioctyloxybenzo- [1,2-b:3,4-b']dithiophene
[BMIm][NTf_2]	1-butyl-3-methylimidazolium bis((trifluoromethyl)sulfonyl)imide
BDMBD-CHO	4,4′-((((2,3-dimethoxy-1,4-phenylene)bis(ethyne-2,1-diyl))-bis(4,1-phenylene))bis(ethyne-2,1-diyl))dibenzaldehyde
CONs	COF nanosheets
CTFs	Covalent triazine frameworks
COFs	Covalent organic frameworks
CP-MAS NMR	Cross polarization/magic angle spinning nuclear magneticresonance
D-A	Donor-acceptor
DFP	2,6-diformylphenol
DAAQ	2,6-diaminoanthraquinone
DVPD	2,5-divinylterephthalaldehyde
DHA	2,5-dihydroxyterephthalaldehyde
DETH	2,5-diethoxyterephthalohydrazide
DCOE	2,8-dicarbaldehydedibenzofuran
DCB	1,4-dicyanobenzene
DABP	4,4'-diaminobiphenyl
DATP	4,4'-diamino-*p*-terphenyl
DABA	2,5-diaminobenzenesulfonic acid
DABDA	2,5-diaminobenzene-1,4-disulfonic acid
DDFB	4,4'-diamino-2,2'-difluorobiphenyl
DCNE	3,6-dicarbaldehyde-N-ethylcarbazole
DCSE	2,8-dicarbaldehydedibenzothiophene
DBT	2,6-diaminobenzo[1,2-d:4,5-d']bisthiazole
DDDP	5,10-di(3,5-diformylphenyl)-5,10-dihydrophenazine
EDA	4,4'-(ethyne-1,2-diyl)dibenzal-dehyde
ETBC	4-[4-[1,2,2-Tris[4-(4-formyl phenyl) phenyl] ethenyl] phenyl] benzaldehyde
FGs	Functional groups
FPFP	2-(4-formylphenyl)-5-formylpyridine
FPD	10-(4-formylphenyl)-10*H*-phenothiazine-3,7-dicarbaldehyde
HOFs	Hydrogen-bonded organic frameworks
HATP	2,3,6,7,10,11-hexaimino-triphenylene
HHTP	2,3,6,7,10,11-hexahydroxytriphenylene
HBT	2-hydroxybenzene-1,3,5-tricarbaldehyde
HFPTP	2,3,6,7,14,15-hexakis(4-formylphenyl)triptycene
HRTEM	High-resolution transmission electron microscopy
INA	Isonicotinic acid
ILs	Ionic liquids
MB	Methylene blue
MOFs	Metal-organic frameworks
NCs	Nanoclusters
NPs	Nanoparticles
NH_2-BDC	2-aminoterephthalic acid
N_0-Ald	1,3,5-tris(4-formylphenyl)benzene
N_1-Ald	2,4,6-tris(4-formylphenyl)pyridine
N_2-Ald	2,4,6-tris(4-formylphenyl)pyrimidine
N_3-Ald	2,4,6-tris(4-formylphenyl)-1,3,5-triazine
N_3-Brp	2,4,6-tris(4-bromophenyl)-1,3,5-triazine
Pa	p-phenylenediamine
PCB 1	2-chlorobiphenyl
PCB 2	3-chlorobiphenyl
PCB 3	4-chlorobiphenyl
PDA	Terephtalaldehyde
POPs	Porous organic polymers
PDAN	1,4-phenylenediacetonitrile
PDDB	Pyrene-2,7-diyldiboronic acid
PBDE-1	Mono-brominated polybrominated diphenyl ether
p-Por-CHO	5,10,15,20-tetrakis(4-benzaldehyde)porphyrin
PyTTA	4, 4',4'',4'''-(pyrene-1,3,6,8-tetrayl)tetraaniline
PXRD	Powder X-ray diffraction
Py	Pyrene
POMs	Polyoxometalates
ppy	2-phenylpyridine
RROP	Radical ring-opening polymerization
RhB	Rhodamine B
SR III	Sudan Red III
SEM	Scanning electron microscope
TC	Tetracycline
TEOA	Triethanolamine
TEA	Trimethylamine
Tz	Thiazolo-[5,4-*d*]thiazole
Tt	1,3,5-triazine-2,4,6-triamine
TFPA	Tris(4-formylphenyl)amine
TMT	2,4,6-trimethyl-1,3,5-triazine
TAPM	Tetra(p-aminophenyl)methane
Tp	1,3,5-triformylphloroglucinol
TAPB	1,3,5-tris(4-aminophenyl)benzene
TABPM	Tetrakis(4-amino biphenyl)methane
TFFPy	1,3,6,8-tetrakis(4-formylphenyl) pyrene
TTA	4,4',4''-(1,3,5-triazine-2,4,6-triyl)trianiline
TDA	[1,1':4',1''-terphenyl]-4,4''-dicarbaldehyde
TTF	2,3,6,7-tetra(4-formylphenyl)tetrathiafulvalene
TAPP	5, 10, 15, 20-tetrakis(para-aminophenyl)porphyrin
TTPPy	5,5',5'',5'''-(pyrene-1,3,6,8-tetrayl)tetrapicolinaldehyde
TPB-Me	1,2,4,5-tetrakis-(4-formylphenyl)-3',6'-dimethyl-benzene
Ttba	4,4',4''-(1,3,5-Triazine-2,4,6-triyl)tris([1,1'-biphenyl]-4-amine)
TDHB-ZnP	zinc(II) 5,10,15,20-tetrakis(4-(dihydroxyboryl)phenyl) porphyrin

THB	1,2,4,5-tetra-hydroxybenzene
TFPM	Tetrakis(4-formylphenyl)methane
tapa	tris(4-aminophenyl)amine

1. Introduction

Massive consumption of fossil fuels in human activity and social development has resulted in serious environmental issues and energy crisis in the world [1-3]. The development of new environmentally friendly and sustainable energy to replace fossil fuels is a highly desired target to alleviate the above problems. Solar energy featuring unlimited, low cost and clean has been considered as one of the most promising alternatives. Despite this, the conversion efficiency of solar energy is still limited, which is an obstacle for practical application. Therefore, numerous efforts have been devoted in developing various strategies to enhance solar conversion efficiency [4-7]. Among them, photocatalysis has been demonstrated as a prospective technology to convert solar energy to chemical energy under mild reaction conditions [8-11]. As a very successful and efficient photocatalytic example, the natural photosynthetic process in green plants that utilizes sunlight as powder source, to efficiently transform carbon dioxide and water into carbohydrates and oxygen by using enzyme catalysts, affords the splendid guidelines for researchers to realize the artificial photocatalysis [12-15]. However, the development of artificial photocatalysts to accomplish this reaction with high efficiency is still challenging.

Since Fujishima and Honda reported the pioneering work of photocatalysis in 1972, in which titanium dioxide was used as an n-type semiconductor to achieve water splitting under UV radiation in a photoelectrochemical cell [16], great efforts have been devoted to this research area and various photocatalytic reactions were carried out [17-20]. In photocatalytic process, there are three main steps, including (i) light harvesting, (ii) electron-hole separation, and (iii) surface redox reactions. To achieve excellent photocatalytic performance, photocatalysts must be efficient in the above three steps. In the past few decades, a huge number of traditional inorganic semiconductor materials such as TiO_2, ZnO, Fe_2O_3 and CdS have been extensively explored as photocatalysts for diverse photocatalytic reactions due to their low cost, high stability and facile modification. Nevertheless, the practical application is greatly hindered because they usually exhibit narrow light response range, rapid recombination of electron-hole pairs and poor utilization efficiency of solar energy [10,21-23]. Therefore, preparing new photocatalysts with high-stability and high-performance has attracted tremendous attention.

Recently, a series of novel porous materials, for example, metal-organic frameworks (MOFs), covalent organic frameworks (COFs), hydrogen-bonded organic frameworks (HOFs) and porous organic polymers (POPs) have been developed for photocatalytic applications [24-31]. Among them, MOFs constructed by metal ions/clusters and organic linkers *via* coordination bonds, demonstrate some unique characteristics such as periodic and well-defined structures, high surface area, structural diversity and tailorability. However, they usually exhibit relatively low chemical stability and poor conductivity, which impede their practical applications [32-34]. HOFs are consisted of organic molecules by hydrogen bonding interactions, which display defined structures and low density. Nevertheless, the poor chemical stability also limits their applications [35,36]. POPs assembled by strong covalent bonds based on organic molecules, are highly stable porous materials. Unfortunately, it is difficult to achieve in-depth insights into the structure-activity relationship because of their undefined structures and irregular pores [37,38]. COFs are a subclass of fully designed crystalline materials formed by polymerization of organic building blocks through strong covalent bonds [39-53]. Compared with MOFs, HOFs and POPs, COFs not only integrate their particular advantages, but also remedy their drawbacks, which have attracted increasing interests in various applications, such as gas adsorption and separation, sensing, catalysis, and drug delivery, *etc* [54–72]. In particular, the desired semiconductor-like behavior and tunable band structure of COFs make them promising candidates for photocatalytic applications [73–78].

In 2008, Jiang et al. reported a boronic ester-based COF that exhibited the semiconducting behavior evidenced by linear I-V profile [79]. Afterwards, researchers have devoted numerous efforts in this field, and Lotsch et al. reported the first hydrazone-linked COF photocatalyst for hydrogen evolution under visible-light irradiation in 2014 [80]. Following this, the other photocatalytic researches of COF-based materials have increased sharply, including photocatalytic CO_2 reduction, organic transformation and pollution degradation, *etc* [81–87]. In order to achieve the high conversion efficiency of solar energy in these photocatalytic reactions, COF-based photocatalysts that possess excellent light harvesting ability and suitable band structures are highly desirable.

Toward the future development of more efficient COF-based materials for various photocatalytic applications, it is timely to

provide a comprehensive overview in this field. In spite of some reviews focusing on COF photocatalysis have been reported [26,27,88–92], an updated review about the structural features and photocatalytic applications of COFs should be provided (Scheme 1). In this review, a systematic introduction of synthetic methods and structural features of COFs are presented at first. Then, the particular advantages and fundamentals of COFs in photocatalysis are discussed. Furthermore, the photocatalytic applications of COF-based materials are introduced, such as H_2 production, CO_2 reduction, organic transformation as well as pollution degradation. Particularly, strategies for improving photocatalytic activity are discussed detailedly for these reactions to reveal the structure-activity relationship. Finally, a perspective on remaining challenges and research opportunities of COF-based materials for photocatalytic applications is also pointed out.

2. Synthetic methods of COFs

As we know, there are various building units, which have been used to construct COFs, while the synthesis of COFs with both high porosity and excellent crystallinity still remains challenging. Suitable synthetic conditions such as reaction temperature, time and pressure, as well as solvent combinations are very important to balance the formation and crystallization of the COFs' framework. Since Yaghi and coworkers first synthesized COF by using the solvothermal method [42], more synthetic approaches have been developed for the fabrication of COFs [54,93]. In this section, we summarize the different methods for the synthesis of COFs, including solvothermal synthesis, microwave synthesis, ionothermal synthesis, room temperature solution synthesis, mechanochemical synthesis and interfacial synthesis (Table 1).

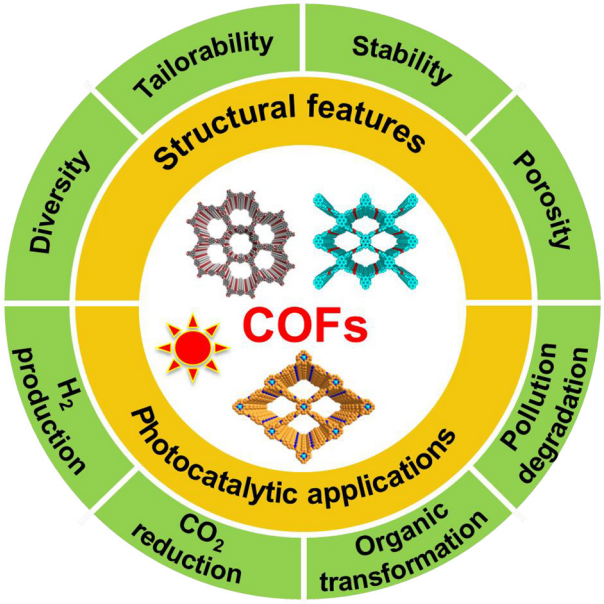

Scheme 1. Schematic showing the structural features and photocatalytic applications of COFs.

2.1. Solvothermal synthesis

Recently, majority of COFs have been prepared by using solvothermal synthetic method. In this way, the COF precursors are added in appropriate solvents, and the reaction occurs in a sealed Pyrex tube. It often requires heating at elevated temperature for several days. After cooling down to room temperature, COFs are obtained by filtration, which are further purified by washing with suitable solvents or Soxhlet extraction. The reaction temperature and time of the reaction system have a great impact on COFs' crystallinity and porosity in the solvothermal reaction. In general, the reaction process is carried out under heating at temperatures ranging from 80 to 200 °C, and the reaction time for synthesis of COFs by this method takes 2 to 9 days. For example, Yaghi et al. synthesized two COFs (COF-1 and COF-5) by solvothermal method in 2005. For the synthesis of COF-1, the 1,4-benzenediboronic acid (BDBA) was dissolved in a solution of mesitylene-dioxane in a Pyrex tube, which was flash frozen at 77 K (liquid N_2 bath). The tube was then evacuated to an internal pressure of 150 mtorr and flame sealed. The reaction proceeded at 120 °C for 3 days to generate white solid, which was collected by filtration and washed with acetone. Using the same procedures as COF-1, BDBA and 2,3,6,7,10,11-hexahydroxytriphenylene (HHTP) was heated at 100 °C for 72 h to produce a free-flowing gray-purple powder of COF-5. COF-1 and COF-5 exhibit high thermal stability up to 500 and 600 °C, and Brunauer-Emmett-Teller (BET) surface areas of 711 and 1590 m^2/g, respectively [42]. Moreover, Yaghi et al. synthesized a series of porphyrinic COFs (COF-366-M and COF-367-M) by the solvothermal condensation between 15,20-tetrakis(4-aminophenyl)porphinato]metal (TAPP-M) and terephtalaldehyde (PDA) or biphenyl-4,4'-dicarboxaldehyde (BPDA) in the mixed solvents of 1,2-dichlorobenzene/butanol/6M aqueous acetic acid under heating at 120 °C for 2 days. COF-366-Co and COF-367-Co show superior activity for electrochemical reduction of CO_2 to CO in water [94].

Table 1
Brief summary of different methods for the synthesis of COFs.

Synthetic method	Temperature	Solvent	Time	Advantages	Disadvantages	Typical examples	Ref.
Solvothermal synthesis	80-200 °C	Organic solvent	2-9 days	Excellent crystallinity	Long reaction time, solvent consumption	COF-1, COF-5, COF-366/367-M, TDHB-ZnP	[42,94,95]
Microwave synthesis	100 °C	Organic solvent	20-60 min	Fast reaction rate, high yield	Polar solvent consumption, few example	COF-5, TpPa-COF	[97,98]
Ionothermal synthesis	400 °C or room temperature	Molten salts or ionic liquids	12-40 h	No solvent consumption	Harsh reaction conditions	CTF-1, 3D-IL-COFs	[99–101]
Room temperature solution synthesis	Room temperature	Organic solvent	1-30 min	Fast reaction rate, mild reaction conditions	Solvent consumption	RT-COF-1, TpBD, TAPB-PDA	[102–104]
Mechanochemical synthesis	Room temperature	No solvent or organic solvent	30 min -3 days	Mild reaction conditions, high yield	Poor crystallinity	TpPa-1, TpPa-2, TpBD, NUS-9, NUS-10, TpBpy-MC	[105–107]
Interfacial synthesis	Room temperature	Organic solvent and water	2-3 days	Mild reaction conditions, large area COF films	Long reaction time, solvent consumption, poor crystallinity	Tp-Bpy, TAPB-PDA, TTA DHTA, polyTB	[108–112]

In the solvothermal synthesis, the chosen of solvent is also of great importance for COF formation as it strongly affects the reactant solubility, which is further related to the crystal nucleation, crystal growth rate and self-healing structure. Mixed solvents containing two or more solvents are often utilized to fabricate COFs, and the proportion of different solvents will affect the crystallinity of COFs. For example, Jiang and coworkers reported a porphyrin-based COF by the condensation reaction of zinc(II) 5,10,15,20-tetrakis(4-(dihydroxyboryl)phenyl) porphyrin (TDHB-ZnP) and 1,2,4,5-tetrahydroxybenzene (THB) in a mixture of mesitylene and dioxane under solvothermal conditions. When the ratio of mesitylene to dioxane was 1:1 (v:v), which gave only an amorphous solid as confirmed by the powder X-ray diffraction (PXRD) measurement. By contrast, the COF with high crystallinity was formed when the ratio of mesitylene to dioxane was changed to 9:1 [95].

In addition to the production of the COF powders, the COF thin films can be also obtained by solvothermal method. As a good example, Dichtel et al. have grown COF thin films on single-layer graphene under solvothermal conditions. First, a mixture of BDBA, HHTP, mesitylene and 1,4-dioxane was added to a cylindrical pressure vessel, which was sonicated for 30 min. The graphene-containing substrate was then added to the above solution. The reaction system was heated at 90 °C for 30 min. The crystalline COF-5 film grown on the graphene surface was obtained with the thickness of 195 ± 20 nm (Fig. 1) [96].

2.2. Microwave synthesis

Microwave-assisted method is a solvothermal synthetic approach by using microwave heating, which has been widely used in synthesis reactions. Compared with the conventional heating methods, microwave heating has several benefits, including accelerated reaction rates, increased yield, cleaned products, energy saving and easy to control during the chemical reaction. However, to achieve a better heating effect, microwave-assisted method needs the use of polar solvents. Until now, a variety of COFs have been prepared *via* microwave-assisted synthetic method. In 2009, Cooper and co-workers synthesized COF-5 by microwave heating within 20 min, which is more than 210 times faster than the reaction time of 72 h required from the solvothermal synthesis. Moreover, the surface area of COF-5 is 2019 m^2/g obtained by microwave synthesis, which is obviously higher than that of solvothermally synthesized (1590 m^2/g) [97]. Besides, Wei et al. synthesized a enamine-linked COF (TpPa-COF) using a rapid microwave-assisted method by the reaction of p-phenylenediamine (Pa) and 1,3,5-triformylphloroglucinol (Tp) in a mixture of mesitylene/1,4-dioxane/3M acetic acid at 100 °C with stirring for 60 min. The yield of TpPa-COF is 83% based on the starting materials obtained by microwave heating, while it is only 8% by the conventional heating method, demonstrating microwave heating is good for COF synthesis. Synthesized TpPa-COF based on microwave method also shows exceptional activities for CO_2 storage and CO_2/N_2 separation [98].

Remarkably, the microwave-assisted method is a simple and efficient strategy to produce COFs with the faster reaction rate and higher yield compared to the conventional solvothermal synthesis, which provides new possibility for industrialized production of COFs.

2.3. Ionothermal synthesis

Ionothermal synthetic method is a novel technique for synthesizing COFs, in which the molten salts or ionic liquids (ILs) are used to create ionothermal conditions. When the metal salts act as solvents, the reaction by this method is taken place under high temperature, thus the thermal stability of the targeted COFs should be high to avoid decomposition during the synthetic process. Generally, covalent triazine frameworks (CTFs) with high thermal and chemical stabilities can be synthesized under molten salts by this method. For instance, Thomas et al. synthesized a highly stable and crystalline porous CTF (CTF-1) by heating a mixture of 1,4-dicyanobenzene (DCB) and $ZnCl_2$ at 400 °C for 40 h. In this reaction, $ZnCl_2$ not only acts as the solvent but also acts as catalyst for the trimerization reaction, which is sufficiently reversible at this tem-

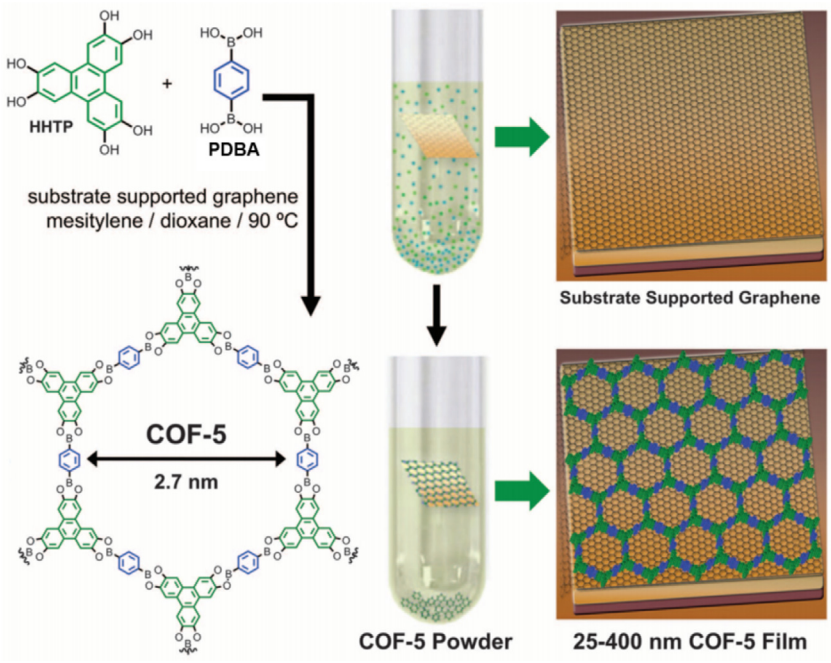

Fig. 1. Solvothermal reaction of HHTP and BDBA in the presence of graphene-containing substrate gives COF-5 film grown on the graphene surface and COF-5 powder precipitated on the bottom of the tube. Reproduced from Ref. [96] with permission from the Science copyright 2011.

perature. The DCB exhibits a good solubility in molten $ZnCl_2$ salt due to the strong Lewis acid base interactions [99]. Furthermore, the Thomas group prepared an ordered and microporous CTF-1 by the conversion of an amorphous and non-porous polymer network under ionothermal conditions through a two-step process. First, the amorphous polymer was synthesized by trimerization of DCB monomers using strong Broensted acids at 40 °C for 12 h. Then, it was heated at 400 °C for 40 h together with $ZnCl_2$, which can be transformed to the crystalline CTF [100].

Apart from CTFs, the IL COFs have also been constructed by ionothermal method. Fang and coworkers reported a series of 3D IL-containing COFs (3D-IL-COFs) by using ionic liquid as a green solvent at room temperature. In the synthesis of these COFs, 1-butyl-3-methylimidazolium bis((trifluoromethyl)sulfonyl)imide ([BMIm][NTf_2]) was chosen as both solvent and catalyst because it is a liquid at room temperature. The Schiff base reactions of tetrahedral building blocks, tetrakis(4-formylphenyl)methane (TFPM), with the linear links, Pa, 4,4'-diaminobiphenyl (DABP) or 4,4'-diamino-*p*-terphenyl (DATP), in [BMIm][NTf_2] within 12 h generate three 3D-IL-COFs. The reaction time for ionothermal method is significantly shorter than those from the solvothermal synthesis (3-7 days). Moreover, the 3D-IL-COFs exhibit excellent performance in the separation of CO_2/N_2 and CO_2/CH_4 [101].

2.4. Room temperature solution synthesis

Although most of COFs have been synthesized by solvothermal method, it often requires a high temperature (> 80 °C), sealed vessels and long reaction time (> 2 days). Therefore, the rapid synthesis of COFs at room temperature and in air has attracted tremendous attention. Room temperature solution synthesis is advantageous, especially for case of sensitive monomers or substrates. For example, Zamora et al. reported the synthesis of imine-based COF (RT-COF-1) by room temperature solution synthetic method. RT-COF-1 was synthesized by the Schiff base reaction between 1,3,5-tris(4-aminophenyl)benzene (TAPB) and 1,3,5-benzenetricarbaldehyde (BTCA) in m-cresol at room temperature and in air for 1 min, which was confirmed by solid-state ^{13}C cross polarization/magic angle spinning nuclear magneticresonance (CP-MAS NMR). RT-COF-1 is crystalline, stable up to 450 °C, and porous to both N_2 and CO_2 [102]. Yan et al. fabricated a spherical COF (TpBD) through a simple and facile room-temperature solution-phase approach by the reaction of Tp and DABP in ethanol at room temperature for 30 min. The obtained TpBD exhibits exceptional stability, not only robust in water and organic solvents, but also stable in 1 M HCl and 0.1 M NaOH [103]. Moreover, Dichtel and coworkers prepared imine-linked COFs (TAPB-PDA) *via* the Schiff base reaction of TAPB and PDA in 1,4-dioxane/mesitylene solution by the addition of metal triflates as catalysts at room temperature for 10 min. The resultant COFs show superior crystallinity and high BET surface areas with optimal value of 2175 m^2/g, which is superior to the solvothermally synthesized COF (S_{BET} < 1000 m^2/g) [104].

2.5. Mechanochemical synthesis

Mechanochemical synthesis is a facile, economical and environmentally benign method, and the reaction process is also carried out at room temperature. In this method, the monomers are placed in a mortar and ground by using a pestle to form COFs. In 2013, the Banerjee group synthesized three high stable isoreticular COFs (TpPa-1, TpPa-2 and TpBD) by mechanochemical method. Taking TpPa-1 as an example, Tp and Pa were added in a mortar and ground at room temperature for 5 min, a light-yellow powder was obtained. With the increased grinding time, the color of powder was changed to orange and then further to dark-red until to 45 min, which is similar to that of solvothermally synthesized COF, indicating the formation of TpPa-1. These COFs exhibit moderate crystallinity and excellent stability in boiling water and 9 M HCl (Fig. 2) [105].

In addition to the use of the room-temperature solvent-free mechanochemical grinding, the liquid-assisted mechanochemical grinding method has also been developed to synthesize COFs. The addition of a small amount of solvent in the reaction system increases the reaction rate, leading to the enhanced crystallinity. For instance, Zhao et al. prepared two fully sulfonated COFs (NUS-9 and NUS-10) by mechanosynthesis with high yields. A mixture of Tp, 2,5-diaminobenzenesulfonic acid (DABA) or 2,5-diaminobenzene-1,4-disulfonic acid (DABDA), and 50 μL of mesitylene/dioxane/aqueous acetic acid (3 M) was placed in a mortar, which was ground for 45-60 min to produce a red powder of NUS-9 with 80% yield and a dark red powder of NUS-10 with 76% yield [106]. Banerjee et al. reported the mechanochemically synthesized COF (TpBpy-MC) by combining Tp and 2,2'-bipyridine-5,5'-diamine (Bpy) through the Schiff base reaction. First, the starting materials of Tp and Bpy with a mixture of 60 μL of *N*,*N*-dimethylacetamide, 30 μL of o-dichlorobenzene and 15 μL of 6 M acetic acid were put into a stainless steel jar. Then, the reaction mixture was ground at room temperature for 90 min at 30 Hz to produce a dark red powder of TpBpy-MC with ~84% isolated yield. TpBpy-MC shows sheet-like morphology, unlike the thread-like morphology that obtained by a solvothermal route [107].

2.6. Interfacial synthesis

Different from the above-mentioned synthetic strategies that mainly give insoluble powders, interfacial synthesis is a widely used method for preparation of COF thin films. In this method, the monomers react with each other at the interface, and the COF growth is limited to the interface region, resulting in the formation of COF thin films. Recently, there are two types of interfaces used to synthesize COF thin films containing liquid/liquid interface and liquid/air interface. Banerjee and coworkers synthesized a ser-

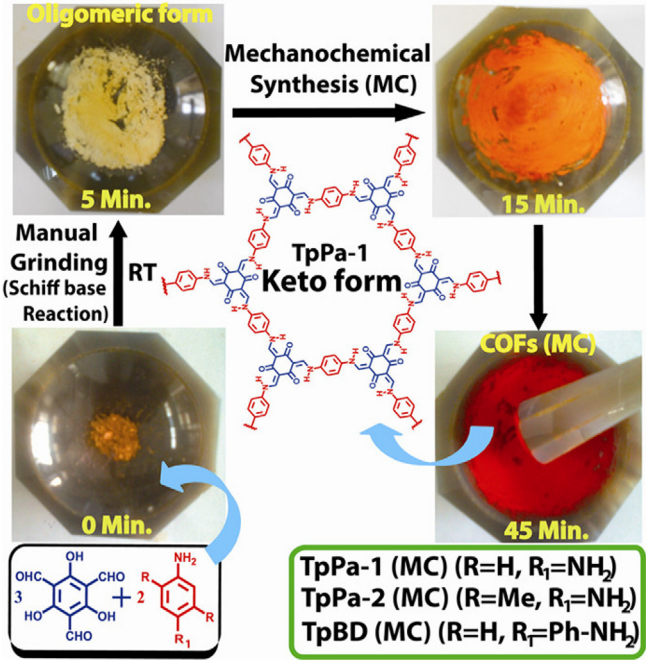

Fig. 2. Schematic representation of the mechanochemical synthesis of TpPa-1, TpPa-2, and TpBD *via* Schiff base reactions. Reprinted from Ref. [105] with permission from the American Chemical Society, copyright 2013.

ies of stable keto-enol tautomerism-based COF thin films by interfacial crystallization technique. Taking Tp-Bpy thin film as an example, Tp was firstly dissolved in dichloromethane on the bottom. Then, the pure water was added on top of the aldehyde solution to create liquid-liquid interface owing to their immiscible with each other. Finally, the aqueous solution of Bpy and amine-*p*-toluene sulfonic acid salt was added slowly on top of the spacer solution. The reaction happens at room temperature. After 72 h, the COF thin film was formed at the interface with the thicknesses of ~75 nm (Fig. 3). Tp-Bpy thin film shows high stability and BET surface area of 1151 m^2 g^{-1}. Moreover, Tp-Bpy thin film exhibits an unprecedented acetonitrile permeance of 339 L m^{-2} h^{-1} bar^{-1} [108]. Wang et al. prepared crystalline COF thin films by the polymerization reaction of amine and aldehyde monomers from oil and hydrogel respectively in thin water layer [109]. Dichtel et al. reported the synthesis of free-standing COF thin films by the interfacial polymerization of polyfunctional amine and aldehyde monomers from an organic solvent in an aqueous solution containing the $Sc(OTf)_3$ catalyst [110].

Through liquid/air interfacial synthesis, the Bao group obtained large-area COF thin films by imine condensation of 2,6-dicarbalde hyde-4,8-dioctyloxybenzo[1,2-b:3,4-b']dithiophene (bdta) and tris (4-aminophenyl)amine (tapa). First, tapa and bdta were dissolved in DMF and acetic acid, which was incubated for 24 h at 100 °C to form bright red precipitate. Then, the precipitate was added to DMF, which was transferred to a petri dish in a sealed container containing saturated H_2O atmosphere. After 48 h, the COF thin film with a green sheen had grown over the surface of the solution. The film thickness of 1.8-29 nm was controlled by the regulation of the incubation times [111]. The Zhang group synthesized a two-dimensional monolayer COF by the Schiff base reaction of aromatic triamine and dialdehyde building blocks at the air/water interface [112].

3. Structural features of COFs

3.1. Diversity

COFs are porous crystalline materials with well-defined two-dimensional (2D) and three-dimensional (3D) structures, obtained by the combination of multi-functional monomers through covalent bonding linkages, in which the 2D structures are further stacked *via* weak interaction (*e.g.*, hydrogen bonding and π-π stacking interactions), between the adjacent layers to generate one-dimensional (1D) channels. Recently, more than 500 COF structures with various linkages, such as boronate ester, imine, imide, triazine, hydrazone, azine, alkene, *etc.* have been designed and prepared [113–115]. Among them, 2D COFs are usually fabricated based on the flat building units (Fig. 4a), and the condensation of stereoscopic precursors leads to the formation of 3D COFs (Fig. 4b) [116,117]. To date, most of COFs exhibit 2D structures, and the major challenges for the construction of 3D COFs are the limited stereoscopic building blocks and serious crystallization problem. Moreover, some COF nanosheets have also been prepared by top-down or bottom-up methods [118–121]. Importantly, the defined and diversified structures of COFs provide great conveniences to study structure-performance correlation, which is of great significance for catalytic mechanism exploration and the development of new COFs toward various functional applications [122–125].

3.2. Tailorability

The flexible tailorability of COF structures affords great opportunity to construct functional COFs for various specific applications [26,126–130]. In general, there are two approaches to modulate the structures of COFs. One is the bottom-up approach, in which the monomers can be preferentially designed to directly synthesize the targeted COFs (Fig. 5a) [131,132]. The other is post-synthetic modification method [133]. In this way, the new functionalized groups are introduced into the pristine COFs to tune their surface or pore environment, while the original COF structures are maintained. After the post-synthetic modification, the application of COFs can be greatly expanded. Post-synthetic metalation by the immobilization of metal ions in COFs through coordination interaction is a common and easy strategy to regulate COF structures. Bipyridine-based monomers within COFs are often employed to bind various metal ions, including Co, Re and Ru *etc* (Fig. 5b). After metallized COFs, a large number of catalytic reactions have been achieved [134–136].

Apart from the post-synthetic metalation, the structures of COFs can also be modulated by the incorporation of additional functional groups (FGs). So far, many techniques have been developed to integrate FGs into COFs to tune their structures and properties. Click reactions are the most commonly used approaches. For example, Jiang et al. prepared a series of azide-appended COFs, in which the azide groups are clicked with alkynes to form triazole-

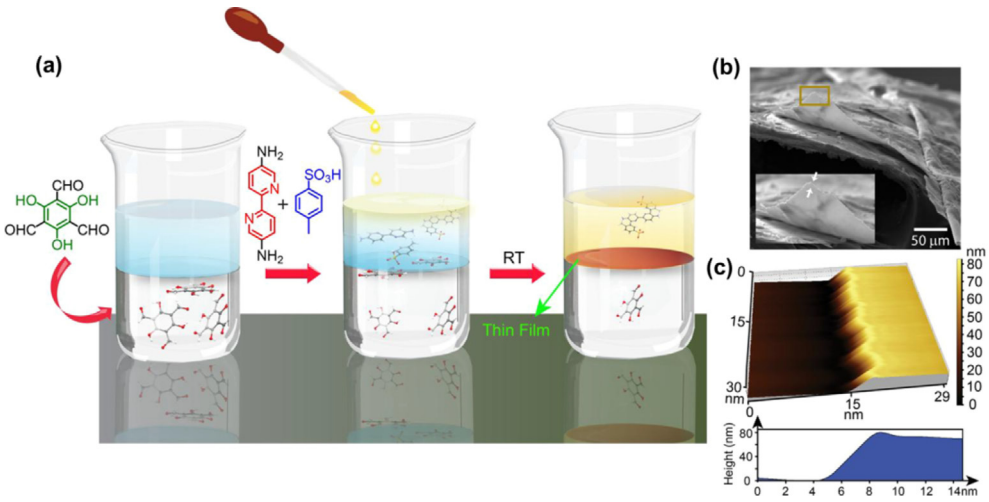

Fig. 3. (a) Schematic illustration for the synthesis of Tp-Bpy by interfacial synthetic method. Scanning electron microscope (SEM) (b) and Atomic force microscope (AFM) (c) images of the Tp-Bpy thin film. Reproduced from Ref. [108] with permission from the American Chemical Society, copyright 2017.

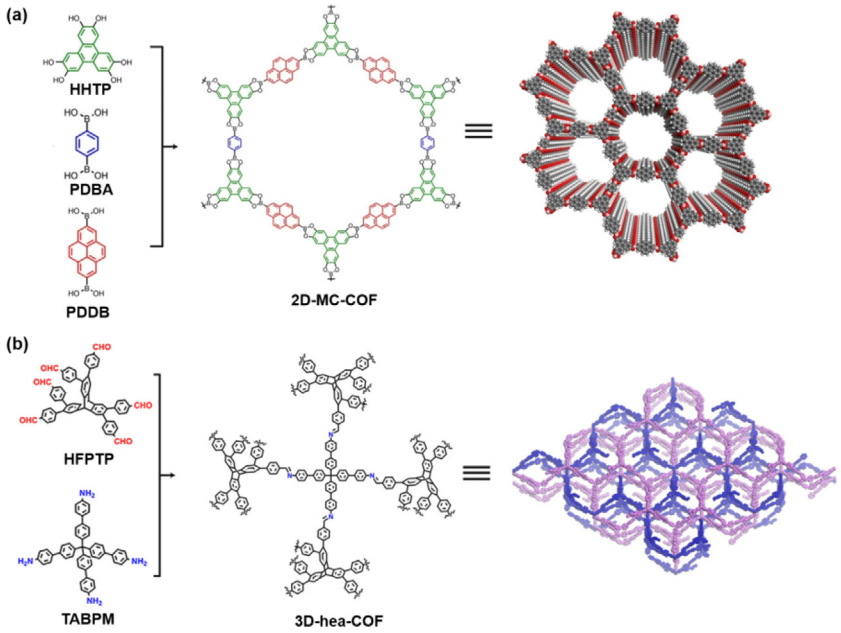

Fig. 4. (a) Schematic illustration for the construction of 2D-MC-COF by using flat HHTP, BDBA and pyrene-2,7-diyldiboronic acid (PDDB). Adapted from Ref. [116] with permission from the Nature Springer, copyright 2016. (b) Schematic showing the synthesis of 3D-hea-COF by using stereoscopic 2,3,6,7,14,15-hexakis(4-formylphenyl) triptycene (HFPTP) and tetrakis(4-amino biphenyl)methane (TABPM). Reproduced from Ref. [117] with permission from the American Chemical Society, copyright 2021.

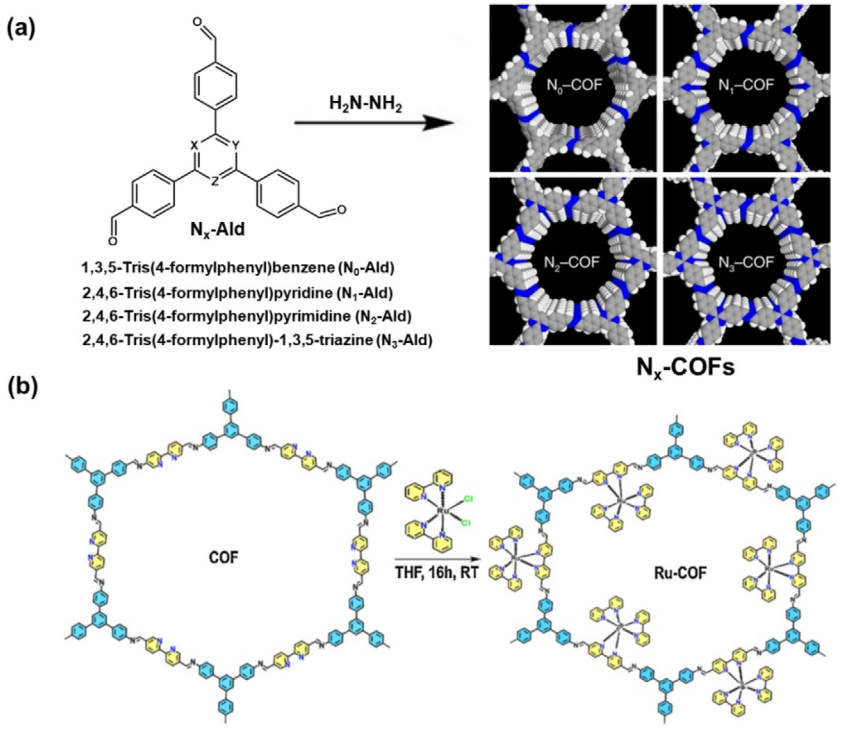

Fig. 5. (a) Schematic showing the synthesis of N_x-COFs with 0-3 nitrogen atoms in the central aryl ring by solvothermal reaction of N_x-Ald and hydrazine. Reprinted from Ref. [132] with permission from the Nature Springer, copyright 2015. (b) The post-synthetic metalation of COF. Adapted from Ref. [136] with permission from Elsevier, copyright 2021.

linked groups on the wall surfaces of COFs [137]. Similarly, an alkyne-incorporated COF prepared by Mancheño et al. undergoes a click reaction for importing both the triazole and thiol moieties in COFs [138]. In addition, the COF structures can also be regulated by chemical conversion of linkages through oxidation-reduction or cyclization reactions [139,140].

3.3. Stability

The stability of COFs is the premise for their post-synthetic modification and practical applications. Generally, COFs possess good thermal stability owing to the robust covalent bonds, which can keep structural integrity between 250 and 450 °C under inert

gas [107,141–143]. Despite the fact that earlier reported boron-based COFs exhibit poor chemical stability in water and acidic/basic solutions, many strategies have been developed to increase the structural stability along with the development of COFs [144–146]. The decomposition of boron-based COFs can be attributed to the hydrolysis of the sensitive B-O bond. Hence, the direct preparation strong linkage is one of the most effective strategies to obtain stable COFs. Up to now, a series of COFs have been constructed with stable linkages such as imine, azine, hydrazine and ether, *etc.*, which show exceptional chemical stability in strong acidic, basic and even oxidizing media (Fig. 6a and 6b) [94,147–150]. Moreover, the stability of COFs can be increased by the predesignation of hydrophobic monomers or the formation of intramolecular hydrogen bonds [151–153].

In addition to the *de novo* synthesis, post-synthetic modification is also a promising strategy to enhance COF stability. For example, Lotsch et al. employed a post-synthetic locking strategy to convert a 2D imine-linked COF into a thiazole-linked one, which displays significantly improved stability [154]. Liu et al. transformed a series of imine-linked COFs into stable aromatic frameworks by an aza-Diels-Alder cycloaddition reaction (Fig. 6c and 6d) [155]. Deng et al. synthesized two amine-linked COFs by direct reduction of their imine linkages with enhanced stability [140].

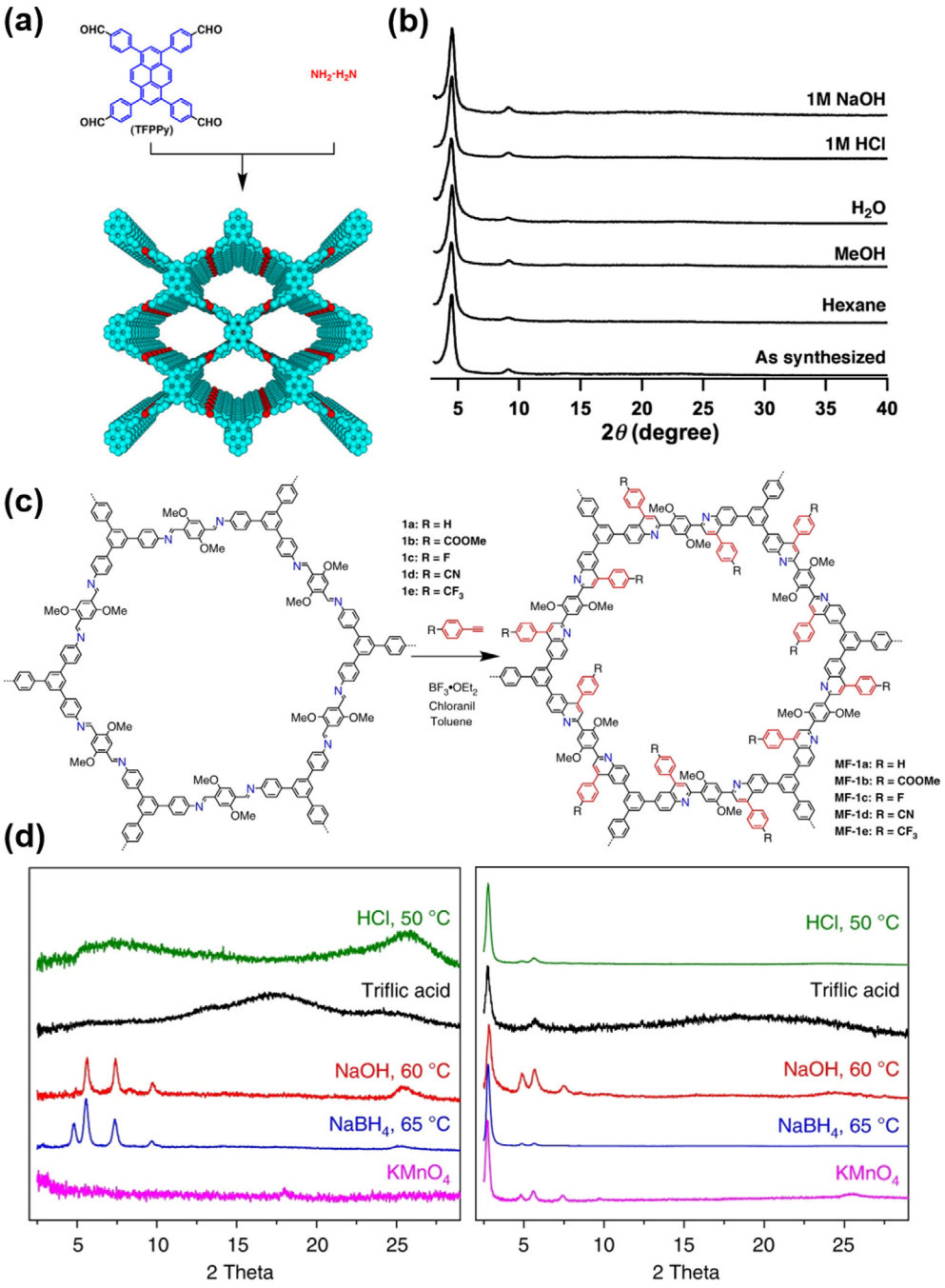

Fig. 6. (a) Illustration showing the synthesis of the azine-linked COF. (b) PXRD patterns of azine-linked COF upon 1-day treatment in different conditions. Adapted from Ref. [147] with permission from the American Chemical Society, copyright 2013. (c) Post-synthetic modification of COF by an aza-Diels-Alder cycloaddition reaction. (d) PXRD patterns of before (left) and after (right) cycloaddition reactions with 12 M HCl, 98% triflic acid, 14 M NaOH, 5 equiv. of $NaBH_4$, and 5 equiv. of $KMnO_4$. Reprinted from Ref. [155] with permission from the Nature Springer, copyright 2018.

3.4. Porosity

COFs are fascinating materials with highly ordered, versatile and permanent porosity, which render them very promising for various functions. Currently, COFs featuring micropores and mesopores have been successfully designed and synthesized. The smallest pore size is 0.52 nm observed for 3D-TPB-COF-Me, which was constructed by the condensation of tetra(p-aminophenyl) methane (TAPM) and 1,2,4,5-tetrakis-(4-formylphenyl)-3',6'-dimethyl-benzene (TPB-Me) (Fig. 7a) [156]. Moreover, TDCOF-3 prepared *via* the polycondensation of 4,4',4''-(1,3,5-Triazine-2,4,6-triyl)tris([1,1'-biphenyl]-4-amine) (Ttba) with 4,4'-((((2,3-dimethoxy-1,4- phenylene)bis(ethyne-2,1-diyl))bis(4,1-phenylene))bis(ethyne-2,1-diyl))-dibenzaldehyde (BDMBD-CHO) exhibits well-aligned hexagonal mesopores with the largest pore size of 10.0 nm (Fig. 7b and 7c) [157]. For 2D COFs with open 1D channels, the pore size and shape can be predetermined by rationally designing monomers, whereas these are difficult to be predicted for 3D COFs because of the possible interpenetrated structures [158–160]. Moreover, the pore size of COFs can be further tuned by three approaches. The first method is to change the length of building units. For example, COF-5 reported by Yaghi et al shows hexagonal layer structure, with pore size of 2.7 nm *via* the condensation of BDBA and HHTP. By using longer 4,4'-diphenylbutadiyne bis(boronic acid) (DPB) instead of BDBA, the HHTP-DPB COF was successfully fabricated, which demonstrates the pore size of 4.7 nm [42,161]. The second one is to modulate the size of substituent groups. For instance, Lavigne et al. reported a series of alkyl-substituted COFs with pore sizes ranging from 1.1 to 1.8 nm [162]. The third one is to tune the stacking modes of COF

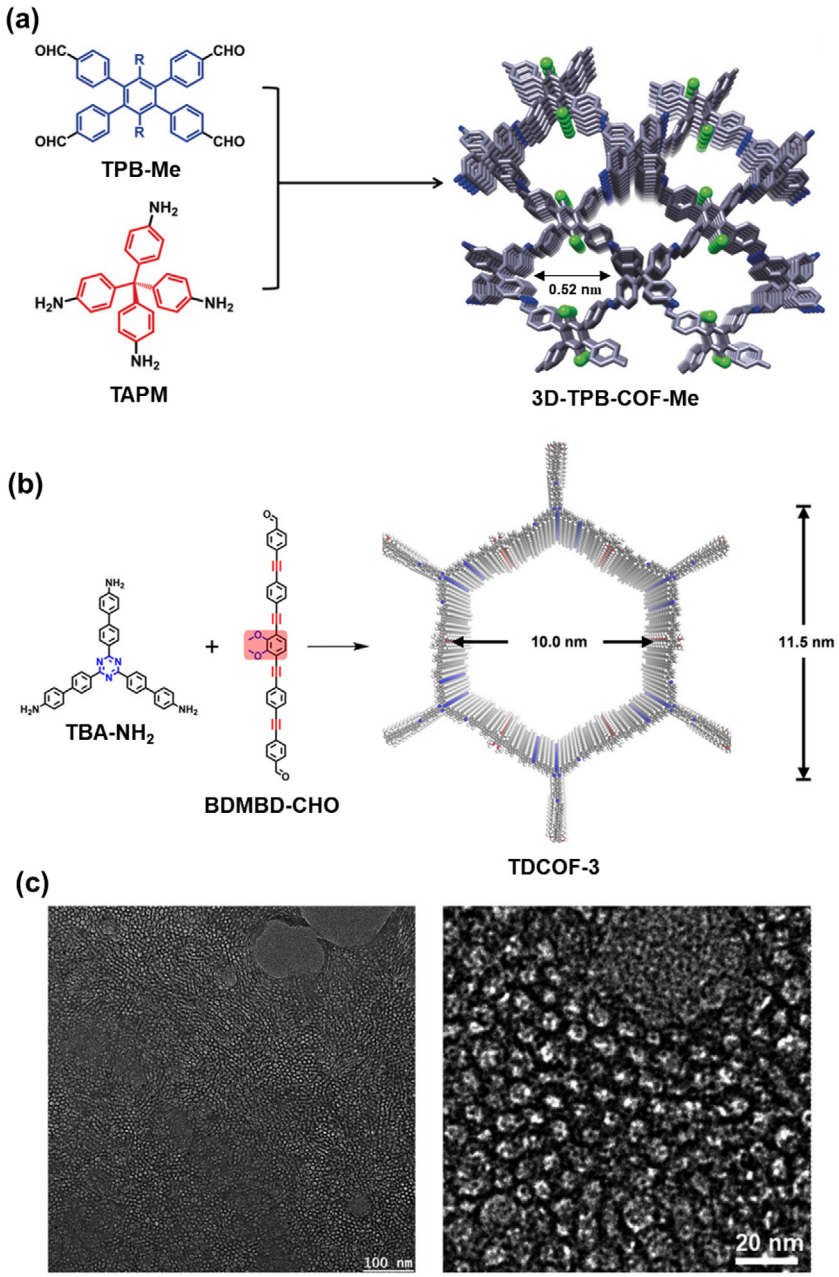

Fig. 7. (a) Schematic showing the synthesis of 3D-TPB-COF-Me with pore size of 0.52 nm. Adapted from Ref. [156] with permission from the Wiley-VCH, copyright 2019. (b) Schematic illustration of the construction of TDCOF-3 with pore size of 10.0 nm. (c) High-resolution transmission electron microscopy (HRTEM) images of TDCOF-3 showing the well-aligned hexagonal mesopores. Reprinted from Ref. [157] with permission from the American Chemical Society, copyright 2022.

nanosheets. In general, the pore size of COFs with AA stacking mode is larger than that of AB stacking mode [163].

In addition to the pore size, the pore environment of COFs can also be precisely tuned. Predesigned functional monomers and post-synthetic modification have been proved to be two acceptable strategies to construct functional COFs with modulated pore environments. Towards this goal, the Chen group reported a series of 2D isostructural COFs by polycondensation of 1,3,6,8-tetrakis(4-formylphenyl)pyrene (TFFPy) with terphenyl based diamines with fluorinated, chlorinated or non-halogenated units, thus the pore environment of COFs is regulated by halogens. The photocatalytic results demonstrate that the chlorine modulation in the COF shows the largest hydrogen evolution rate [164]. Moreover, the Lan group developed a kind of functionalizing exfoliation agent to modify and exfoliate bulk porphyrine COFs into functional nanosheets. The obtained COF nanosheets with 2,4-diamino-6-cholo-triazine functional groups anchored on the pore walls, exhibit enhanced electrocatalytic CO_2 reduction activity over the bare COF [165].

4. Fundamentals of COF photocatalysis

Photocatalysis converting solar to chemical energy is a complicated process, which is affected by a number of factors. Generally, there are three main steps in photocatalytic process, including: (i) the photocatalysts harvest UV, visible or near-infrared (NIR) light to form electron-hole pairs, which relying on their band gaps; (ii) the electrons in the highest occupied molecular orbitals (HOMO) are excited into the lowest unoccupied molecular orbitals (LUMO), leaving the holes in the HOMO and generating charge separation; (iii) the photoinduced electrons and holes can further migrate to catalyst surface to take part in redox reactions. For photocatalytic redox reactions to happen, the HOMO of the photocatalysts must be lower than the energy of a donor ($E_{(D^-/D)}$) redox couple, while the LUMO must be higher than the energy of an acceptor ($E_{(A^+/A)}$) redox couple. Hence, the band edges of photocatalysts are of great importance for the estimation of a photocatalytic reaction to occur. For example, for photocatalytic reduction of CO_2 to CO, the redox potential is -0.53 V, and it is 0.81 V for photocatalytic H_2O oxidation to O_2 (Fig. 8) [166–168]. The redox potentials are with reference to NHE (pH = 7). In this context, the theoretical LUMO of photocatalysts should be more negative than -0.53 V to reduce CO_2 to CO, and the HOMO has to be more positive than 0.81 V to oxidize H_2O to O_2. Moreover, charge separation also plays a key role in photocatalytic process since most of the photoinduced electrons and holes tend to the fast recombination in the bulk or at the surface of catalysts. Therefore, the rational design of the photocatalysts with reasonable band gaps, appropriate energy levels and high charge separation efficiency is an urgently desired target.

Recently, COFs have attracted tremendous attention as a kind of special photocatalysts. According to the photocatalytic mechanism mentioned above, the building units of COFs serves as antennas to absorb light to generate exciton (electron-hole pair), which can be split into charge. The exciton binding energy (E_{XBE}) depending on the HOMO and LUMO energy levels of COFs, decides charge separation efficiency. The lower E_{XBE} means the more efficient charge separation. Both HOMO and LUMO energy levels of COFs are relevant to the building blocks, which are different from MOFs that are usually mainly contributed by the organic ligands and the metal nodes, respectively [81,169,170]. The structural designability and tunability of COFs afford possibility to regulate HOMO and LUMO energy levels and thus optimize photocatalytic performance. After charge separation, the electrons and holes transfer to catalyst surface and participate in redox reactions. Usually, sacrificial agents are used in photocatalytic reactions to annihilate the photogenerated holes or electrons and ensure the high catalytic efficiency. Triethanolamine (TEOA), trimethylamine (TEA), dimethylphenylbenzimidazoline (BIH) and ascorbic acid (AA) are often employed as electron donors, whereas $AgNO_3$, $Na_2S_2O_8$ and $NaIO_3$ can serve as hole donors [171–177].

Based on the above fundamentals of COF photocatalysis, an efficient COF photocatalyst should possess the following features: (a) excellent visible light harvesting ability to generate electron-hole pairs as many as possible; (b) appropriate band structures to make the photocatalytic reaction thermodynamical downhill process ($\Delta G < 0$); (c) low E_{XBE} to promote charge separation; (d) high surface area to expose high-density active sites.

5. Advantages of COFs for photocatalysis

In 2014, the Lotsch group reported the first COF photocatalyst (TFPT-COF) for hydrogen evolution. TFPT-COF was constructed from 1,3,5-tris-(4-formyl-phenyl)- triazine (N_3-Ald) and 2,5-diethoxy-terephthalohydrazide (DETH), which exhibits an excellent photocatalytic activity with hydrogen production rate of 230 μmol g^{-1} h^{-1} in the presence of Pt cocatalyst under visible-light irradiation [80]. Afterwards, COFs have been dramatically developed in photocatalytic applications containing energy conversion and environmental remediation [26,27,91]. Compared with traditional photocatalysts including metal oxides [178], MOFs [179] and organic polymers [180], COFs exhibit numerous special advantages in photocatalysis (Fig. 9): (1) The structural designability means that the topologies, pore shapes and sizes, as well as light harvesting ability of COFs can be easily foreseen by utilizing various building blocks; (2) High crystallinity of COFs is in favor of the separation and transport of photogenerated electrons and holes in catalytic process; (3) The high surface area and porosity of COFs not only ensure abundant available catalytic sites to adsorb and activate substrate molecules, but also are beneficial for the mass transfer during the photocatalytic process; (4) Most of COFs show high stability, especially chemical stability originated from strong covalent bond between the building blocks, which can avoid the corrosion of photoactive units and improve the lifetime of

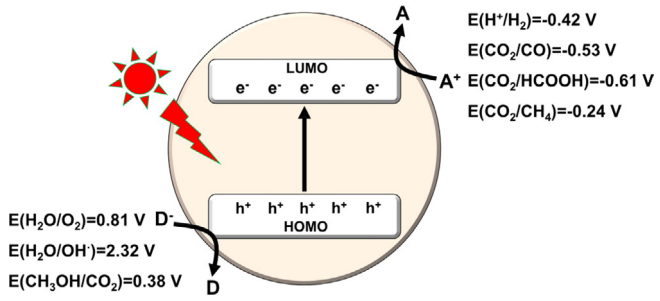

Fig. 8. Schematic illustration of the redox potentials for various photocatalytic reactions (E^0 (V) *vs* NHE at pH = 7).

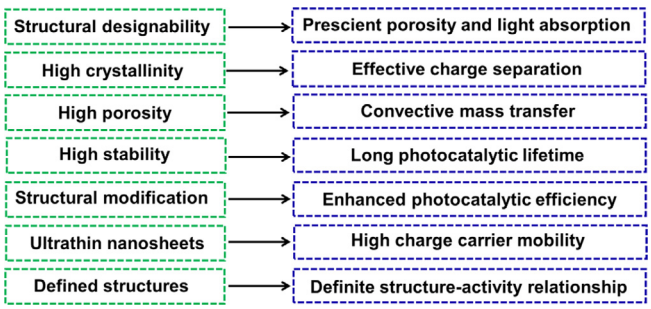

Fig. 9. The special advantages of COFs for photocatalysis.

photocatalysts; (5) The facile modification of COF structures provides great opportunity to incorporate additional functional groups, to enhance charge separation efficiency and thus photocatalytic performance; (6) The 2D COF nanosheets with π-conjugated plane structures enables high charge carrier mobility; (7) Well-defined structures of COFs make them ideal candidates in the understanding of the catalytic mechanism and structure-activity relationship.

Based on the above fascinating inherent features of COFs, a series of outstanding strategies have been proposed to enhance photocatalytic efficiency [26,27,181–183]. One of approach is to extend light harvesting ability. Porphyrins with large conjugated systems can absorb light in the whole visible region. Therefore, incorporating porphyrins into COFs has been proven to be an efficient approach to obtain COFs with strong visible light harvesting ability. The examples include COF-367, TTCOFs and 3D-Por-COF, etc, which exhibit excellent photocatalytic performance for various reactions [184–186]. Moreover, the introduction of functional groups (such as -CH_3, -OH and halogens, *etc*) can also regulate light absorption [187–189]. For example, Baeg et al. prepared a series of 2D COFs by the self-condensation of Ttba and 1,3,5-triformylbenzene (BT) with varying number of hydroxyl units. The resulting COFs containing one (COF-3) or two (COF-4) -OH groups on the phenyl ring show better visible light absorption than COFs without (COF-1) or with three (COF-2) hydroxyl units. The improved optical properties of COF-3 and COF-4 greatly enhance their photocatalytic activities for the reduction of CO_2 to HCOOH [187].

Given most of COFs are made entirely of non-metallic elements, which show low efficiency of photogenerated charge separation and limited catalytic active sites. Therefore, it is highly desirable to introduce active sites within COFs to enhance charge separation and photocatalytic efficiencies. Impressively, metal active centers can be bound on the skeleton of COFs through coordination interactions. For example, Huang and coworkers synthesized a 2D triazine COF by solvothermal reaction of 2,2'-b ipyridine-5,5'-dicarbaldehyde (2,2'-BPDA) and 4,4',4''-(1,3,5-tria zine-2,4,6-triyl)trianiline (TTA). Then Re ions were immobilized on the skeleton of COF through coordination by post-synthetic modification, which exhibits efficiently photocatalytic CO_2 reduction to CO with better activity than pristine COF [190]. Furthermore, single-atom Pt was anchored on the pore walls of β-ketoenamine-linked TpPa-1-COF for photocatalytic water splitting to hydrogen. The optimized Pt_1@TpPa-1 shows a high hydrogen evolution rate of 719 μmol g^{-1} h^{-1}, which is 48 times higher than that of bare TpPa-1 [191].

Besides, the integration of cocatalysts with COFs to form composites is also an effective strategy to promote charge separation. Metal nanoparticles (NPs) have been considered to be the outstanding cocatalysts in photocatalysis. For instance, Ghosh et al. prepared a series of 2D isoreticular COFs by the condensation reaction of Tp with 4,4'-diamino-substituted p-terphenyl and analogous derivatives for photocatalytic hydrogen production. Among them, BtCOF150 shows the best catalytic activity with hydrogen production rate of 750 μmol g^{-1} h^{-1} in the presence of low Pt NPs (1 wt %) cocatalyst [192]. Moreover, the integration of COFs and semiconductors to form heterojunction is another effective approach to enhance charge separation. As typical examples, Lan and coworkers fabricated a series of covalently linked organic-inorganic *Z*-scheme heterojunctions containing COF-318 and semiconductors (TiO_2, Bi_2WO_6 and α-Fe_2O_3) for artificial photosynthesis (Fig. 10a). As shown in Fig. 10b and 10c, taking TiO_2 as a representative, it was completely covered by COF-318 with a thickness of 5-10 nm COF shell. The results of photocatalytic CO_2 reduction show that COF-318-TiO_2 heterojunction exhibits the highest CO production rate of 69.67 μmol g^{-1} h^{-1} with H_2O as the electron donor (Fig. 10d) [193].

6. Photocatalytic applications of COFs

The excellent physical and chemical properties of COFs make them splendid materials for large-scale applications, particularly in photocatalysis. In this part, we summarize the recent research progresses of COFs in photocatalytic H_2 production, CO_2 reduction, organic transformation and pollution degradation.

6.1. Photocatalytic H_2 production

Hydrogen (H_2) is regarded as a promising energy carrier owing to its high energy density (120 MJ kg^{-1}) and environment-friendly characteristic [194]. The generation of H_2 by photocatalytic water splitting is an ideal strategy, which can directly convert solar energy into chemical energy [195–197]. Thus, the development of efficient photocatalysts for water splitting is a very active research field. As a new class of crystalline porous materials, COFs provide an emerging platform for photocatalytic H_2 production. To facilitate H_2 evolution, predesigning functional building units and linkages, and modifying COFs with metal ions and semiconductors, are the most widely used strategies. Furthermore, the metal-based cocatalysts are often introduced into the COF-based photocatalytic system to improve charge separation efficiency and further boost catalytic performance [198–230].

6.1.1. Pristine COFs

Recently, a series of COFs have been investigated for photocatalytic H_2 production. For instance, Dong and coworkers constructed a 2D donor-acceptor (D-A) COF (BDF-TAPT-COF) by the solvothermal reaction of the electron-rich 4,4'-(benzo[1,2-*b*:4,5-*b*']difuran-4,8-diyl)dibenzaldehyde (BDF-CHO) and electron-deficient 2,2'-BPDA. The organized D-A system within BDF-TAPT-COF enables effective charge separation and transport. Thus, BDF-TAPT-COF exhibits a superior photocatalytic performance for H_2 production with the rate of 1390 μmol g^{-1} h^{-1}, by using aqueous ascorbic acid as sacrificial electron donor and Pt as cocatalyst under simulated sunlight (AM 1.5) [208]. The same conclusion was also reported by Wen and coworkers with a 2D D-A COF (PyTz-COF), which was constructed based on the electron-rich pyrene (Py) and electron-deficient thiazolo-[5,4-*d*]thiazole (Tz). The obtained PyTz-COF shows a high photocatalytic H_2 production rate of 2072.4 μmol g^{-1} h^{-1} [209].

The structural designability of COFs is an attractive character, which makes them promising candidates for structure-to-property design at an atomic/molecular level. In 2021, Wang et al. designed and synthesized four isostructural porphyrinic 2D COFs (MPor-DETH-COF, M = H_2, Co, Ni, Zn) through condensation reaction of porphyrinic aldehydes (p-MPor-CHO) and DETH (Fig. 11a). By incorporating different transition metals into the porphyrin rings, the performance of photocatalytic H_2 evolution can be tuned with the rate order of CoPor-DETH-COF < H_2Por-DETH-COF < NiPor-DETH-COF < ZnPor-DETH-COF (Fig. 11b) [210]. Moreover, the photocatalytic H_2 production performance can also be regulated in COF photocatalysts through substituting different non-metallic atoms in organic building units. To achieve this, the Tan group successfully fabricated a series of D-A CTFs by condensation of benzene-1,4-dicarboximidamide hydrochloride (BDCH) with 3,6-dicarbaldehyde-N-ethylcarbazole (DCNE), 2,8-dicarbaldehydedibenzothi- ophene (DCSE) and 2,8-dicarbaldehydedibenzofuran (DCOE), which are denoted as CTF-X (X = N, S and O, respectively). The N-doped fluorene possesses the strongest electron donating ability, thus CTF-N exhibits the best charge separation efficiency. Consequently, it achieves an exceptionally high hydrogen evolution rate of 538 μmol h^{-1} under

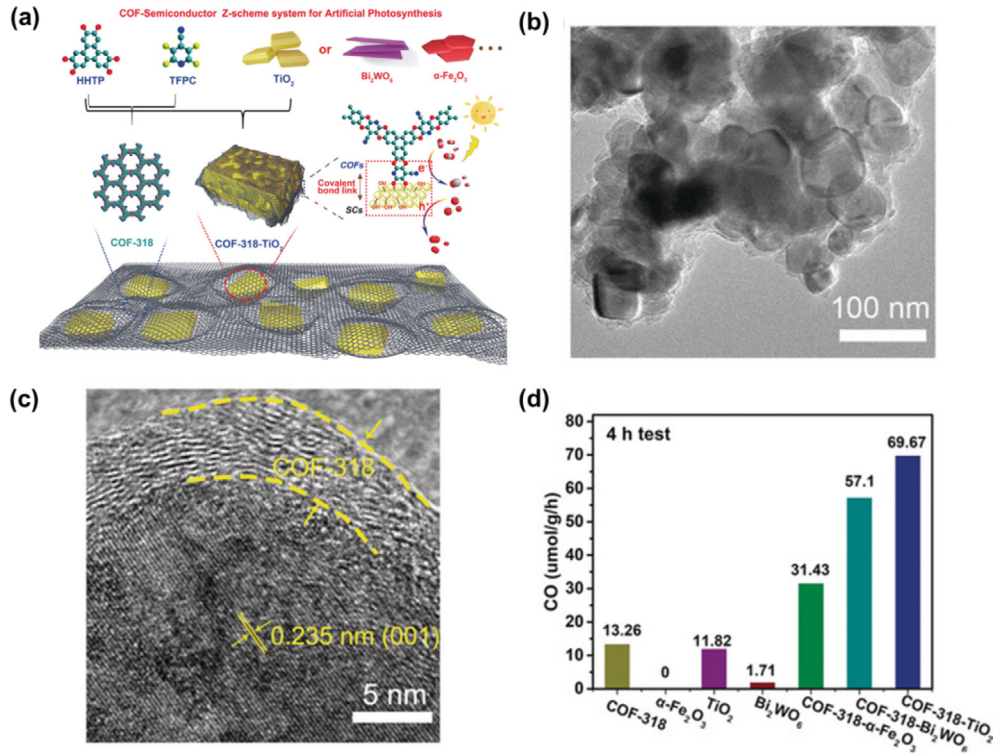

Fig. 10. (a) Schematic showing the preparation of COF-318 based heterojunctions *via* the integration of COF-318 and TiO_2, Bi_2WO_6 or α-Fe_2O_3. (b) TEM image of COF-318-TiO_2. (c) HRTEM image and lattice fringes (the lattice fringe of 0.235 nm is attributed to the (001) face of TiO_2). (d) Photocatalytic activities of COF-318 based heterojunctions compared with pristine COF-318, TiO_2, Bi_2WO_6 and α-Fe_2O_3. Reprinted from Ref. [193] with permission from the Wiley-VCH, copyright 2020.

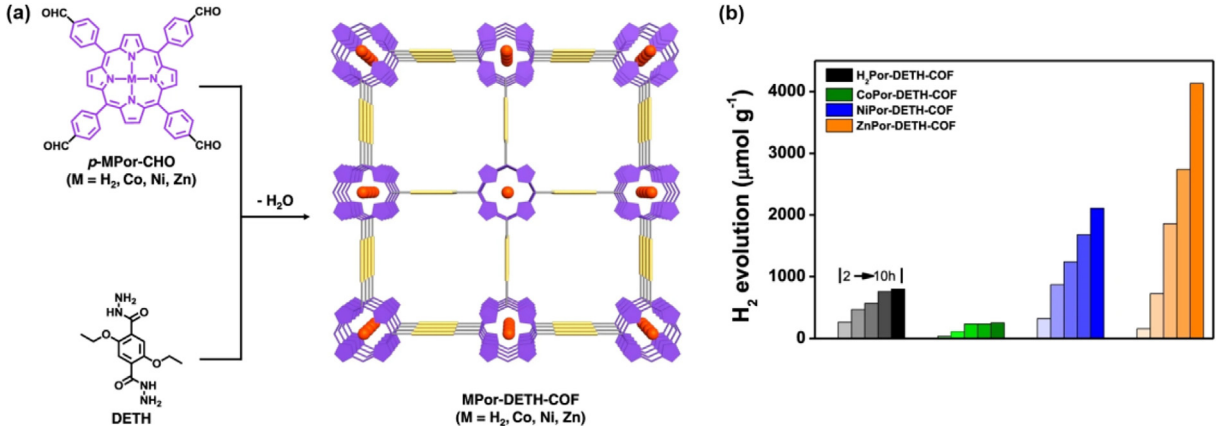

Fig. 11. (a) Schematic illustration for the fabrication of MPor-DETH-COFs. (b) Photocatalytic performances for H_2 evolution over MPor-DETH-COFs. Adapted from Ref. [210] with permission from the Nature Springer, copyright 2021.

visible light irradiation, which is about 7 and 2 times higher than those of CTF-O and CTF-S, respectively [211].

Besides, COFs with various functional groups usually exhibit different photocatalytic performance for H_2 production. For example, Yang et al. synthesized a cyano-containing COF (CYANO-COF) with D-A (ketene-cyano) pair *via* a Schiff-base condensation reaction of Tp and 4,4'-diamino-[1,1'-biphenyl]-3,3'- dicarbonitrile (BD-CYANO). The ball milling of CYANO-COF results in the formation of COF nanosheet (CYANO-CON). Interestingly, CYANO-CON achieved a high photocatalytic activity for H_2 production with a rate of 2684 μmol h^{-1}, which was about 17 times higher than that of a control sample (BD-CON) with similar structure but without cyano group [212]. The $-CH_3$ group as the electron-donating unit and $-NO_2$ group as the electron-withdrawing moiety were respectively introduced in the same host framework of COFs, to explore the effect of functional groups on photocatalytic performance. The resulted TpPa-COF-X (X = -H, $-(CH_3)_2$, and $-NO_2$) with different functional groups attached on the backbone were constructed. The results of photocatalytic H_2 production demonstrate that TpPa-COF-$(CH_3)_2$ shows the best activity with H_2 evolution rate of 8.33 mmol g^{-1} h^{-1}, which is 6 and 38 times higher than those of TpPa-COF and TpPa-COF-NO_2, respectively [213]. Furthermore, Jiang and coworkers prepared two 2D D-A COFs (BT-COF and HBT-COF) by the acid-catalyzed condensation of 4,4'-(Benzo[*c*][1,2,5]thiadiazole-4,7-diyl)dianiline (BTDA) with BT or 2-hydroxybenzene-1,3,5-tricarbaldehyde (HBT). The introduction of electron-donating unit (-OH group) in HBT-COF enhances internal D-A effect and hydrophilicity. As a consequence, HBT-COF shows 5-fold

improvement of activity for photocatalytic H_2 evolution over BT-COF under visible light irradiation [214].

Apart from building units, the type and number of linkages can also affect the H_2 production rate in COF photocatalysis. In 2020, the Yu group constructed three structurally related COFs with different linkages (imine-, imide-, and alkene linkages), to investigate the effect of the linkage chemistry on photocatalytic H_2 evolution. The alkene linkage exhibits stronger electron-withdrawing ability and electron delocalization than the other two linkages, which facilitates the charge separation efficiency. Consequently, alkene-linked COF shows the highest photocatalytic performance with H_2 production rate of 2330 μmol h^{-1} g^{-1}, far superior to the imine- and imide-linked COFs (< 40 μmol h^{-1} g^{-1}) under visible light irradiation [215]. Furthermore, the Zhao group prepared three kinds of COFs with different ratios of β-ketoenamine to imine moieties in the linkages, by an acid-catalyzed Schiff base reaction of Pa with BT derivatives. The photocatalytic H_2 production rate gradually enhances along with the increased numbers of β-ketoenamine linkages. The excited state of the mixed-linkage COFs are suppressed by the imine moiety, which accounts for their different photocatalysis [216].

The 2D layer structures of COFs make them outstanding candidates for the fabrication of nanosheets (NSs) with enhanced catalytic efficiency. Recently, various strategies have been developed to construct COF NSs for photocatalytic H_2 production. For instance, the Xu group reported a novel redox exfoliation strategy for efficient preparation of ultrathin amide-functionalized CTF NSs. The crystalline CTF bulk materials were firstly treated with concentrated sulfuric acid to achieve oxidative intercalation of layered CTF. Afterwards, water was added to exfoliate layered CTF into o-CTF NSs, which were further reduced by hydrazine hydrate to obtain amide-functionalized CTF NSs with a thickness of 1.5 nm (r-CTF NSs) (Fig. 12a-12c). The resulted r-CTF NSs show 17-fold improvement of photocatalytic H_2 evolution activity compared with the pristine bulk CTF (Fig. 12d) [217]. Moreover, Osakada and coworkers synthesized several 2D porphyrin COF NSs with average thickness of 1 nm by the exfoliation technique, through the addition of metal ions and axial ligands to disrupt the π-π stacking between the COF layers. The photocatalytic results demonstrate that COF NSs show significantly increased activity for H_2 production over the bulk materials upon irradiation with visible or NIR light [218].

6.1.2. Metallized COFs

COFs with well-defined structures and high porosity provide a good platform for metalation to improve catalytic performance. Towards this goal, Zang et al. prepared binuclear Cu-salphen based COF nanosheets for photocatalytic H_2 production. The salphen-HDCOF was firstly synthesized by solvothermal polycondensation of 2,3,6,7,10,11-hexaimino-triphenylene (HATP·6HCl) and 2,6-diformylphenol (DFP). Subsequently, the metalation of the salphen-HDCOF was performed by stirring it with $Cu(OAc)_2$ in CH_3-OH to produce Cu-salphen-HDCOFs, which was further exfoliated into ultrathin nanosheets by facile solvent-assisted liquid sonication (denoted as Cu-salphen-HDCOF-NSs). The photocatalytic results demonstrate that Cu-salphen-HDCOF-NSs shows an excellent activity with H_2 production rate of 36.99 mmol g^{-1} h^{-1}, which is higher than that of salphen-HDCOF-NSs without Cu complexation (~4.50 mmol g^{-1} h^{-1}) [219]. Furthermore, the Yu group reported a Zn/Co ion-implantation pathway to regulate the electronic structure of a series of hollow COF cages for photocatalytic H_2 production. Taking Zn@H-TpPa as an example, ZIF-8 was prepared by reaction of Zn and 2-methylimidazole to act as a sacrificial template. Afterwards, the Zn@H-TpPa with Zn ions in the shell was obtained by a condensation of Tp and Pa outside of ZIF-8 core, following by etching ZIF-8 with acetic acid.

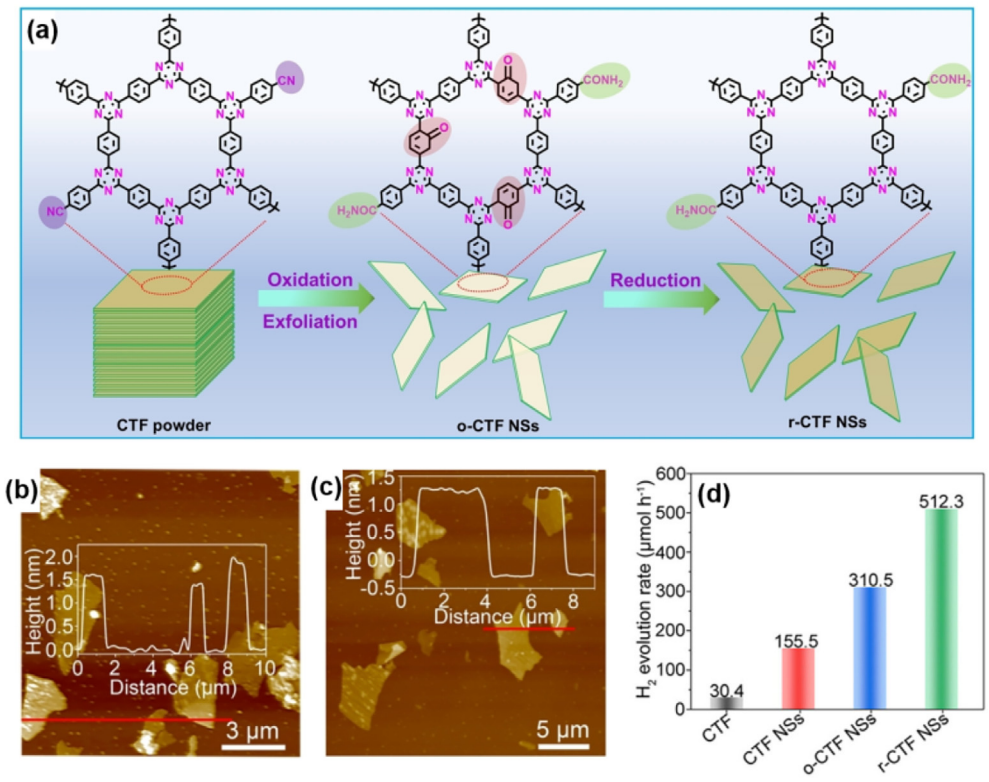

Fig. 12. (a) Schematic showing the preparation of o-CTF NSs and r-CTF NSs. (b) and (c) AFM images of o-CTF NSs and r-CTF NSs (Inset: height plot). (d) Photocatalytic H_2 evolution rates of bulk CTF, CTF NSs, o-CTF NSs and r-CTF NSs. Reproduced from Ref. [217] with permission from the Wiley-VCH, copyright 2021.

The incorporation of Zn within COFs not only increases the polarity of the framework, but also upshifts the conduction band of COF, thus facilitating the charge separation. As a consequence, Zn@H-TpPa exhibits an ultrahigh H_2 production rate of 28.00 mmol g^{-1} h^{-1}, far superior to that of pure TpPa (Fig. 13) [220].

6.1.3. COF-based composites

The electron-hole separation plays an important role in photocatalysis. The photogenerated electron-hole pairs in single COF photocatalysts often tend to the fast recombination, which result in the low catalytic efficiency for H_2 evolution. To conquer this, one of the promising strategies is to construct COF-based composite photocatalysts by the combination of COFs with inorganic semiconductors, MOFs and C_3N_4, *etc* [221–230].

Traditional inorganic semiconductors such as metal oxide and sulfide have not only been explored as photocatalysts, but also regarded as outstanding candidates to form composites. Therefore, functionally combining these semiconductors with COFs to form COF-based composites have been demonstrated to be a feasible strategy to improve photocatalytic efficiency. To this end, the Zhang group reported a series of TiO_2-COF composites by combining TiO_2 and COF through covalent bonds. First, the TiO_2 nanosheets were modified with Tp to obtain aldehyde-functionalized TiO_2 (CHO-TiO_2) by a two-step strategy. Then, the Schiff base reaction between Tp and Pa results in covalent binding of TiO_2 to the surface of TpPa-1-COF to form TiO_2-TpPa-1-COF hybrid materials (Fig. 14a). The photocatalytic results show that the TiO_2-TpPa-1-COF (1:3), with the weight ratio of 1:3 for CHO-TiO_2:TpPa-1-COF, exhibits H_2 evolution rate of 11.19 mmol g^{-1} h^{-1}, which is 5.3, 3.0 and 4.6 times higher than those of TpPa-1-COF, TiO_2/TpPa-1-COF composite without covalent connection and their physical mixture, respectively (Fig. 14b and 14c) [225]. Moreover, the Shi group constructed a 2D-2D SnS_2/TpPa-1-COF composite for photocatalytic H_2 evolution without the addition of cocatalyst. In this study, the COF nanosheets (TpPa-1-COF) was prepared by Schiff base reaction between Pa and Tp firstly, which was further added into thioacetamide and $SnCl_4{\cdot}5H_2O$ solution, to form SnS_2/TpPa-1-COF composite by hydrothermal synthesis process. The photocatalytic results demonstrate that

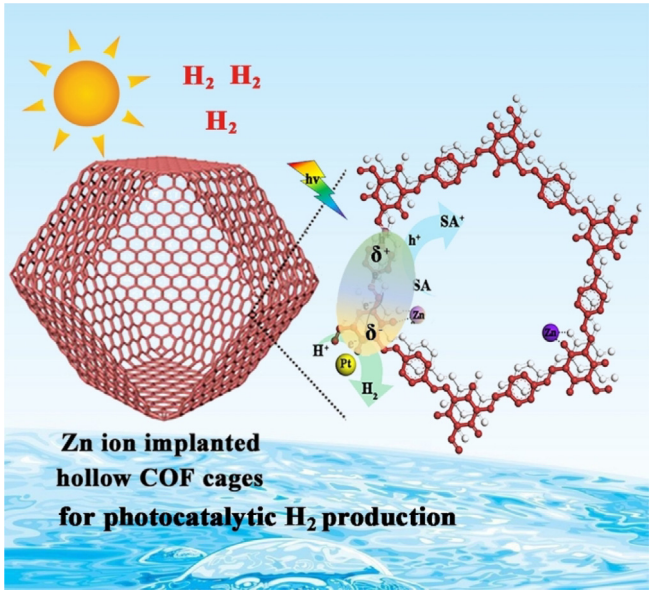

Fig. 13. Schematic showing the Zn ion implanted hollow COF cages for photocatalytic H_2 production by using Pt as a cocatalyst. Adapted from Ref. [220] with permission from the Wiley-VCH, copyright 2022.

SnS_2/TpPa-1-COF, with the mass ratio of 3:7 for SnS_2:TpPa-1-COF, shows H_2 production rate of 37.11 μmol h^{-1}, which is 21.7 times and 51.5 times higher than those of bare TpPa-1-COF and SnS_2, respectively [226].

Similar to the COFs, the facile modification of MOFs is one of the most fascinating features, which enables their intermesh into MOF/COF composites. For example, the Lan group fabricated a covalently integrated MOF/COF hybrid material for photocatalytic H_2 evolution. First, NH_2-UiO-66 was prepared by reaction of $ZrCl_4$ and 2-aminoterephthalic acid (NH_2-BDC) with exposed -NH_2 functional groups. Then, the addition of different amounts of NH_2-UiO-66 in the reaction system of TpPa-1-COF containing Tp and Pa led to a series of NH_2-UiO-66/TpPa-1-COF hybrid materials (Fig. 15a). The TEM images demonstrate that NH_2-UiO-66 grows on the surface of the TpPa-1-COF (Fig. 15b and 15c). The element mapping images reveals the homogeneous distribution of C, N, and Zr in NH_2-UiO-66/TpPa-1-COF (Fig. 15d). The composite with weight ratio of 4:6 for MOF:COF, exhibits the best photocatalytic activity with H_2 evolution of 23.41 mmol g^{-1} h^{-1}, which is 20-fold improvement over TpPa-1-COF (Fig. 15e). Moreover, it shows excellent photocatalytic stability, which can retain activity in the 20 consecutive runs in 480 h (Fig. 15f) [227]. Using a similar strategy, the Chen group synthesized PdTCPP⊂PCN-415(NH_2)/TpPa composites by introducing PdTCPP⊂PCN-415(NH_2) into the synthesis system of TpPa, which exhibits an excellent photocatalytic performance with H_2 evolution rate of 13.98 mmol g^{-1} h^{-1}, far superior to those of PdTCPP⊂PCN-415(NH_2) (0.21 mmol g^{-1} h^{-1}) and TpPa (6.51 mmol g^{-1} h^{-1}), respectively [228].

Graphitic carbon nitride (g-C_3N_4), a type of fascinating metal-free semiconductor, has emerged as a promising photocatalyst. However, the photocatalytic efficiency of pure g-C_3N_4 is hampered due to insufficient visible light utilization and rapid recombination of photogenerated electron-hole pairs. To overcome these drawbacks, the integration of g-C_3N_4 and COF to form g-C_3N_4/COF composites has been proved as an efficient strategy. For instance, the combination of a D-A type COF (TBTA) and g-C_3N_4 together generates TBTA/g-C_3N_4 hybrids *via in situ* condensation procedure of Tp and BTDA on g-C_3N_4, reported by the Jiang group. The obtained hybrids exhibit excellent photocatalytic activity for H_2 evolution, with an optimized rate of 11.73 mmol g^{-1} h^{-1}, which is higher than those of individual components [229].

Apart from the combination of COFs with other semiconductors, the COF/COF composites can also be constructed to increase photocatalytic performance. Towards this goal, Fan et al. prepared a series of P-COF-1/CTF heterojunction composites with different mass ratios of COF and CTF *via* intermolecular π-π interactions. As expected, the heterojunctions not only enhance the visible-light absorption, but also promote the effective charge separation, thus significantly improving photocatalytic activity for H_2 evolution. The optimum H_2 production rate of P-COF-1/CTF is 14,100 μmol h^{-1} g^{-1}, which is about 2.5 times higher than those of pure CTF and their mechanical mixture [230].

6.2. Photocatalytic CO_2 reduction

In recent years, excessive CO_2 discharged from the combustion of fossil fuels has resulted in serious environmental and energy problems [231,232]. Photocatalytic CO_2 reduction to fuels or high value-added chemicals is an effective way to alleviate the above issues [233–236]. However, the activation and conversion of CO_2 are particularly difficult due to the high kinetic and thermodynamic stabilities of CO_2 molecule, which requires efficient photocatalysts to achieve this process. COFs with excellent CO_2 adsorption capacity and tunable interactions with CO_2, represent ideal candidates for photocatalytic CO_2 reduction [184,185,237–248].

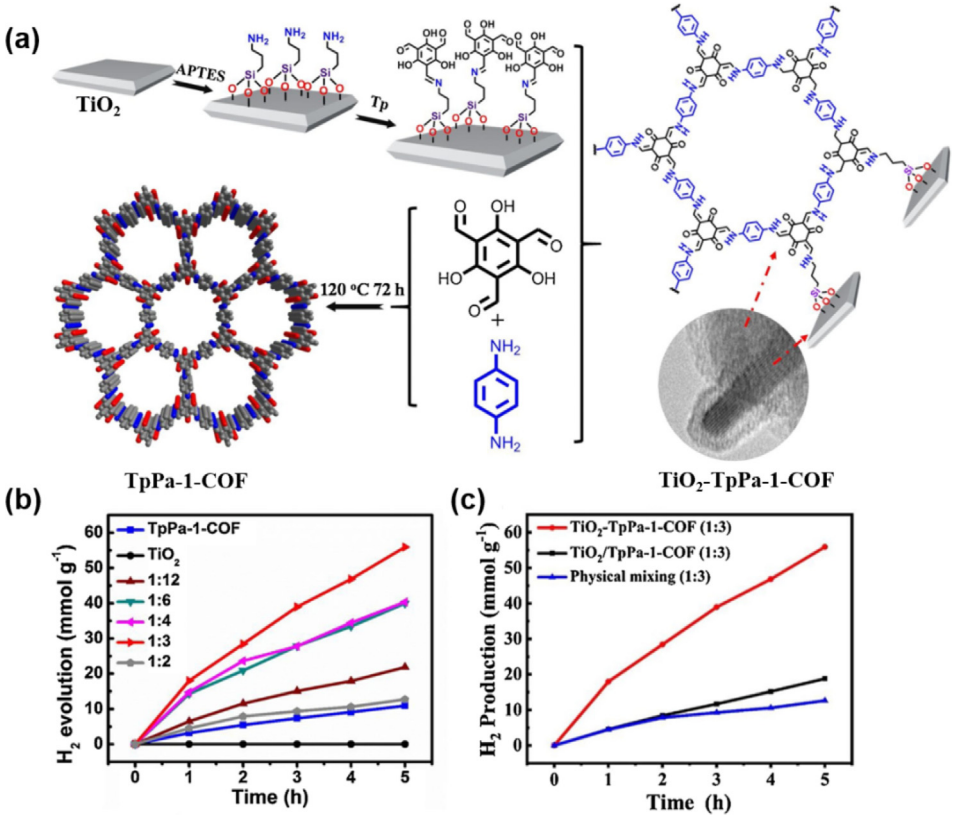

Fig. 14. (a) Schematic showing the construction of TiO_2-TpPa-1-COF composite. (b) The photocatalytic H_2 production performances of TiO_2, TpPa-1-COF and a series of TiO_2-TpPa-1-COF composites. (c) The photocatalytic H_2 production performances of TiO_2-TpPa-1-COF (1:3), TiO_2/TpPa-1-COF (1:3) and physical mixture (1:3). Reproduced from Ref. [225] with permission from the Elsevier, copyright 2020.

6.2.1. Pristine COFs

In 2018, Zhu et al. synthesized two 2D azine-based COFs by condensation reaction of BT or 2,4,6-tris(4-bromophenyl)-1,3,5-triazine (N_3-Brp) with hydrazine hydrate. The two metal-free COFs can catalyze CO_2 and H_2O into methanol under visible light irradiation without any sacrificial agents, which exhibit higher performance than g-C_3N_4 and some inorganic semiconductor photocatalysts [237]. Next, the same group also constructed a series of ketoenamine-based COFs to explore the effects of the different functional groups for photocatalytic CO_2 reduction. The amine-aldehyde condensation reaction of Tp and benzidine (BD-H_2), *o*-tolidine [BD-$(CH_3)_2$], *o*-dianisidine [BD-$(OCH_3)_2$], or 3,3'-dinitrobenzidine [BD-$(NO_2)_2$] was performed to generate imine-linked COFs, following by an irreversible enol-keto tautomerism to produce *β*-ketoenamine bond within COFs, named TpBD-X [X = -H_2, -$(CH_3)_2$, -$(OCH_3)_2$, and -$(NO_2)_2$] (Fig. 16a). The photocatalytic results demonstrate that all TpBD-X samples can reduce CO_2 to HCOOH with the rate order of TpBD-$(OCH_3)_2$>TpBD-$(CH_3)_2$>TpBD-H_2>TpBD-$(NO_2)_2$ under visible-light irradiation (Fig. 16b). Furthermore, TpBD-$(OCH_3)_2$ exhibits an excellent catalytic stability in the five successive runs (Fig. 16c). The electron-donating groups have a stronger conjugation effect than the electron-withdrawing groups in TpBD-X, which enhance charge separation efficiency, thus explaining their discriminative CO_2 photoreduction performances [238].

Porphyrin-based COFs can not only incorporate various metal ions to serve as catalytic centers, but also possess excellent visible-light absorption due to the large conjugated systems, which have shown great potential in photocatalytic CO_2 reduction. For instance, Jiang and coworkers developed a facile strategy to tune the cobalt spin state by the manipulation of its oxidation state in porphyrinic COF-367-Co for photocatalytic CO_2 reduction. The results of experiments and density functional theory (DFT) calculations demonstrate that Co^{II} and Co^{III} are implanted into the porphyrin centers of COF-367-Co with S = 1/2 and 0 spin ground states, respectively. The photocatalytic results show that COF-367-Co^{III} exhibits higher activity and selectivity to HCOOH than COF-367-Co^{II} (Fig. 17) [185]. In another example, the Lan group designed and synthesized a series of 2D porphyrin-tetrathiafulvalene COFs (TTCOF-M, M = 2H, Zn, Ni, Cu) by Schiff base condensation between metallized TAPP-M and 2,3,6,7-tetra (4-formylphenyl)tetrathiafulvalene (TTF), for artificial photosynthesis including CO_2 reduction and H_2O oxidation. Among these COFs, TTCOF-Zn shows the highest catalytic activity with CO yield of 12.33 μmol along with H_2O oxidation to O_2, under visible light illumination after 60 h without additional photosensitize and sacrificial agents [186].

6.2.2. Metallized COFs

Most of COFs show the prominent drawback of lacking bare metal catalytic centers, which is an obstacle for them to activate CO_2 molecule. Post-synthetic metalation through the immobilization of individual catalytic metal centers in COFs, is a promising strategy to improve the performance of photocatalytic CO_2 reduction. As a good example, a bipyridine-based COF (TpBpy) with keto moieties was designed and synthesized by the condensation of Tp and Bpy under solvothermal conditions, following by a simple treatment with $Ni(ClO_4)_2$ to form Ni-TpBpy, in which the bipyridine units can stabilize single Ni sites through coordination (Fig. 18a). Ni-TpBpy exhibits an excellent activity for photoreduction of CO_2 to CO using $[Ru(bpy_3)]Cl_2$ (bpy = 2,2'-bipyridine) as a photosensitizer and TEOA as an electron donor, giving a CO

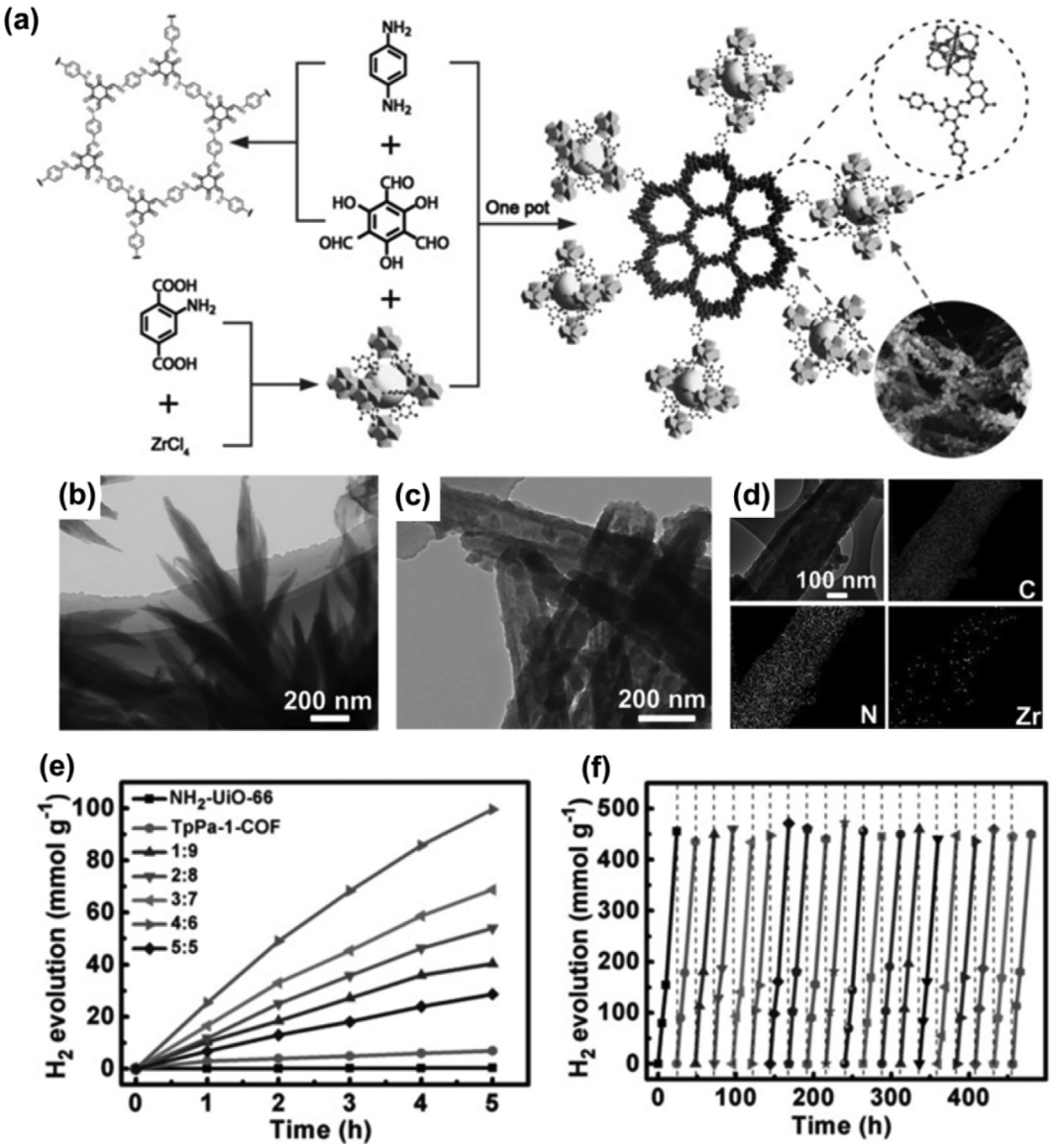

Fig. 15. (a) Schematic illustration for the synthesis of NH_2-UiO-66/TpPa-1-COF composites. (b, c) TEM images of TpPa-1-COF and NH_2-UiO-66/TpPa-1-COF. (d) HRTEM image and the corresponding elemental mappings of C, N and Zr for NH_2-UiO-66/TpPa-1-COF. (e) The photocatalytic H_2 evolution activities of NH_2-UiO-66/TpPa-1-COF, NH_2-UiO-66 and TpPa-1-COF. (f) The photocatalytic recyclability for H_2 production of NH_2-UiO-66/TpPa-1-COF. Reproduced from Ref. [227] with permission from the Wiley-VCH, copyright 2018.

production rate of 811.4 μmol g^{-1} h^{-1} with a selectivity of 96%. For comparison, Ni-TpPa and TbBpy COFs without 2,2'-bypridine coordination units and keto moieties respectively show much lower photocatalytic activities than that of Ni-TpBpy, demonstrating that the coordinated Ni sites and keto moieties play important roles in the activation and conversion of CO_2 (Fig. 18b) [239]. Using a similar strategy, a series of other bipyridine-based COFs were prepared, which can also immobilize metals (such as Re, Mo and Co) to enhance catalytic activity for CO_2 photoreduction, indicating a general and powerful method to modify COFs [134–136,240].

Apart from bipyridine, the metal ions or clusters can be anchored in the skeleton of COFs through other functional groups to serve as catalytic centers. In this respect, the Lan group prepared a 2D anthraquinone-contained COF (DQTP) by Schiff base condensation reaction of Tp with 2,6-diaminoanthraquinone (DAAQ). The adjacent quinone oxygen atoms can ligate different kinds of metal active species to form DQTP COF-M (M = Co/Ni/Zn). The results of photocatalytic CO_2 reduction demonstrate that DQTP COF-Co exhibits a high performance for CO production (1020 μmol h^{-1} g^{-1}), while DQTP COF-Zn shows a high activity for the formation of HCOOH (152.5 μmol h^{-1} g^{-1}) [241]. Besides, the Cooper group synthesized two bulk 2D COFs (Py-COF and FPy-COF) by Schiff base condensation of 5,5',5'',5'''-(pyrene- 1,3,6,8-tetrayl)-tetrapicolinal dehyde (TTPPy) with benzidine and 4,4'-diamino-2,2'-difluorobi phenyl (DDFB), respectively. Next, the ultrasonic exfoliation of them in acetonitrile containing $CoCl_2$ generates Co-loaded COF nanosheets (CONs), in which Co sites are anchored by pyridine units and adjacent imine groups. The partially fluorinated Co-FPy-CON shows an excellent photocatalytic performance for CO_2 reduction with the CO yield of 10.1 μmol for 6 h, which is higher than that of Co-Py-CON (7.4 μmol) under the same conditions. The enhanced photocatalytic activity of Co-FPy-CON is attributed to the improved binding affinity toward CO_2 [242]. The Lan group designed two COFs with uncondensed aldehyde functionalities (TCOF and ECOF) by the Schiff-base condensation of TTA and TTF/4-[4-[1,2,2-Tris[4-(4-formyl phenyl) phenyl] ethenyl] phenyl]

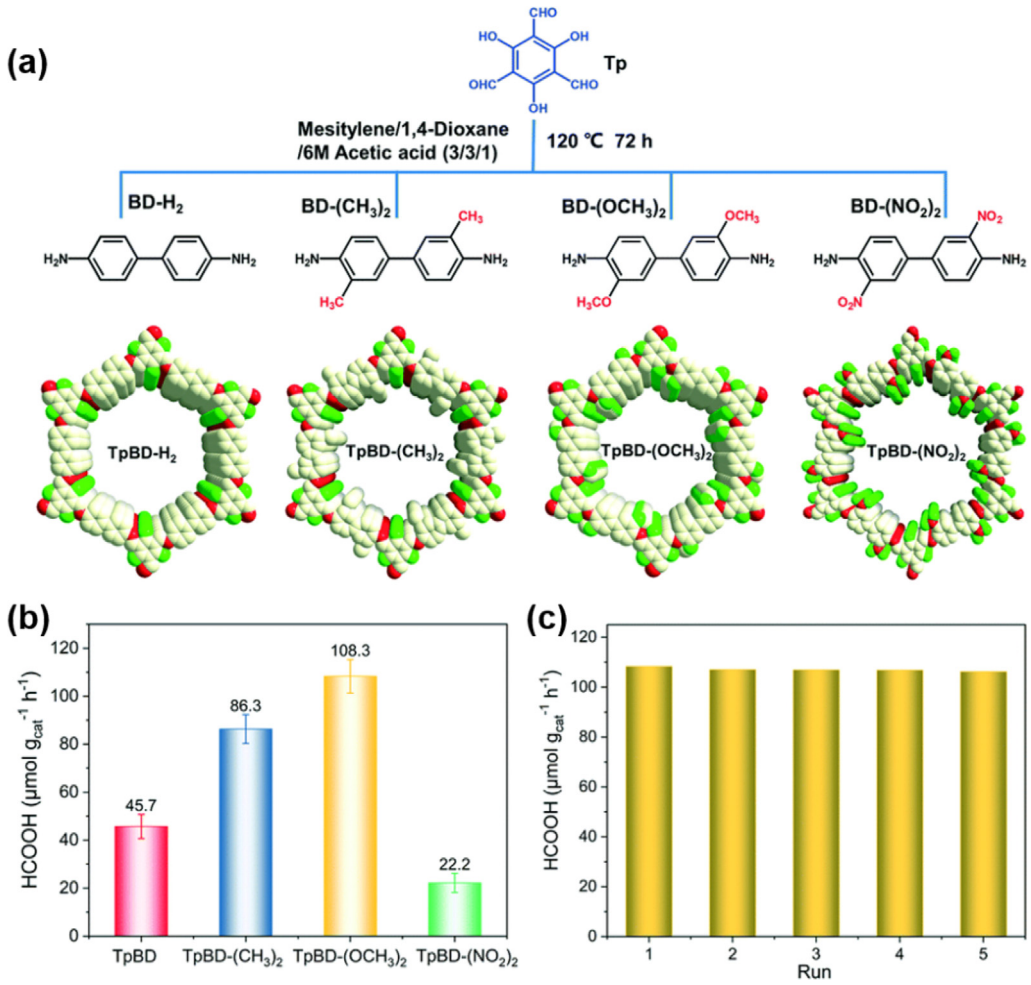

Fig. 16. (a) Schematic showing the construction of TpBD-X [X = -H_2, -$(CH_3)_2$, -$(OCH_3)_2$ and -$(NO_2)_2$]. (b) The photocatalytic activity for HCOOH production over TpBD-X. (c) The rate of HCOOH produced in five consecutive runs over TpBD-$(OCH_3)_2$. Adapted from Ref. [238] with permission from Royal Society of Chemistry, copyright 2021.

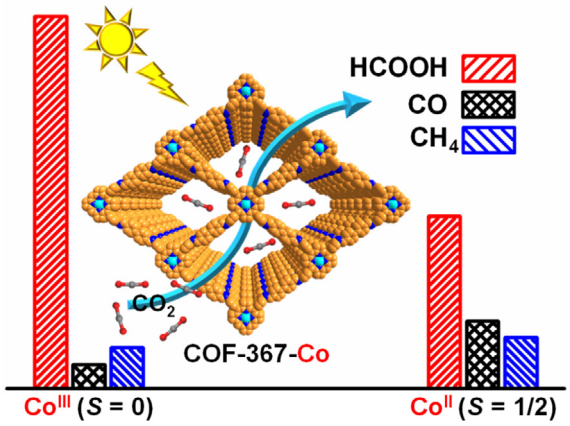

Fig. 17. The COF-367-Co with different spin states of Co for photocatalytic CO_2 reduction. Reprinted from Ref. [185] with permission from the American Chemical Society, copyright 2020.

benzaldehyde (ETBC). Next, the polyoxometalates (POMs) clusters ($MnMo_6$) were stably confined into the nanopores of TCOF and ECOF by covalent linkages to form TCOF-$MnMo_6$ and ECOF-$MnMo_6$. They showed excellent activities for photocatalytic CO_2 reduction with CO production rates of 37.25 and 16.60 μmol g^{-1} h^{-1} respectively with H_2O as the electron donor, which are much higher than those of TCOF and ECOF [243].

Additionally, the free guest molecules containing metal catalytic sites can be also loaded on COFs to enhance photocatalytic CO_2 reduction performance. For instance, the Wang group prepared a 2D COF (TD-COF) by the acid-catalyzed Schiff base reaction of Tp with 2,6-diaminobenzo[1,2-d:4,5-d']bisthiazole (DBT). Afterwards, the metalloporphyrin-based carbon dots (Ni-PCD) were filled into the 1D channels of the TD-COF *via* ultrasonic treatment of TD-COF, TAPP-Ni and glucose in the ethanol/water solution, following by selective pyrolysis of glucose under N_2 at 200 °C. The introduction of Ni-PCD in the 1D channels of TD-COF provides suitable microenvironment for CO_2 adsorption and activation. When the amount of TAPP-Ni used is 0.15 μmol, the Ni-PCD@TD-COF shows the highest photocatalytic activity for CO_2 reduction with CO production rate and selectivity of 478 μmol g^{-1} h^{-1} and 98%, respectively [244]. Furthermore, different amounts of Ru NPs were loaded on TpPa-1 to form Ru/TpPa-1 catalysts, reported by Zhu and coworkers, which exhibit obviously increased photocatalytic performance for the reduction of CO_2 to HCOOH, in sharp contrast to TpPa-1 [245]. Islam et al. prepared a mesoporous COF by reacting Tp and DAAQ, which was used as photocatalyst for the reduction of CO_2 to HCOOH by using $Co(dmg)_2$ complex as cocatalyst (dmg = dimethylglyoxime). The photocatalytic reaction goes with a TON of 125, but it can't proceed without the cocatalyst [246].

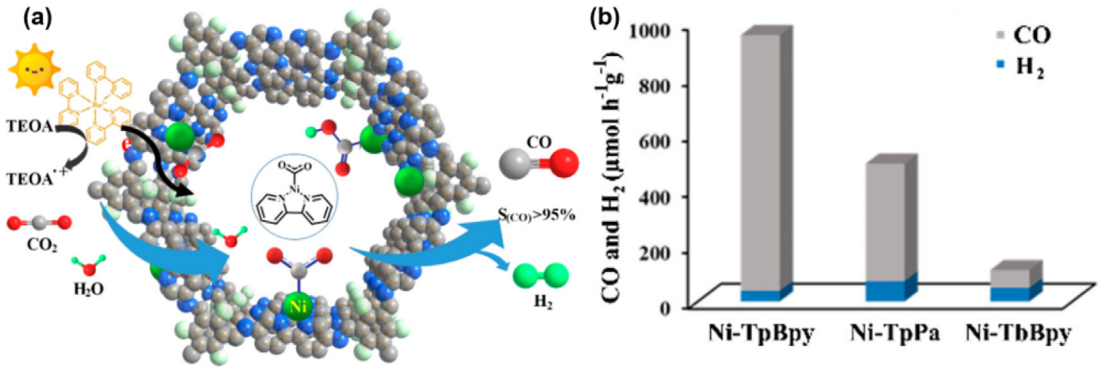

Fig. 18. (a) Schematic showing photocatalytic CO_2 reduction to CO over Ni-TpBpy. (b) The photocatalytic performance for the reduction of CO_2 to CO over Ni-TpBpy, Ni-TpPa and NiTbBpy. Adapted from Ref. [239] with permission from the American Chemical Society, copyright 2019.

6.2.3. COF-based composites

Similar to that of photocatalytic H_2 production, COF-based composites have also been reported to show the improved photocatalytic performance for CO_2 reduction. In 2021, the Wang group constructed a Z-scheme hybrid between copper(II) porphyrin-based COF and TiO_2 by the addition of TiO_2-INA (INA = isonicotinic acid) into the DMF solution of as-prepared CuP-Ph COF, in which the INA is used as a bridge ligand to link CuP-Ph and TiO_2 through coordination bonds. The TiO_2-INA@CuP-Ph composite can catalyze CO_2 conversion under simulated solar light without sacrificial agents, with CO production rate of 50.5 μmol g^{-1} h^{-1}, which is 9.9-fold and 24.5-fold improvements than those of pristine COF and TiO_2, respectively [247]. Besides, the Lan group reported a yolk-shell MOFs/TiO_2@COFs, a core-shell MOFs@COFs and a hollow-sphere TiO_2@COFs composites for photocatalytic CO_2 reduction. As shown in Fig. 19a, NH_2-MIL-125 was firstly prepared by solvothermal reaction of titanium isopropoxide ($Ti(OC_4H_9)_4$) and NH_2-BDC, which was further added into a mixture of 2,5-dihy droxyterephthalaldehyde (DHA), Ni-TAPP and o-dichlorobenzene/ethanol to form core-shell NH_2-MIL-125@COF-366-Ni-OH-HAc composite. Following this, partial NH_2-MIL-125 was transformed to TiO_2 in acetic acid (HAc) by controlling the content of HAc, generating the yolk-shell NH_2-MIL-125/TiO_2@COF-366-Ni- OH-HAc composite. In the end, all NH_2-MIL-125 was decomposed to TiO_2 in HAc to form hollow-sphere TiO_2@COF-366-Ni-OH-HAc composite. The photocatalytic results demonstrate that the CO yield is about 67.49 μmol g^{-1} for NH_2-MIL-125/TiO_2@COF-366-Ni-OH-HAc in 4 h with H_2O as the electron donor, much higher than those of NH_2-MIL-125@COF-366-Ni-OH-HAc (≈5.78 μmol g^{-1}) and TiO_2@COF-366-Ni-OH-HAc (≈44.12 μmol g^{-1}) (Fig. 19b). The NH_2-MIL-125/TiO_2@COF-366-Ni-OH-HAc composite not only exhibits the coexistence of Z-scheme and II type heterojunction, but also possesses both photocatalytic oxidation and reduction sites, thus showing the enhanced photocatalytic activity [248].

6.3. Photocatalytic organic transformation

The light-driven organic transformation is recognized as a green and sustainable approach for the synthesis of fine chemicals [30,249]. Over the last few decades, organic dyes and metal complexes have been proved to be efficient catalysts in photocatalytic organic transformation. However, they often suffer from poor stability, low recyclability and high cost, which are still obstacles for practical applications [250–256]. Therefore, the development of efficient and stable photocatalysts to achieve organic transformation is highly desirable. Recently, COFs featuring tunable structures, high stability, large surface area, easy-adjustable band structure, have been shown as promising photocatalysts in many organic transformation reactions such as oxidation, reduction, addition, ring-opening polymerization, isomerization, dehalogenation, *etc* [257–278].

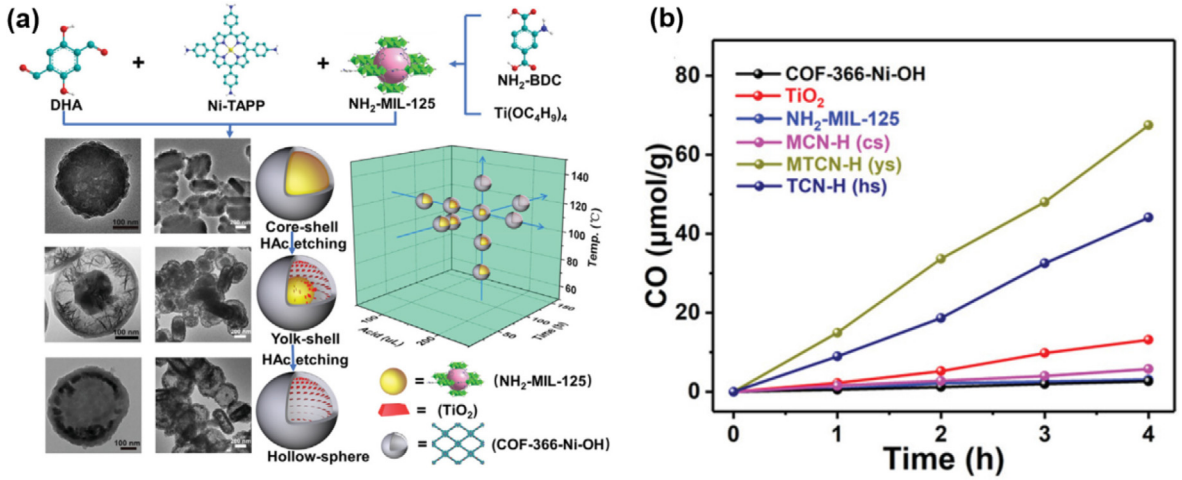

Fig. 19. (a) The schematic illustration of the fabrication of yolk-shell NH_2-MIL-125/TiO_2@COF-366-Ni-OH-HAc, core-shell NH_2-MIL-125@COF-366-Ni-OH-HAc and hollow-sphere TiO_2@COF-366-Ni-OH-HAc composites. (b) Photocatalytic CO_2-to-CO performances for COF-366-Ni-OH, TiO_2, NH_2-MIL-125, NH_2-MIL-125/TiO_2@COF-366-Ni- OH-HAc, NH_2-MIL-125@COF-366-Ni-OH-HAc and TiO_2@COF-366-Ni-OH-HAc. Adapted from Ref. [248] with permission from the Wiley-VCH, copyright 2021.

6.3.1. Pristine COFs

Photocatalytic aerobic oxidation through COFs presents an eco-friendly approach for organic synthesis. To this end, Zhang et al. synthesized a series of 2D COFs by Knoevenagel condensation of tricyanomesitylene with ditopic or tritopic aromatic aldehydes. Thanks to the excellent semiconducting properties, they exhibit photocatalytic aerobic oxidation of arylboronic acids to phenols with high efficiency under visible light irradiation [270]. In another work, the Bai group prepared an anthraquinone functionalized COF (AQ-COF) with a noodle-like nanofiber morphology, which exhibits higher photocatalytic activity than the AQ-COF_{DMF} with spherical particles morphology, for the selective aerobic oxidation of sulfides to sulfoxides. The unique morphology of AQ-COF facilitates charge separation and transfer, thus explaining the enhanced photocatalytic activity [271].

Besides, Jiang et al. prepared three porphyrinic COFs (DhaTph-M, M = 2H, Zn and Ni) with different metals in porphyrin centers to regulate excitonic effects for photocatalytic oxidation reactions. The introduction of Zn^{2+} in porphyrin center promotes the conversion of singlet to triplet excitons, while the Ni^{2+} introduction can efficiently dissociate excitons to hot carriers. Under the irradiation of visible light, DhaTph-Zn and DhaTph-Ni can activate O_2 to $^1O_2$ and $O_2^{\cdot-}$, respectively. Notably, they exhibit selective oxidation of α-terpinene to ascaridole and p-cymene, respectively. Moreover, DhaTph-Zn shows superior photocatalytic activity for the oxidation of organic sulfides, whereas DhaTph-Ni possesses excellent performance for the hydroxylation of phenylboronic acid (Fig. 20) [272].

COFs can be also used as photocatalysts for the aerobic oxidation of amines. For instance, Li and coworkers designed and synthesized a 2D porphyrinic COF (Por-BC-COF) with an AA stacking mode by Schiff-base condensation reaction of 4,4',4'',4'''-([9,9'-bicarbazole]-3,3',6,6'-tetrayl)tetrabenzaldehyde (BCTB) with H_2TAPP. Upon white and red lights irradiation, Por-BC-COF can catalyze the aerobic oxidative coupling of benzylamine to N-benzylidenebenzylamine with high yield (97%) [273]. Also, the Wang group synthesized a 2D porphyrin-based sp^2 carbon-conjugated COF (Por-sp^2c-COF) with an eclipsed AA stacking structure by the Knoevenagel condensation reaction of 5,10,15,20-tetrakis(4-benzaldehyde)porphyrin (*p*-Por-CHO) and 1,4-phenylenediacetonitrile (PDAN). Por-sp^2c-COF can catalyze the aerobic oxidation of dibenzylamine to N-benzylidenebenzylamine with the yield of 99% in 30 min [274].

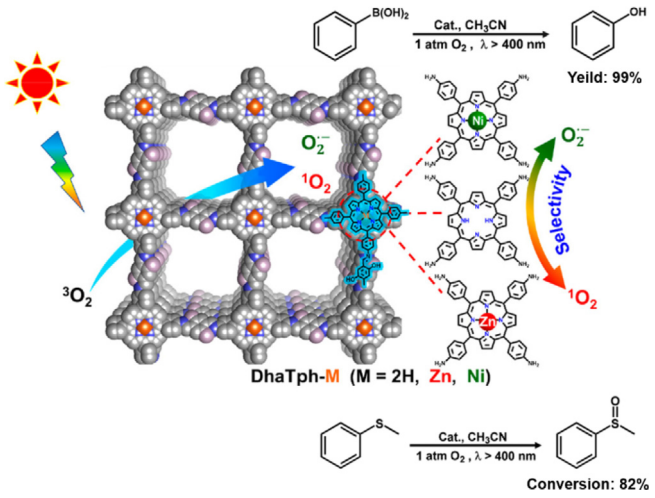

Fig. 20. Schematic showing DhaTph-M COFs (M = 2H, Zn and Ni) with discriminative oxygen activation selectivity to $^1O_2$ and $O_2^{\bullet-}$, for the oxidation of thioanisole and the hydroxylation of phenylboronic acid. Adapted from Ref. [272] with permission from the Wiley-VCH, copyright 2021.

In addition to the aerobic oxidation reaction, COFs can be employed as photocatalysts for reduction and addition reactions. Tang et al. synthesized a series of 2D [3+3] COFs *via* the polycondensation reaction between N_0-Ald containing -H, -OH and -CF_3 substituents in the aromatic ring and TTA or TAPB for photocatalytic reductive dehalogenation reaction. Among them, OH-N_0-Ald-TTA bearing both the -OH group and triazine skeleton, exhibits the highest catalytic activity due to the narrow band gap, high conductivity and efficient charge separation [275]. In another study, Gu et al. constructed an anionic 3D titanium-based COF (Ti-COF-1) by the imine condensation reaction of $Na_2Ti(2,3\text{-}DHTA)_3$ (2,3-DHTA = 2,3-dihydroxyterephthalaldehyde) complex and 4,4',4'',4'''-(pyrene-1, 3, 6, 8-tetrayl)tetraaniline (PyTTA). Ti-COF-1 can catalyze Meerwein addition reactions of arenediazonium salts and alkenes with yields of 49-75% under the white LED irradiation [276].

Radical ring-opening polymerization (RROP) has been considered as an efficient approach to synthesize functional polymers. For example, the Cui group designed and synthesized a series of 2D-PN and 3D-PN COFs, which were used as photocatalysts to drive RROP of vinylcyclopropanes (VCPs). In this work, the imine condensations of 5,10-di(3,5-diformylphenyl)-5,10-dihydrophenazine (DDDP) and six linear aromatic diamines and a tetrahedral tetraamine, produce six 2D-PN COFs with slipped AA stacking and a 3D-PN COF with a 2-fold interpenetrated pts network (Fig. 21a). All COFs can drive RROP of various VCP monomers, whereas the 2D-PN-2-OMe exhibits higher catalytic activity than the 3D-PN-1 (Fig. 21b). The increased catalytic efficiency of 2D-PN COFs can be attributed to the enhanced internal surface areas, catalytically active sites, visible-light harvesting ability and electron transfer efficiency [277].

The *trans* (*E*)/*cis* (*Z*) configuration of olefins is very important for the synthesis of anticancer drugs. In recent years, COFs have been employed as photocatalysts for the *E* to *Z* transformation of olefins. For example, Banerjee et al. constructed a triazine and keto functionalized COF (TpTt) by performing reaction of1,3,5-triazine-2,4,6-triamine (Tt) with Tp for the *E* to *Z* transformation of alkenes. Generally, the triazine core can facilitate strong π–π interaction with *E* alkene, and keto functionalities within β-ketoenamine core contribute to increase the lifetime of the excited triplet state. Therefore, the TpTt photocatalyst with the two distinct photoactive building blocks is used for isomerization reaction of *trans*- to *cis*-stilbene, which exhibits an excellent activity with a yield of 90% after 18 h [278].

6.3.2. Metallized COFs

To enhance the photocatalytic performance of COFs for organic transformation, anchoring metals in the framework to facilitate charge separation and transfer is considered as an efficient strategy. In this respect, the Chen group synthesized a highly stable olefin linked 2D COF (sp^2c-COF_{dpy}) with bipyridine units *via* Knoevenagel polymerization between TFFPy and 5,5'-bis(cyanomethyl)-2,2'- bipyridine (BCPy). Afterwards, the Ni was stabilized at the bipyridine unit through coordination interaction to generate sp^2c-COF_{dpy}-Ni (Fig. 22a). The obtained sp^2c-COF_{dpy}-Ni has been proved to be a promising photocatalyst for C-O coupling from aryl bromide, which exhibits significantly improved catalytic activity over sp^2c-COF_{dpy} without Ni (Fig. 22b) [279]. Beyzavi et al. prepared an imine COF (COF-UARK-49) assembled from 2-(4-formylphenyl)-5-formylpyridine (FPFP) and PyTTA, which can anchor Pt by imine or pyridyl N atoms to form COF-UARK-49-Pt. The incorporation of Pt in the framework not only expands the visible-light harvesting ability, but also provides openings in axial sites to enhance

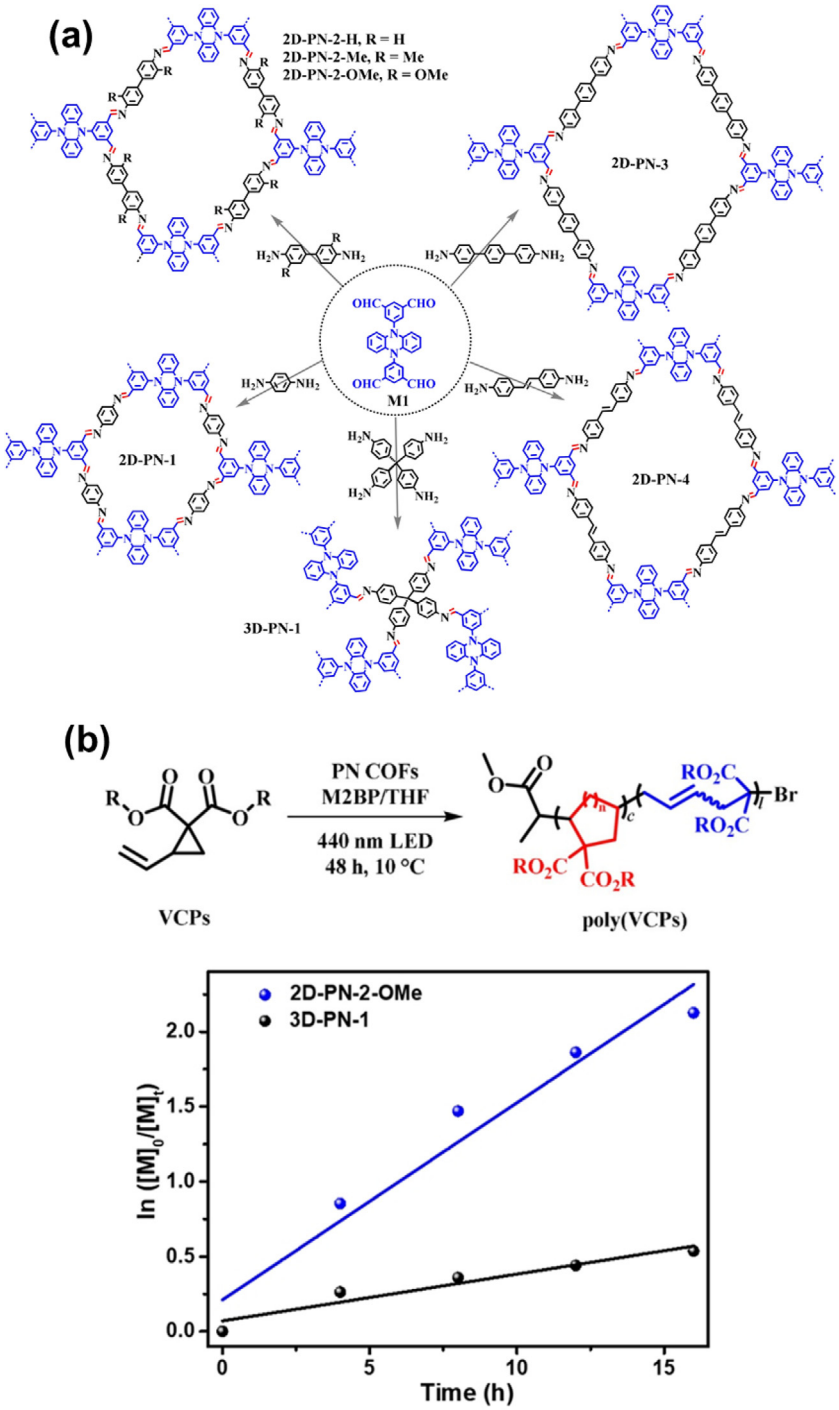

Fig. 21. (a) Schematic showing the synthesis of 2D-PN and 3D-PN COFs. (b) RROP of VCP monomers and kinetic plots of the RROP over 2D-PN-2-OMe and 3D-PN-1. Reproduced from Ref. [277] with permission from the Wiley-VCH, copyright 2021.

interactions with substrates. As a consequence, COF-UARK-49-Pt displays obviously higher photocatalytic performance toward decarboxylative difluoroalkylation and oxidative cyclization reactions than COF-UARK-49 [280]. Moreover, Maji and coworkers firstly synthesized a bipyridine-based COF (Tp-Bpy) by reaction of Tp and Bpy via mechanochemical grinding process. Afterwards, the Tp-Bpy COF was treated with $[Ir(ppy)_2(CH_3CN)_2]PF_6$; [ppy = 2-phenylpyridine], and further treated with $NiCl_2$ to generate Ni-Ir@Tp-Bpy COF, in which Ir and Ni were anchored at the bipyridine unit. The resulting Ni-Ir@Tp-Bpy exhibits high photocatalytic activity for catalyzing C-N coupling reactions [281].

6.3.3. COF-based composites

The construction of COF-based composites by coupling COFs with other active species is another effective strategy to improve photocatalytic efficiency for organic transformation. For example, the Huang group reported a series of COF/CdS composites by the deposition of different contents of CdS on the surface of COFs, *via* a two-step method for the oxidation of aromatic alcohols. First,

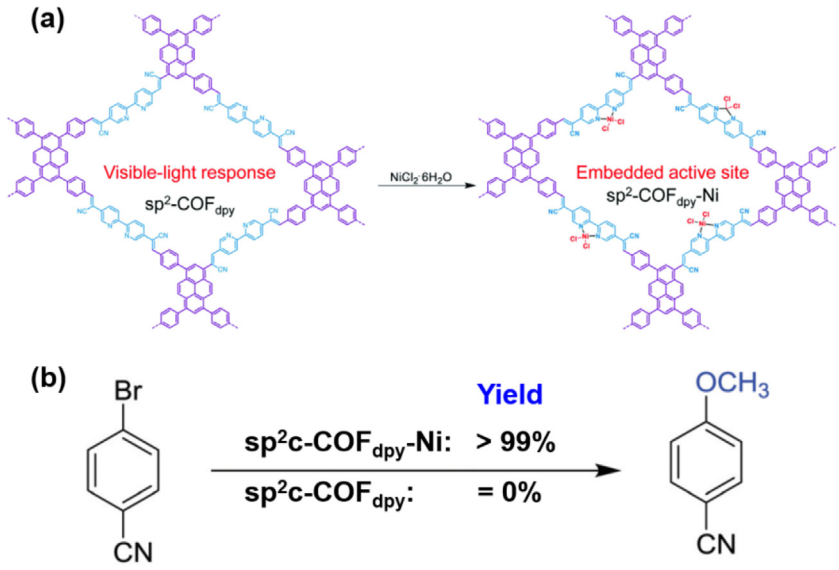

Fig. 22. (a) Schematic showing the modification of sp^{2}c-COF$_{dpy}$ with Ni through coordination interaction. (b) Photocatalytic C-O coupling reaction over sp^{2}c-COF$_{dpy}$ and sp^{2}c-COF$_{dpy}$-Ni. Reproduced from Ref. [279] with permission from the Royal Society of Chemistry, copyright 2021.

pure COF was synthesized through the Schiff base reaction of TAPB with terephthalaldehyde. Then, a mixture of cadmium acetate, thioacetamide and COF with different mass ratios was added into ethanol solution at 80 °C for 40 min to form COF/CdS composites (named, COF/CdS-1, COF/CdS-2, COF/CdS-3 and COF/CdS-4, respectively). Among these composites, COF/CdS-3 shows the best catalytic activity for the production of benzaldehyde with a yield of 97.1%, which is about 2.5 and 15.9 times higher than those of parental CdS and COF, respectively. The integration of CdS and COF can enhance the visible light harvesting ability and charge separation efficiency, unambiguously explaining its high photocatalytic performance [282].

Additionally, Wang and coworkers successfully constructed a range of core-shell MOF@COF photocatalysts based on a seed growth method for the selective oxidation of alcohols. In detail, the NH_2-MIL-125 was firstly prepared by solvothermal reaction of 2-aminoterephtalic acid and titaniumtetraisopropoxide. Afterwards, a little amount of PDA and TAPB were added in the suspension of NH_2-MIL-125, the Schiff base reaction between aldehyde of PDA and -NH_2 groups on PAPB/NH_2-MIL-125 led to the formation of heterogeneous seed nuclei coated on surface of NH_2-MIL-125. Next, the high concentration of PDA and PAPB were used to connect seed forming NH_2-MIL-125@TAPB-PDA hybrid materials with different thickness of COF shell (Fig. 23a). The images of TEM and HRTEM demonstrate that TAPB-PDA grows on the surface of NH_2-MIL-125 to form composite featuring the porous structure (Fig. 23b and 23c). The optimized NH_2-MIL-125@TAPB-PDA-3 with COF shell thickness of ~20 nm shows the best photocatalytic activity for the oxidation of benzyl alcohol to benzaldehyde with the yield of 94.7%, which is approximately 2.5 and 15.5 times higher than those of NH_2-MIL-125 and TAPB-PDA, respectively (Fig. 23d). As shown in Fig. 23e, NH_2-MIL-125@TAPB-PDA-3 also possesses high catalytic stability, only a little photocatalytic deactivation is observed after 5 cycles [283].

6.4. Photocatalytic pollution degradation

Organic contaminants (such as organic dyes, antibiotics, phenol derivatives, *etc.*) and heavy metals (e.g. Cr(VI)) from industrial wastes are hazardous to the environment and humans [284–287]. Photocatalysis has been recognized to an environment-friendly method to degrade these pollutants [288–313]. However, most of pollutants are difficult to be degraded and the degradation process is relatively complicated, which requires photocatalysts with high efficiency and stability. COFs have demonstrated potential for the degradation of pollutants due to their good stability and excellent photoelectronic properties.

6.4.1. Pristine COFs

High toxic organic dyes such as rhodamine B (RhB), methylene blue (MB) and Sudan Red III (SR III), etc. are ubiquitous in industrial wastewater that need to be eliminated urgently. Photoactive COFs have been proved as outstanding catalysts for the degradation of these dyes [85,291–299]. For example, Liu et al. synthesized two amide-linked 2D COFs *via* a two-step method for the photocatalytic degradation of RhB. The imine-linked COFs (COF-JLU16 and COF-JLU17) were prepared by the condensation reaction of TTA with N_3-Ald and N_0-Ald respectively, following by oxidation of the imine bonds with $NaClO_2$ to form amide-linked COFs (COF-JLU18 and COF-JLU19). The photocatalytic results demonstrate that COF-JLU19 shows fast degradation of RhB to N-deethylated intermediates within 4 min in water, which is 4 times higher catalytic efficiency than that of COF-JLU18. The enhanced photocatalytic efficiency of COF-JLU19 can be attributed to the ampliative visible light absorption and incremental electron-hole separation [85]. Moreover, Alemán et al. reported a series of 2D imine-based COFs for photocatalytic degradation of three different pollutants (MB, SR III and mono-brominated polybrominated diphenyl ether (PBDE-1)). The solvothermal reaction of 10-(4-formylphenyl)-10*H*-phenothiazine- 3,7-dicarbaldehyde (FPD), tris(4-formylphenyl) amine (TFPA) and TAPB with the FPD/TFPA molar ratios of 0/1, 1/7, 1/3, 1/1 and 1/0 generates five COFs (4a-e). All COFs can degrade the above pollutants, in which COFs 4a and 4e exhibit the best catalytic efficiencies for the degradation of MB and SR III/PBDE-1, respectively [295].

COFs can also be used as photocatalysts for the degradation of sulfonamides, as typical antibiotics that will increase drug resistance among microorganisms. For example, by Schiff base reaction of Tp and Tt under different methods (ball milling and solvothermal), two COFs (TpMA and TpMA-1) have been prepared for the photodegradation of sulfathiazole. Under visible light irradiation, TpMA can quickly degrade sulfathiazole with degradation rate of

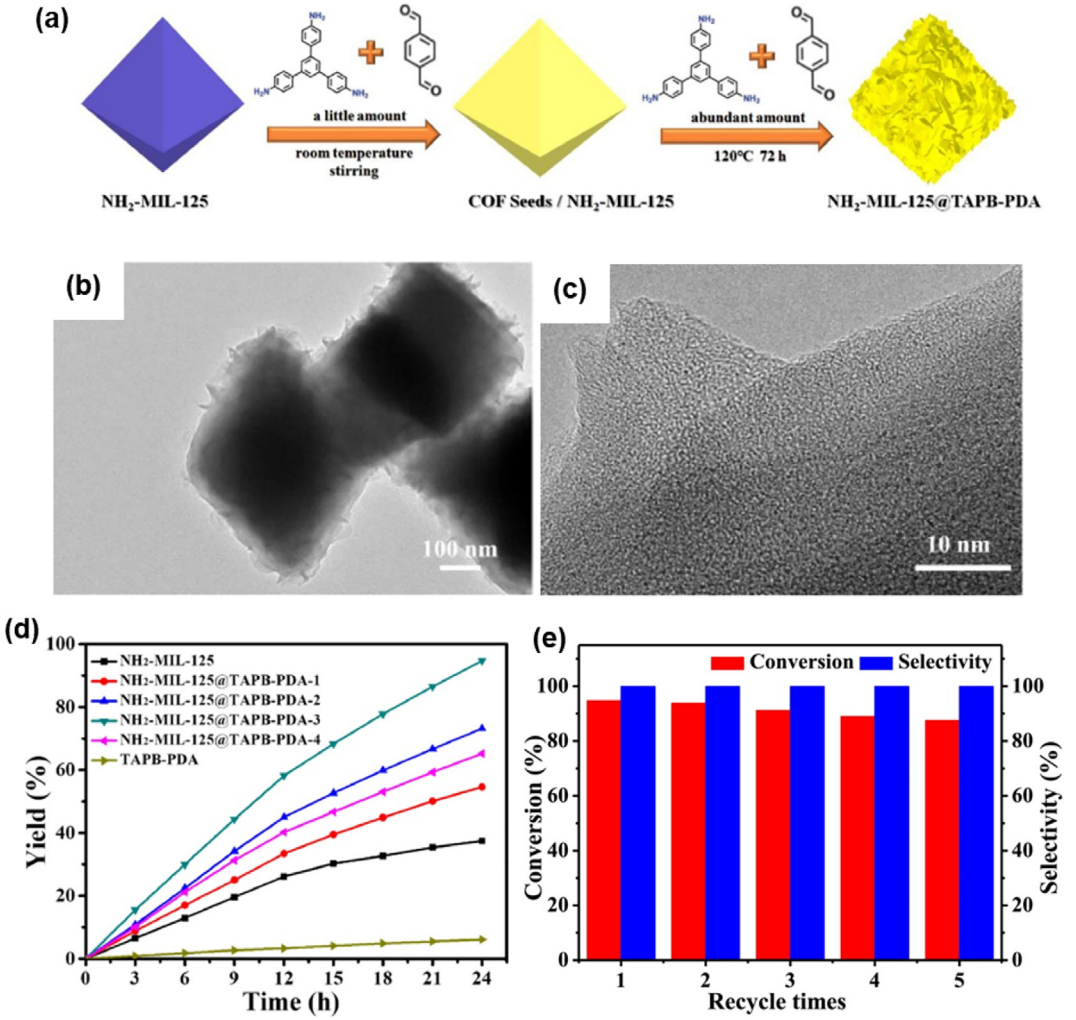

Fig. 23. (a) Schematic showing the construction of NH_2-MIL-125@TAPB-PDA hybrids. (b) TEM image of NH_2-MIL-125@TAPB-PDA-3. (c) HRTEM image of NH_2-MIL-125@TAPB-PDA-3. (d) The conversion of photooxidative benzyl alcohol to benzaldehyde over NH_2-MIL-125, TAPB-PDA and NH_2-MIL-125@TAPB-PDA composites. (e) Recycling experiment of NH_2-MIL-125@TAPB-PDA-3 in the oxidation of benzyl alcohol. Reproduced from Ref. [283] with permission from the Elsevier, copyright 2020.

0.1498 min^{-1}, which is more than three times than TpMA-1. This result suggests the ball milling method with less solvent might be efficient to prepare COFs for the degradation of organic pollutants [297]. In addition, Qiu et al. constructed three vinylene-linked COFs, BDA-TMT, EDA-TMT, and TDA-TMT, by reacting 2,4,6-trimethyl-1,3,5-triazine (TMT) with 4,4'-(buta-1,3-diyne-1,4-diyl)dibenzaldehyde (BDA), 4,4'-(ethyne-1,2-diyl)diben zal- dehyde (EDA) and [1,1':4',1''-terphenyl]-4,4''-dicarbaldehyde (TDA) respectively for photocatalytic degradation of phenol and norfloxacin. The introduction of diacetylene moieties in the skeleton of BDA-TMT increases conjugated π-electrons delocalization and optimizes the electronic band structures, as well as charge separation efficiency. Therefore, BDA-TMT shows ultrafast photodegradation efficiencies for phenol and norfloxacin (> 96% in 15 min) with reaction rate constants of 0.1675 and 0.1764 min^{-1} respectively under visible light irradiation, which is the best performance among all prepared COFs [298].

Apart from photodegradation organic contaminants, COFs can also be employed as photocatalysts to degrade heavy metals from wastewater. Cr(VI) is a toxic heavy metal, while Cr(III) is indispensable to human nutrition. Thus, the reduction of Cr(VI) to Cr(III) is highly desired to address the environmental pollution. Towards this goal, Chen and coworkers synthesized two hexagonal 2D D-A COFs for photoreduction of Cr(VI) to Cr(III) under visible light irradiation (Fig. 24). In this work, the acid-catalyzed Schiff base reaction of benzo[*c*][1,2,5]thiadiazole-4,7-dicarbaldehyde (BTD) with TAPB and TTA generates TAPB-BTD-COF and TTA-BTD-COF respectively, in which benzothiadiazole is known as the electron acceptor to tune bandgaps and enhance charge separation. The photocatalytic results show that 99% Cr(VI) is reduced to Cr(III) by using the two COFs without any sacrificial agents, while TTA-BTD-COF exhibits faster rate than TAPB-BTD-COF [299].

6.4.2. Metallized COFs

The majority of COFs exhibit poor visible light harvesting ability and low charge separation efficiency, which give rise to unsatisfactory activity for photocatalytic pollution degradation. To overcome these issues, metallized COFs has been regarded as facile and effective approach. For example, the Zhao group fabricated a 2D lamellar COF-909(Cu) nanorods for photocatalytic degradation of sulfamethoxazole. COF-909 nanorods containing terpyridyl-based construction unit were firstly prepared by solvothermal reaction of Pa and 4,4',4''-(1,4-phenylene)bis([2,2':6',2''-terpyridine]-5,5'-d icarbaldehyde (PBDT), which was further soaked in copper chloride-methanol solution to generate COF-909(Cu) (Fig. 25a). The introduction of Cu not only increases the visible light

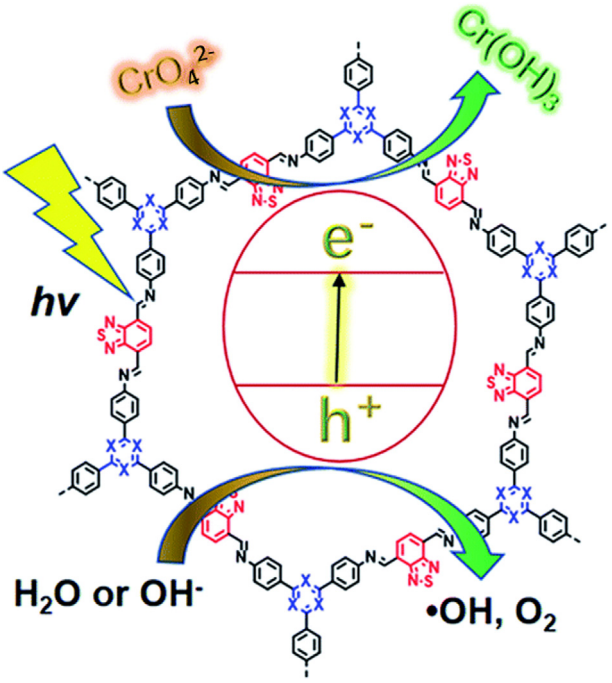

Fig. 24. The photoreduction of Cr(VI) to Cr(III) over TAPB-BTD-COF and TTA-BTD-COF. Reproduced from Ref. [299] with permission from the Royal Society of Chemistry, copyright 2019.

absorption, but also facilitates charge separation. As a consequence, COF-909(Cu) shows an excellent catalytic activity for degradation of sulfamethoxazole with degradation rate of 0.133 min^{-1}, which is 27 times higher than that of COF-909 (Fig. 25b) [296]. In addition, Lu et al. successfully encapsulated Au nanoclusters (NCs) into a thiol chains by post-modified COF to form Au@COF for photocatalytic degradation of RhB. First, the COF-V with vinyl groups was constructed by Schiff base reaction between 2,5-divinylterephthalaldehyde (DVPD) and TAPB, which was further modified with thiol chains. Then, the Au@COF was obtained by the growth of Au NCs into the pores of COF-V through the formation of strong S-Au bonds. Upon visible light irradiation for 30 min, 97.3% RhB is degraded by Au@COF with the degradation rate of 0.0904 min^{-1}, which is 2-fold higher catalytic efficiency than that of COF-V [300].

6.4.3. COF-based composites

COF-based composites have also been shown to improve photocatalytic activity for the degradation of pollutants [301–313]. For instance, the Zhang group fabricated a 2D/2D TpPa-1/MoS_2 heterojunction by adding TpPa-1 into the water solution of sodium molybdate dehydrate and thiourea through a facile hydrothermal method (Fig. 26a). The photocatalytic properties of MoS_2, TpPa-1 and TpPa-1/MoS_2 were assessed by the degradation of RhB and tetracycline (TC). For RhB, the degradation efficiency is 98% for MoS_2/TpPa-1 (20) with a weight ratio of 4:1 for MoS_2:TpPa-1, which is higher than pure MoS_2 (37.5%) and TpPa-1 (35.6%). The degradation rate constant of MoS_2/TpPa-1 (20) is 0.118 min^{-1}, which shows approximately 7-fold and 8-fold improvements over pure MoS_2 and TpPa-1, respectively (Fig. 26b). For TC, the degradation efficiency of MoS_2/TpPa-1 (20) is 85.9%, whereas it is only 47% and 37.8% for pure MoS_2 and TpPa-1, respectively. The degradation rate constant for MoS_2/TpPa-1 (20) is 0.0316 min^{-1}, which is ~3 and ~4 times higher than those of pure MoS_2 and TpPa-1, respectively (Fig. 26c) [308]. Similar to Zhang's work, a series of other 2D/2D heterojunctions such as COF/g-C_3N_4 [309], COF/MOF [310] and COF/COF [311], have also been constructed, which show enhanced photocatalytic performance for the degradation of pollutants compared with the pristine counterparts.

COF-based composites with three components can be also prepared for photocatalytic degradation of pollutants. Towards this goal, Xu et al. synthesized a matryoshka Fe_3O_4@$MOF_{UIO\ 66}$@TzDa-COF composite for the photodegradation of Congo Red (CR). First, Fe_3O_4 NPs were loaded into the skeleton of $MOF_{UIO\ 66}$ to generate Fe_3O_4@$MOF_{UIO\ 66}$. Then, a triazine-containing TzDa-COF is grown on the surface of Fe_3O_4@$MOF_{UIO\ 66}$ to form Fe_3O_4@$MOF_{UIO\ 66}$@-TzDa-COF composite. As a result, Fe_3O_4@$MOF_{UIO\ 66}$@TzDa-COF shows an excellent photodegradation performance to anionic dye CR with degradation efficiency of 97%. The photocatalytic rate constant is 0.65 min^{-1}, which is higher than $MOF_{UIO\ 66}$ (0.069 min^{-1}), TzDa-COF (0.11 min^{-1}), Fe_3O_4 (0.086 min^{-1}) and Fe_3O_4@$MOF_{UIO\ 66}$ (0.137 min^{-1}) [312]. In another study, Bachas et al. prepared a composite Cu_2O-ACOF-1@Pd for photocatalytic degradation of 2-chlorobiphenyl (PCB 1), 3-chlorobiphenyl (PCB 2), 4-chlorobiphenyl (PCB 3). ACOF-1 was synthesized by the condensation reaction of BT with hydrazine hydrate, which was further loaded onto Cu_2O cubes to form Cu_2O-ACOF-1. Subsequently, the Cu_2O-ACOF-1@Pd composite was obtained by the decoration of Cu_2O-ACOF-1 with Pd NPs. The photocatalytic results demonstrate that the Cu_2O-ACOF-1@Pd exhibits better activity than those of the other counterparts, for the degradation of PCB 1, PCB 2 and PCB 3

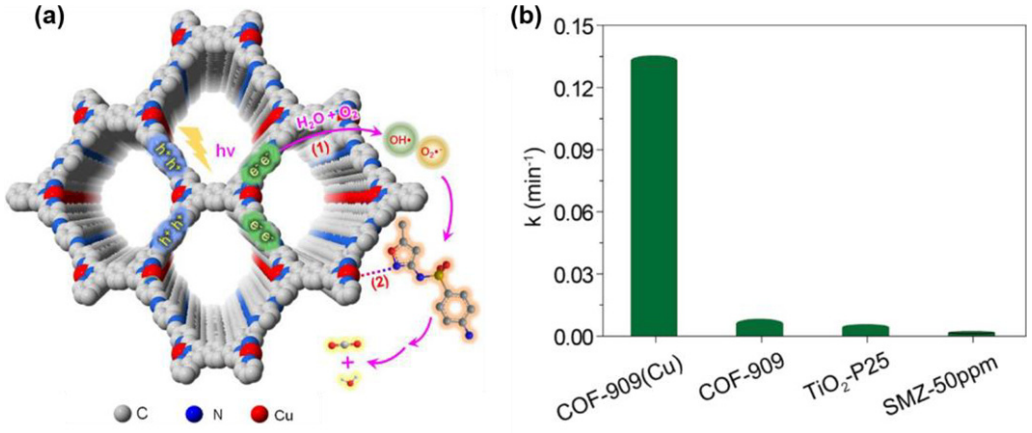

Fig. 25. (a) Schematic illustration for the photodegradation of sulfamethoxazole to CO_2 and H_2O over COF-909(Cu). (b) Pseudo-first-order kinetic constants (k) of COF-909 (Cu), COF-909 and TiO_2-P25 in the photocatalytic degradation of sulfamethoxazole. Reproduced from Ref. [296] with permission from the Elsevier, copyright 2021.

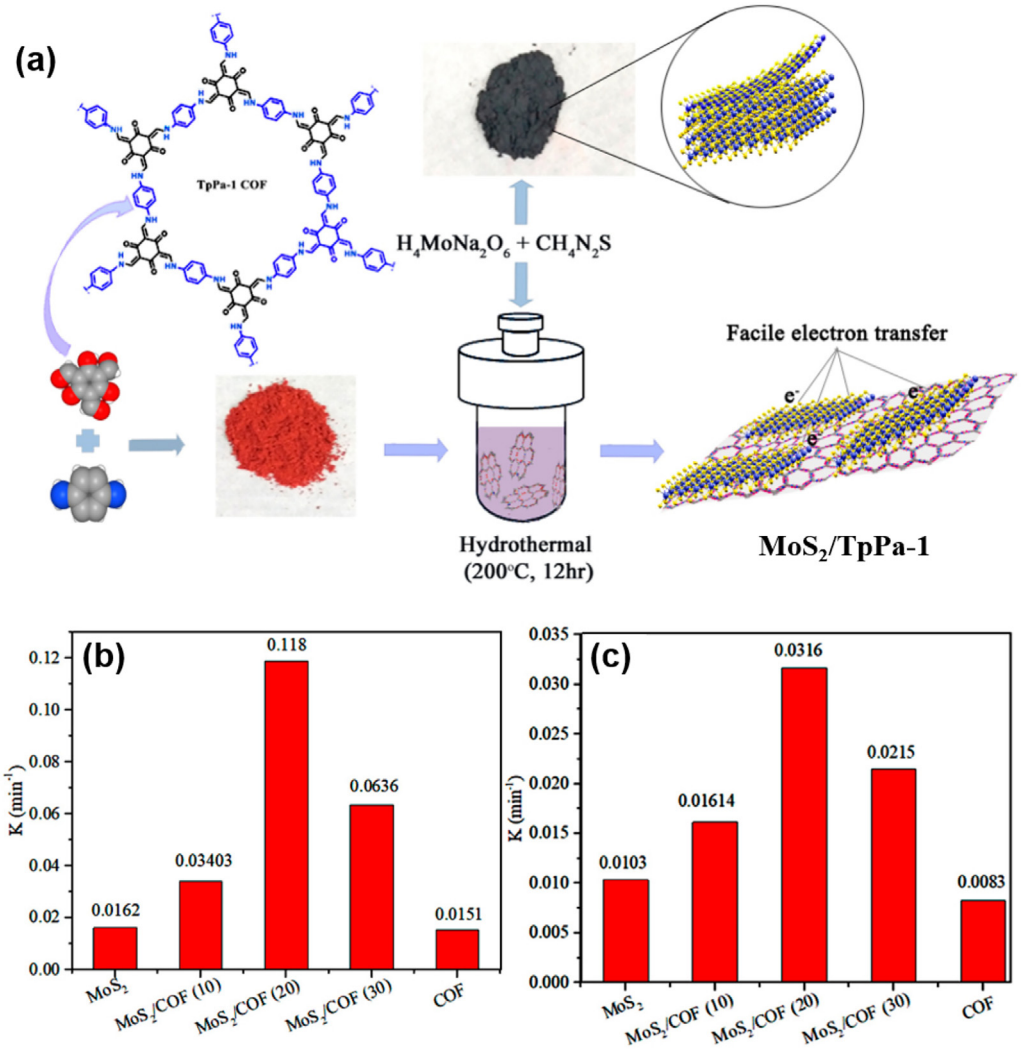

Fig. 26. (a) Schematic showing the preparation of 2D-2D MoS_2/TpPa-1 composites. The kinetic rate constants for photocatalytic degradation of (b) RhB and (c) TC to CO_2 and H_2O over various as-prepared samples. Adapted from Ref. [308] with permission from the American Chemical Society, copyright 2020.

with the activity order of Cu_2O-ACOF-1@Pd>Cu_2O-ACOF-1>ACOF-1@Pd>ACOF-1. The outstanding performance of Cu_2O-ACOF-1@Pd can be attributed to the synergistic effect among the three components [313].

7. Conclusion and outlook

COFs are a subclass of porous crystalline materials built from organic building blocks through covalent bond linkages, which have shown incredible promise as outstanding photocatalysts for diverse photocatalytic reactions. In this review, the synthesis, structural features and photocatalytic applications of COFs are presented. Six synthetic methods including solvothermal synthesis, microwave synthesis, ionothermal synthesis, room temperature solution synthesis, mechanochemical synthesis and interfacial synthesis have been introduced for the preparation of a variety of COFs. Generally, COFs exhibit uniquely ordered 2D and 3D polymeric structures. The 2D COFs are further stacked *via* weak interlayer interactions to generate 1D channels, which will be favorable for the mass transfer during the catalytic process. Various functional COFs can be obtained by *de novo* synthesis and post-synthetic modification techniques. Apart from boron-based COFs, they often show excellent chemical stability in water and acidic/basic solutions due to the strong covalent bonds. Some effective methods have also been applied to further increase the structural stability for practical applications. In addition, the pore size and environment of COFs can be easily engineered, which render them very promising for diverse catalytic reactions.

Based on these attractive structural characteristics, COFs have been deemed as one of the most outstanding photocatalytic candidates. It is well-known that photocatalytic process involves light harvesting, electron-hole separation and redox reaction, in which charge separation plays an important role in this process. A series of accepted strategies have been developed to enhance charge separation efficiency. The introduction of functionalized groups and metal ions in the skeleton of COFs to tune their surface and pore environments, has been proven facile and effective approaches to facilitate charge separation. Moreover, the construction of COF-based composites by the combination of COFs with other active species is another efficient strategy.

As a result, COF-based materials have been employed for various photocatalytic applications including H_2 production, CO_2 reduction, organic transformation and pollution degradation. For H_2 production, researchers have fabricated a series of D-A COFs that exhibit strong light absorption ability and effective charge separation, and thus excellent photocatalytic activity. To further

enhance catalytic activity towards H_2 production, the regulation of the building blocks with different metal ions, non-metallic atoms or functional groups, and modulating the type and number of linkages as well as the thickness of the structure, have shown to be promising approaches. Furthermore, the metallization of COFs by post-synthetic modification method, and the composition of COFs with metal oxides, metal sulfides, MOFs, g-C_3N_4 or the other COFs present some other potential strategies to promote charge separation, ultimately yielding materials with increased photocatalytic performance for H_2 evolution. In the field of CO_2 reduction, research to improve the photocatalytic performance by predesigning building blocks with functional groups and integrating porphyrins in the skeleton of COFs is indicated. Post-synthetic metalation to import catalytic metal centers in COFs and the combination of COFs with metal oxides and/or MOFs, are ideal for duplicating the photocatalytic activity of CO_2 reduction. In the case of organic transformation, COF-based materials have been widely applied as photocatalysts for diverse organic reactions such as oxidation, reduction, addition, ring-opening polymerization, isomerization, dehalogenation, *etc.* The photocatalytic performance of organic transformation can be enhanced by pre-fixed metal ion in the building blocks. The immobilization of metal ions in the skeleton of COFs by post-synthetic technique, and the fabrication of COF-based composites by coupling COFs with metal sulfides or MOFs, can also improve photocatalytic activity for organic transformance. Investigations on pollution degradation by COF-based photocatalysts have been shown promising results. Up to now, a series of COF-based materials were reported for the degradation of organic dyes, sulfonamides, phenol, norfloxacin and Cr(VI) ion. Among them, COFs with functional groups or metal ions exhibit the enhanced catalytic activity due to the increased charge separation efficiency. Also, metallized COFs and the integration of COFs with metal oxides, metal sulfides, MOFs and g-C_3N_4, *etc.* can promote photocatalytic performance for the degradation of pollutants.

Despite the fact that the dramatic advances have been achieved in the COF-based photocatalysis, a number of challenges are still to be addressed. (1) Most COFs exhibit partial crystallinity, the synthesized COFs with overall structural regularity is a very significant and challenging task for the clarification of the structure-activity relationship. (2) The achievements in the development of 3D COFs for photocatalysis are still poor compared with the 2D analogues. (3) The construction of the thin layer COFs in large size to increase the dispersion of COFs in solvent and accelerate the charge migration, as well as enhance energy transfer and mass transfer in the photocatalytic process remains a challenge. (4) Currently, the majority of products are CO, HCOOH and CH_4 in the photocatalytic CO_2 reduction by COF-based photocatalysts, it is highly desired to obtain hydrocarbons, especially for C_2H_4. (5) The realization of full photocatalytic reactions in the absence of sacrificial agents such as TEOA and TEA, is still in their infancy. In this regard, efforts for the fabrication of COFs with suitable bandgaps to simultaneously drive oxidation and reduction half-reactions in one catalytic system are encouraged. (6) The study for the fundamental mechanism of photocatalytic reaction by COF-based catalysts is insufficient. Some *in situ* characterization technologies such as *in situ* Fourier transform infrared spectroscopy (FTIR), *in situ* electron paramagnetic resonance (EPR), *in situ* X-ray absorption spectroscopy (XPS) and *in situ* extended X-ray absorption fine structure (EXAFS) are highly recommended to monitor reactive intermediates and active sites. (7) Investigations should also be focused on more innovative photocatalytic applications through COF-based materials to further broaden their application scopes. (8) The COF-based photocatalysts with high catalytic activity have to be further developed, which will be beneficial for their practical applications. (9) Although some COF-based photocatalysts exhibit outstanding stabilities under acid and base conditions for several days, explorations on the long-term stability are urgently demanded for them to achieve practical applications. (10) At present, researches in this field are still in the laboratory level, the large-scale applications of COF-based photocatalysts in industrial manufacturing are rarely reported currently. Therefore, it is imperative to optimize synthetic routes and search raw materials with low cost.

In summary, we have detailedly discussed the structural features of COFs including diversity, tailorability, stability and porosity for photocatalysis, as well as the photocatalytic applications of COF-based materials toward H_2 production, CO_2 reduction, organic transformation and pollution degradation. We believe that this review will offer guidance for the fabrication of functional COF-based photocatalysts. It is noteworthy that COFs have shown a rapid development for photocatalytic applications in the past several years. Though many obstacles need to be solved, the challenges and opportunities coexist. With constant research efforts toward the above challenges, we are confident to see a bright future for COF photocatalysis.

Data availability

Data will be made available on request.

Declaration of Competing Interest

The authors declare that they have no known competing financial interests or personal relationships that could have appeared to influence the work reported in this paper.

Acknowledgements

This work was supported by the National Key Research and Development Program of China (2021YFA1500400), the National Natural Science Foundation of China (21725101, 22161142001, 21871244 and 22001043), International Partnership Program of CAS (211134KYSB20190109) and the Fundamental Research Funds for the Central Universities (WK3450000007, WK2060000038, WK2060000041).

References

[1] D. Shindell, C.J. Smith, Nature 573 (2019) 408–411.
[2] F. Green, Nat. Clim. Change 8 (2018) 449–451.
[3] R. Fouquet, Nat. Energy 1 (2016) 16098.
[4] N.S. Lewis, Science 315 (2007) 798–801.
[5] A.J. Carrillo, J. González-Aguilar, M. Romero, J.M. Coronado, Chem. Rev. 119 (2019) 4777–4816.
[6] J.-L. Gong, C. Li, M.R. Wasielewski, Chem. Soc. Rev. 48 (2019) 1862–1864.
[7] P.A. Maggard, Acc. Chem. Res. 54 (2021) 3160–3171.
[8] J.-D. Xiao, H.-L. Jiang, Acc. Chem. Res. 52 (2019) 356–366.
[9] C. Gao, J. Low, R. Long, T. Kong, J. Zhu, Y. Xiong, Chem. Rev. 120 (2020) 12175–12216.
[10] C. Xu, P.R. Anusuyadevi, C. Aymonier, R. Luque, S. Marre, Chem. Soc. Rev. 48 (2019) 3868–3902.
[11] A. Hu, J.-J. Guo, H. Pan, Z. Zuo, Science 361 (2018) 668–672.
[12] D.K. Dogutan, D.G. Nocera, Acc. Chem. Res. 52 (2019) 3143–3148.
[13] S. Ye, C. Ding, R. Chen, F. Fan, P. Fu, H. Yin, X. Wang, Z. Wang, P. Du, C. Li, J. Am. Chem. Soc. 140 (2018) 3250–3256.
[14] H. Liu, C. Xu, D. Li, H.-L. Jiang, Angew. Chem. Int. Ed. 57 (2018) 5379–5383.
[15] L. Lin, Z. Lin, J. Zhang, X. Cai, W. Lin, Z. Yu, X. Wang, Nat. Catal. 3 (2020) 649–655.
[16] A. Fujishima, K. Honda, Nature 238 (1972) 37–38.
[17] L. Yang, Y. Peng, X. Luo, Y. Dan, J. Ye, Y. Zhou, Z. Zou, Chem. Soc. Rev. 50 (2021) 2147–2172.
[18] X. Ren, D. Philo, Y. Li, L. Shi, K. Chang, J. Ye, Coord. Chem. Rev. 424 (2020) 213516.
[19] J. Kou, C. Lu, J. Wang, Y. Chen, Z. Xu, R.S. Varma, Chem. Rev. 117 (2017) 1445–1514.
[20] C. Feng, Z.-P. Wu, K.-W. Huang, J. Ye, H. Zhang, Adv. Mater. 34 (2022) 2200180.
[21] Q. Guo, Z. Ma, C. Zhou, Z. Ren, X. Yang, Chem. Rev. 119 (2019) 11020–11041.

[22] M.D. Regulacio, M.-Y. Han, Acc. Chem. Res. 49 (2016) 511–519.
[23] A. Meng, L. Zhang, B. Cheng, J. Yu, Adv. Mater. 31 (2019) 1807660.
[24] T. Zhang, W. Lin, Chem. Soc. Rev. 43 (2014) 5982–5993.
[25] J. Cao, Z. Yang, W. Xiong, Y. Zhou, Y. Wu, M. Jia, C. Zhou, Z. Xu, Coord. Chem. Rev. 439 (2021) 213924.
[26] H. Wang, H. Wang, Z. Wang, L. Tang, G. Zeng, P. Xu, M. Chen, T. Xiong, C. Zhou, X. Li, D. Huang, Y. Zhu, Z. Wang, J. Tang, Chem. Soc. Rev. 49 (2020) 4135–4165.
[27] C. Xia, K.O. Kirlikovali, T.H.C. Nguyen, X.C. Nguyen, Q.B. Tran, M.K. Duong, M. T.N. Dinh, D.L.T. Nguyen, P. Singh, P. Raizada, V.-H. Nguyen, S.Y. Kim, L. Singh, C.C. Nguyen, M. Shokouhimehr, Q.V. Le, Coord. Chem. Rev. 446 (2021) 214117.
[28] Q. Yin, E.V. Alexandrov, D.-H. Si, Q.-Q. Huang, Z.-B. Fang, Y. Zhang, A.-A. Zhang, W.-K. Qin, Y.-L. Li, T.-F. Liu, D.M. Proserpio, Angew. Chem. Int. Ed. 61 (2022) e202115854.
[29] B. Wang, R.-B. Lin, Z. Zhang, S. Xiang, B. Chen, J. Am. Chem. Soc. 142 (2020) 14399–14416.
[30] Z. Zhang, J. Jia, Y. Zhi, S. Ma, X. Liu, Chem. Soc. Rev. 51 (2022) 2444–2490.
[31] L. Wang, Y. Zhang, L. Chen, H. Xu, Y. Xiong, Adv. Mater. 30 (2018) 1870369.
[32] H.-C. Zhou, S. Kitagawa, Chem. Soc. Rev. 43 (2014) 5415–5418.
[33] L. Jiao, Y. Wang, H.-L. Jiang, Q. Xu, Adv. Mater. 30 (2018) 1703663.
[34] C. Xu, R. Fang, R. Luque, L. Chen, Y. Li, Coord. Chem. Rev. 388 (2019) 268–292.
[35] R.-B. Lin, Y. He, P. Li, H. Wang, W. Zhou, B. Chen, Chem. Soc. Rev. 48 (2019) 1362–1389.
[36] J. Luo, J.-W. Wang, J.-H. Zhang, S. Lai, D.-C. Zhong, CrystEngComm 20 (2018) 5884–5898.
[37] D. Hetemi, J. Pinson, Chem. Soc. Rev. 46 (2017) 5701–5713.
[38] W. Ji, T.-X. Wang, X. Ding, S. Lei, B.-H. Han, Coord. Chem. Rev. 439 (2021) 213875.
[39] P.J. Waller, F. Gandara, O.M. Yaghi, Acc. Chem. Res. 48 (2015) 3053–3063.
[40] X. Feng, X. Ding, D. Jiang, Chem. Soc. Rev. 41 (2012) 6010–6022.
[41] C. Kang, K. Yang, Z. Zhang, A.K. Usadi, D.C. Calabro, L.S. Baugh, Y. Wang, J. Jiang, X. Zou, Z. Huang, D. Zhao, Nat. Commun. 13 (2022) 1370.
[42] A.P. Côté, A.I. Benin, N.W. Ockwig, M. O'Keeffe, A.J. Matzger, O.M. Yaghi, Science 310 (2005) 1166–1170.
[43] R.-R. Liang, S.-Y. Jiang, X. Zhao, Chem. Soc. Rev. 49 (2020) 3920–3951.
[44] B. Gui, G. Lin, H. Ding, C. Gao, A. Mal, C. Wang, Acc. Chem. Res. 53 (2020) 2225–2234.
[45] Z. Wang, S. Zhang, Y. Chen, Z. Zhang, S. Ma, Chem. Soc. Rev. 49 (2020) 708–735.
[46] T. Ma, E.A. Kapustin, S.X. Yin, L. Liang, Z. Zhou, J. Niu, L.H. Li, Y. Wang, J. Su, J. Li, X. Wang, W.D. Wang, W. Wang, J. Sun, O.M. Yaghi, Science 361 (2018) 48–52.
[47] A.M. Evans, L.R. Parent, N.C. Flanders, R.P. Bisbey, E. Vitaku, M.S. Kirschner, R. D. Schaller, L.X. Chen, N.C. Gianneschi, W.R. Dichtel, Science 361 (2018) 52–57.
[48] H.M. El-Kaderi, J.R. Hunt, J.L. Mendoza-Cortés, A.P. Côté, R.E. Taylor, M. O'Keeffe, O.M. Yaghi, Science 316 (2007) 268–272.
[49] E. Jin, M. Asada, Q. Xu, S. Dalapati, M.A. Addicoat, M.A. Brady, H. Xu, T. Nakamura, T. Heine, Q. Chen, D. Jiang, Science 357 (2017) 673–676.
[50] X. Guan, H. Li, Y. Ma, M. Xue, Q. Fang, Y. Yan, V. Valtchev, S. Qiu, Nat. Chem. 11 (2019) 587–594.
[51] A. Acharjya, P. Pachfule, J. Roeser, F.J. Schmitt, A. Thomas, Angew. Chem. Int. Ed. 58 (2019) 14865–14870.
[52] O. Yahiaoui, A.N. Fitch, F. Hoffmann, M. Froba, A. Thomas, J. Roeser, J. Am. Chem. Soc. 140 (2018) 5330–5333.
[53] L. Ascherl, T. Sick, J.T. Margraf, S.H. Lapidus, M. Calik, C. Hettstedt, K. Karaghiosoff, M. Döblinger, T. Clark, K.W. Chapman, F. Auras, T. Bein, Nat. Chem. 8 (2016) 310–316.
[54] X. Liu, D. Huang, C. Lai, G. Zeng, L. Qin, H. Wang, H. Yi, B. Li, S. Liu, M. Zhang, R. Deng, Y. Fu, L. Li, W. Xue, S. Chen, Chem. Soc. Rev. 48 (2019) 5266–5302.
[55] L. Zhang, Q.-C. Yang, S. Wang, Y. Xiao, S.-C. Wan, H. Deng, Z.-J. Sun, Adv. Mater. 34 (2022) 2108174.
[56] I. Ahmed, S.H. Jhung, Coord. Chem. Rev. 441 (2021) 213989.
[57] S. Liu, T. Qian, M. Wang, H. Ji, X. Shen, C. Wang, C. Yan, Nat. Catal. 4 (2021) 322–331.
[58] X. Wang, L. Sun, W. Zhou, L. Yang, G. Ren, H. Wu, W.Q. Deng, Cell Rep. Phys. Sci. 3 (2022) 100804.
[59] C.J. Doonan, D.J. Tranchemontagne, T.G. Glover, J.R. Hunt, O.M. Yaghi, Nat. Chem. 2 (2010) 235–238.
[60] X. Ren, C. Li, J. Liu, H. Li, L. Bing, S. Bai, G. Xue, Y. Shen, Q. Yang, ACS Appl. Mater. Interfaces 14 (2022) 6885–6893.
[61] Y. Zeng, R. Zou, Y. Zhao, Adv. Mater. 28 (2016) 2855–2873.
[62] M. Traxler, S. Gisbertz, P. Pachfule, J. Schmidt, J. Roeser, S. Reischauer, J. Rabeah, B. Pieber, A. Thomas, Angew. Chem. Int. Ed. 61 (2022) e202117738.
[63] B.Q. Li, S.Y. Zhang, B. Wang, Z.J. Xia, C. Tang, Q. Zhang, Energy Environ. Sci. 11 (2018) 1723–1729.
[64] R.K. Sharma, P. Yadav, M. Yadav, R. Gupta, P. Rana, A. Srivastava, R. Zbořil, R.S. Varma, M. Antonietti, M.B. Gawande, Mater. Horiz. 7 (2020) 411–454.
[65] S. Bhunia, S.K. Das, R. Jana, S.C. Peter, S. Bhattacharya, M. Addicoat, A. Bhaumik, A. Pradhan, ACS Appl. Mater. Interfaces 9 (2017) 23843–23851.
[66] P. Yadav, M. Yadav, R. Gaur, R. Gupta, G. Arora, A. Srivastava, A. Goswami, M.B. Gawande, R.K. Sharma, Mater. Adv. 3 (2022) 1432–1458.
[67] X. Zhao, P. Pachfule, S. Li, T. Langenhahn, M. Ye, C. Schlesiger, S. Praetz, J. Schmidt, A. Thomas, J. Am. Chem. Soc. 141 (2019) 6623–6630.
[68] H. Xu, J. Gao, D. Jiang, Nat. Chem. 7 (2015) 905–912.
[69] H. Xu, S. Tao, D. Jiang, Nat. Mater. 15 (2016) 722–727.
[70] C. Li, J. Yang, P. Pachfule, S. Li, M.Y. Ye, J. Schmidt, A. Thomas, Nat. Commun. 11 (2020) 4712.
[71] W. Zhang, L. Chen, S. Dai, C. Zhao, C. Ma, L. Wei, M. Zhu, S.Y. Chong, H. Yang, L. Liu, Y. Bai, M. Yu, Y. Xu, X.W. Zhu, Q. Zhu, S. An, R.S. Sprick, M.A. Little, X. Wu, S. Jiang, Y. Wu, Y.B. Zhang, H. Tian, W.H. Zhu, A.I. Cooper, Nature 604 (2022) 72–79.
[72] Y. Zhang, J. Guo, G. Han, Y. Bai, Q. Ge, J. Ma, C.H. Lau, L. Shao, Sci. Adv. 7 (2021) eabe8706.
[73] W. Huang, W. Luo, Y. Li, Mater. Today 40 (2020) 160–172.
[74] Q. Yang, M. Luo, K. Liu, H. Cao, H. Yan, Appl. Catal. B Environ. 276 (2020) 119174.
[75] G.-B. Wang, S. Li, C.-X. Yan, F.-C. Zhu, Q.-Q. Lin, K.-H. Xie, Y. Geng, Y.-B. Dong, J. Mater. Chem. A 8 (2020) 6957–6983.
[76] X. Wang, L. Chen, S.Y. Chong, M.A. Little, Y. Wu, W.-H. Zhu, R. Clowes, Y. Yan, M.A. Zwijnenburg, R.S. Sprick, A.I. Cooper, Nat. Chem. 10 (2018) 1180–1189.
[77] S. Xu, M. Richter, X. Feng, Acc. Mater. Res. 2 (2021) 252–265.
[78] J. Xie, S.A. Shevlin, Q. Ruan, S.J.A. Moniz, Y. Liu, X. Liu, Y. Li, C.C. Lau, Z.X. Guo, J. Tang, Energy Environ. Sci. 11 (2018) 1617–1624.
[79] S. Wan, J. Guo, J. Kim, H. Ihee, D. Jiang, Angew. Chem. Int. Ed. 47 (2008) 8826–8830.
[80] L. Stegbauer, K. Schwinghammer, B.V. Lotsch, Chem. Sci. 5 (2014) 2789–2793.
[81] H.L. Nguyen, A. Alzamly, ACS Catal. 11 (2021) 9809–9824.
[82] W. Liu, X. Li, C. Wang, H. Pan, W. Liu, K. Wang, Q. Zeng, R. Wang, J. Jiang, J. Am. Chem. Soc. 141 (2019) 17431–17440.
[83] X. Kan, J.-C. Wang, Z. Chen, J.-Q. Du, J.-L. Kan, W.-Y. Li, Y.-B. Dong, J. Am. Chem. Soc. 144 (2022) 6681–6686.
[84] P.-F. Wei, M.-Z. Qi, Z.-P. Wang, S.-Y. Ding, W. Yu, Q. Liu, L.-K. Wang, H.-Z. Wang, W.-K. An, W. Wang, J. Am. Chem. Soc. 140 (2018) 4623–4631.
[85] S. Ma, Z. Li, J. Jia, Z. Zhang, H. Xia, H. Li, X. Chen, Y. Xu, X. Liu, Chin. J. Catal. 42 (2021) 2010–2019.
[86] Y.H. Kim, N. Kim, J.-M. Seo, J.-P. Jeon, H.-J. Noh, D.H. Kweon, J. Ryu, J.-B. Baek, Chem. Mater. 33 (2021) 8705–8711.
[87] M. Tian, Y. Wang, X. Bu, Y. Wang, X. Yang, Catal. Sci. Technol. 11 (2021) 4272–4279.
[88] H. Li, L. Wang, G. Yu, Nano Today 40 (2021) 101247.
[89] Z. Qian, Z.J. Wang, K.A.I. Zhang, Chem. Mater. 33 (2021) 1909–1926.
[90] T. Banerjee, K. Gottschling, G. Savasci, C. Ochsenfeld, B.V. Lotsch, ACS Energy Lett. 3 (2018) 400–409.
[91] Y. Zhi, Z. Wang, H.-L. Zhang, Q. Zhang, Small 16 (2020) 2001070.
[92] H. Lin, C. Chen, T. Zhou, J. Zhang, Sol. RRL 5 (2021) 2000458.
[93] L. Guo, L. Yang, M. Li, L. Kuang, Y. Song, L. Wang, Coord. Chem. Rev. 440 (2021) 213957.
[94] S. Lin, C.S. Diercks, Y.B. Zhang, N. Kornienko, E.M. Nichols, Y. Zhao, A.R. Paris, D. Kim, P. Yang, O.M. Yaghi, C.J. Chang, Science 349 (2015) 1208–1213.
[95] X. Feng, L. Chen, Y. Dong, D. Jiang, Chem. Commun. 47 (2011) 1979–1981.
[96] J.W. Colson, A.R. Woll, A. Mukherjee, M.P. Levendorf, E.L. Spitler, V.B. Shields, M.G. Spencer, J. Park, W.R. Dichtel, Science 332 (2011) 228–231.
[97] N.L. Campbell, R. Clowes, L.K. Ritchie, A.I. Cooper, Chem. Mater. 21 (2009) 204–206.
[98] H. Wei, S. Chai, N. Hu, Z. Yang, L. Wei, L. Wang, Chem. Commun. 51 (2015) 12178–12181.
[99] P. Kuhn, M. Antonietti, A. Thomas, Angew. Chem. Int. Ed. 47 (2008) 3450–3453.
[100] S. Kuecken, J. Schmidt, L. Zhi, A. Thomas, J. Mater. Chem. A 3 (2015) 24422–24427.
[101] X. Guan, Y. Ma, H. Li, Y. Yusran, M. Xue, Q. Fang, Y. Yan, V. Valtchev, S. Qiu, J. Am. Chem. Soc. 140 (2018) 4494–4498.
[102] A.P. Ruigómez, D. Rodríguez-San-Miguel, K.C. Stylianou, M. Cavallini, D. Gentili, F. Liscio, S. Milita, O.M. Roscioni, M.L. Ruiz-González, C. Carbonell, D. Maspoch, R. Mas-Ballesté, J.L. Segura, F. Zamora, Chem. Eur. J. 21 (2015) 10666–10670.
[103] C.X. Yang, C. Liu, Y.M. Cao, X.P. Yan, Chem. Commun. 51 (2015) 12254–12257.
[104] M. Matsumoto, R.R. Dasari, W. Ji, C.H. Feriante, T.C. Parker, S.R. Marder, W.R. Dichtel, J. Am. Chem. Soc. 139 (2017) 4999–5002.
[105] B.P. Biswal, S. Chandra, S. Kandambeth, B. Lukose, T. Heine, R. Banerjee, J. Am. Chem. Soc. 135 (2013) 5328–5331.
[106] Y. Peng, G. Xu, Z. Hu, Y. Cheng, C. Chi, D. Yuan, H. Cheng, D. Zhao, ACS Appl. Mater. Interfaces 8 (2016) 18505–18512.
[107] D.B. Shinde, H.B. Aiyappa, M. Bhadra, B.P. Biswal, P. Wadge, S. Kandambeth, B. Garai, T. Kundu, S. Kurungot, R. Banerjee, J. Mater. Chem. A 4 (2016) 2682–2690.
[108] K. Dey, M. Pal, K.C. Rout, S. Kunjattu, A. Das, R. Mukherjee, U.K. Kharul, R. Banerjee, J. Am. Chem. Soc. 139 (2017) 13083–13091.
[109] Q. Hao, C. Zhao, B. Sun, C. Lu, J. Liu, M.J. Liu, L.J. Wan, D. Wang, J. Am. Chem. Soc. 140 (2018) 12152–12158.
[110] M. Matsumoto, L. Valentino, G.M. Stiehl, H.B. Balch, A.R. Corcos, F. Wang, D.C. Ralph, B.J. Mariñas, W.R. Dichtel, Chem 4 (2018) 308–317.
[111] J.I. Feldblyum, C.H. McCreery, S.C. Andrews, T. Kurosawa, E.J.G. Santos, V. Duong, L. Fang, A.L. Ayzner, Z. Bao, Chem. Commun. 51 (2015) 13894–13897.
[112] W. Dai, F. Shao, J. Szczerbiński, R. McCaffrey, R. Zenobi, Y. Jin, A.D. Schlîter, W. Zhang, Angew. Chem. Int. Ed. 55 (2016) 213–217.
[113] Y. Li, W. Chen, G. Xing, D. Jiang, L. Chen, Chem. Soc. Rev. 49 (2020) 2852–2868.
[114] Z. Li, T. He, Y. Gong, D. Jiang, Acc. Chem. Res. 53 (2020) 1672–1685.
[115] H. Lyu, Z. Ji, S. Wuttke, O.M. Yaghi, Chem 6 (2020) 2219–2241.

[116] N. Huang, L. Zhai, D.E. Coupry, M.A. Addicoat, K. Okushita, K. Nishimura, T. Heine, D. Jiang, Nat. Commun. 7 (2016) 12325.
[117] Z. Li, L. Sheng, C. Hsueh, X. Wang, H. Cui, H. Gao, Y. Wu, J. Wang, Y. Tang, H. Xu, X. He, Chem. Mater. 33 (2021) 9618–9623.
[118] J. Dong, L. Liu, C. Tan, Q. Xu, J. Zhang, Z. Qiao, D. Chu, Y. Liu, Q. Zhang, J. Jiang, Y. Han, A.P. Davis, Y. Cui, Nature 602 (2022) 606–611.
[119] W. Wang, W. Zhao, H. Xu, S. Liu, W. Huang, Q. Zhao, Coord. Chem. Rev. 429 (2021) 213616.
[120] H. Duan, K. Li, M. Xie, J.-M. Chen, H.-G. Zhou, X. Wu, G.-H. Ning, A.I. Cooper, D. Li, J. Am. Chem. Soc. 143 (2021) 19446–19453.
[121] Y. Peng, Y. Huang, Y. Zhu, B. Chen, L. Wang, Z. Lai, Z. Zhang, M. Zhao, C. Tan, N. Yang, F. Shao, Y. Han, H. Zhang, J. Am. Chem. Soc. 139 (2017) 8698–8704.
[122] K. Geng, T. He, R. Liu, S. Dalapati, K.T. Tan, Z. Li, S. Tao, Y. Gong, Q. Jiang, D. Jiang, Chem. Rev. 120 (2020) 8814–8933.
[123] X. Li, P. Yadav, K.P. Loh, Chem. Soc. Rev. 49 (2020) 4835–4866.
[124] S. Zhao, C. Jiang, J. Fan, S. Hong, P. Mei, R. Yao, Y. Liu, S. Zhang, H. Li, H. Zhang, C. Sun, Z. Guo, P. Shao, Y. Zhu, J. Zhang, L. Guo, Y. Ma, J. Zhang, X. Feng, F. Wang, H. Wu, B. Wang, Nat. Mater. 20 (2021) 1551–1558.
[125] C. Kang, Z. Zhang, V. Wee, A.K. Usadi, D.C. Calabro, L.S. Baugh, S. Wang, Y. Wang, D. Zhao, J. Am. Chem. Soc. 142 (2020) 12995–13002.
[126] X. Zhao, P. Pachfule, A. Thomas, Chem. Soc. Rev. 50 (2021) 6871–6913.
[127] Z. Meng, K.A. Mirica, Chem. Soc. Rev. 50 (2021) 13498–13558.
[128] C. Kang, Z. Zhang, A.K. Usadi, D.C. Calabro, L.S. Baugh, K. Yu, Y. Wang, D. Zhao, J. Am. Chem. Soc. 144 (2022) 3192–3199.
[129] K. Wang, D. Qi, Y. Li, T. Wang, H. Liu, J. Jiang, Coord. Chem. Rev. 378 (2019) 188–206.
[130] Z.-C. Guo, Z.-Q. Shi, X.-Y. Wang, Z.-F. Li, G. Li, Coord. Chem. Rev. 422 (2020) 213465.
[131] S.-Y. Ding, W. Wang, Chem. Soc. Rev. 42 (2013) 548–568.
[132] V.S. Vyas, F. Haase, L. Stegbauer, G. Savasci, F. Podjaski, C. Ochsenfeld, B.V. Lotsch, Nat. Commun. 6 (2015) 8508.
[133] J.L. Segura, S. Royuela, M.M. Ramos, Chem. Soc. Rev. 48 (2019) 3903–3945.
[134] Z. Fu, X. Wang, A.M. Gardner, X. Wang, S.Y. Chong, G. Neri, A.J. Cowan, L. Liu, X. Li, A. Vogel, R. Clowes, M. Bilton, L. Chen, Chem. Sci. 11 (2020) 543–550.
[135] Y. Xiang, W. Dong, P. Wang, S. Wang, X. Ding, F. Ichihara, Z. Wang, Y. Wada, S. Jin, Y. Weng, H. Chen, J. Ye, Appl. Catal. B Environ. 274 (2020) 119096.
[136] G. Kumar, R.S. Pillai, N.H. Khan, Appl. Catal. B Environ. 292 (2021) 120149.
[137] A. Nagai1, Z. Guo, X. Feng, S. Jin, X. Chen, X. Ding, D. Jiang, Nat. Commun. 2 (2011) 536.
[138] L. Merí-Bofí, S. Poyuela, F. Zamora, M.L. Ruiz-González, J.L. Segura, R. Muñoz-Olivas, M.J. Mancheño, J. Mater. Chem. A 5 (2017) 17973–17981.
[139] P.J. Waller, S.J. Lyle, T.M.O. Popp, C.S. Diercks, J.A. Reimer, O.M. Yaghi, J. Am. Chem. Soc. 138 (2016) 15519–15522.
[140] H. Liu, J. Chu, Z. Yin, X. Cai, L. Zhuang, H. Deng, Chem 4 (2018) 1696–1709.
[141] Q. Fang, S. Gu, J. Zheng, Z. Zhuang, S. Qiu, Y. Yan, Angew. Chem. Int. Ed. 126 (2014) 2922–2926.
[142] S. Karak, S. Kandambeth, B.P. Biswal, H.S. Sasmal, S. Kumar, P. Pachfule, R. Banerjee, J. Am. Chem. Soc. 139 (2017) 1856–1862.
[143] B. Zhang, M. Wei, H. Mao, X. Pei, S.A. Alshmimri, J.A. Reimer, O.M. Yaghi, J. Am. Chem. Soc. 140 (2018) 12715–12719.
[144] X. Huang, C. Sun, X. Feng, Sci. China Chem. 63 (2020) 1367–1390.
[145] Y. Yusran, X. Guan, H. Li, Q. Fang, S. Qiu, Nat. Sci. Rev. 7 (2019) 170–190.
[146] S. Kandambeth, D.B. Shinde, M.K. Panda, B. Lukose, T. Heine, R. Banerjee, Angew. Chem. Int. Ed. 52 (2013) 13052–13056.
[147] S. Dalapati, S. Jin, J. Gao, Y. Xu, A. Nagai, D. Jiang, J. Am. Chem. Soc. 135 (2013) 17310–17313.
[148] F.J. Uribe-Romo, J.R. Hunt, H. Furukawa, C. Klöck, M. O'Keeffe, O.M. Yaghi, J. Am. Chem. Soc. 131 (2009) 4570–4571.
[149] M.A. Khayum, S. Kandambeth, S. Mitra, S.B. Nair, A. Das, S.S. Nagane, R. Mukherjee, R. Banerjee, Angew. Chem. Int. Ed. 55 (2016) 15604–15608.
[150] S. Chandra, S. Kandambeth, B.P. Biswal, B. Lukose, S.M. Kunjir, M. Chaudhary, R. Babarao, T. Heine, R. Banerjee, J. Am. Chem. Soc. 135 (2013) 17853–17861.
[151] X. Wu, X. Han, Y. Liu, Y. Liu, Y. Cui, J. Am. Chem. Soc. 140 (2018) 16124–16133.
[152] A. Halder, S. Karak, M. Addicoat, S. Bera, A. Chakraborty, S.H. Kunjattu, P. Pachfule, T. Heine, R. Banerjee, Angew. Chem. Int. Ed. 57 (2018) 5797–5802.
[153] A. Halder, M. Ghosh, S. Bera, M. Addicoat, H.S. Sasmal, S. Karak, S. Kurungot, R. Banerjee, J. Am. Chem. Soc. 140 (2018) 10941–10945.
[154] F. Haase, E. Troschke, G. Savasci, T. Banerjee, V. Duppel, S. Dörfler, M.M.J. Grundei, A.M. Burow, C. Ochsenfeld, S. Kaskel, B.V. Lotsch, Nat. Commun. 9 (2018) 2600.
[155] X. Li, C. Zhang, S. Cai, X. Lei, V. Altoe, F. Hong, J.J. Urban, J. Ciston, E.M. Chan, Y. Liu, Nat. Commun. 9 (2018) 2998.
[156] C. Gao, J. Li, S. Yin, G. Lin, T. Ma, Y. Meng, J. Sun, C. Wang, Angew. Chem. Int. Ed. 58 (2019) 9770–9775.
[157] Z. Mu, Y. Zhu, B. Li, A. Dong, B. Wang, X. Feng, J. Am. Chem. Soc. 144 (2022) 5145–5154.
[158] P. Zhang, Z. Wang, P. Cheng, Y. Chen, Z. Zhang, Coord. Chem. Rev. 438 (2021) 213873.
[159] S.B. Alahakoon, S.D. Diwakara, C.M. Thompson, R.A. Smaldone, Chem. Soc. Rev. 49 (2020) 1344–1356.
[160] X. Guan, F. Chen, Q. Fang, S. Qiu, Chem. Soc. Rev. 49 (2020) 1357–1384.
[161] E.L. Spitler, B.T. Koo, J.L. Novotney, J.W. Colson, F.J. Uribe-Romo, G.D. Gutierrez, P. Clancy, W.R. Dichtel, J. Am. Chem. Soc. 133 (2011) 19416–19421.
[162] R.W. Tilford, S.J. Mugavero III, P.J. Pellechia, J.J. Lavigne, Adv. Mater. 20 (2008) 2741–2746.
[163] X. Ding, L. Chen, Y. Honsho, X. Feng, O. Saengsawang, J. Guo, A. Saeki, S. Seki, S. Irle, S. Nagase, V. Parasuk, D. Jiang, J. Am. Chem. Soc. 133 (2011) 14510–14513.
[164] W. Chen, L. Wang, D. Mo, F. He, Z. Wen, X. Wu, H. Xu, L. Chen, Angew. Chem. Int. Ed. 59 (2020) 16902–16909.
[165] Y.-R. Wang, H.-M. Ding, X.-Y. Ma, M. Liu, Y.-L. Yang, Y. Chen, S.-L. Li, Y.-Q. Lan, Angew. Chem. Int. Ed. 61 (2022) e202114648.
[166] D. Li, M. Kassymova, X. Cai, S.-Q. Zang, H.-L. Jiang, Coord. Chem. Rev. 412 (2020) 213262.
[167] Y. Liu, Z. Liu, D. Huang, M. Cheng, G. Zeng, C. Lai, C. Zhang, C. Zhou, W. Wang, D. Jiang, H. Wang, B. Shao, Coord. Chem. Rev. 388 (2019) 63–78.
[168] M. Xiao, Z. Wang, M. Lyu, B. Luo, S. Wang, G. Liu, H.-M. Cheng, L. Wang, Adv. Mater. 31 (2019) 1801369.
[169] Y. Fang, Y. Ma, M. Zheng, P. Yang, A.M. Asiri, X. Wang, Coord. Chem. Rev. 373 (2018) 83–115.
[170] Y.-Z. Chen, Z.U. Wang, H. Wang, J. Lu, S.-H. Yu, H.-L. Jiang, J. Am. Chem. Soc. 139 (2017) 2035–2044.
[171] H.-Q. Xu, J. Hu, D. Wang, Z. Li, Q. Zhang, Y. Luo, S.-H. Yu, H.-L. Jiang, J. Am. Chem. Soc. 137 (2015) 13440–13443.
[172] Z. Guo, G. Chen, C. Cometto, B. Ma, H. Zhao, T. Groizard, L. Chen, H. Fan, W.-L. Man, S.-M. Yiu, K.-C. Lau, T.-C. Lau, M. Robert, Nat. Catal. 2 (2019) 801–808.
[173] Y.-N. Gong, J.-H. Mei, J.-W. Liu, H.-H. Huang, J.-H. Zhang, X. Li, D.-C. Zhong, T.-B. Lu, Appl. Catal. B Environ. 292 (2021) 120156.
[174] W.R. McNamara, Z. Han, P.J. Alperin, W.W. Brennessel, P.L. Holland, R. Eisenberg, J. Am. Chem. Soc. 133 (2011) 15368–15371.
[175] J. Lin, X. Liang, X. Cao, N. Wei, Y. Ding, Chem. Commun. 54 (2018) 12515–12518.
[176] D. Wang, H. Jiang, X. Zong, Q. Xu, Y. Ma, G. Li, C. Li, Chem. Eur. J. 17 (2011) 1275–1282.
[177] R. Li, H. Han, F. Zhang, D. Wang, C. Li, Energy Environ. Sci. 7 (2014) 1369–1376.
[178] M.J. Limo, A. Sola-Rabada, E. Boix, V. Thota, Z.C. Westcott, V. Puddu, C.C. Perry, Chem. Rev. 118 (2018) 11118–11193.
[179] G. Cai, P. Yan, L. Zhang, H.-C. Zhou, H.-L. Jiang, Chem. Rev. 121 (2021) 12278–12326.
[180] D.-H. Yang, Y. Tao, X. Ding, B.-H. Han, Chem. Soc. Rev. 51 (2022) 761–791.
[181] S. Wang, Q. Sun, W. Chen, Y. Tang, B. Aguila, Y. Pan, A. Zheng, Z. Yang, L. Wojtas, S. Ma, F.-S. Xiao, Matter 2 (2020) 416–427.
[182] S. Yang, H. Lv, H. Zhong, D. Yuan, X. Wang, R. Wang, Angew. Chem. Int. Ed. 61 (2022) e202115655.
[183] S.-Y. Hu, Y.-N. Sun, Z.-W. Feng, F.-O. Wang, Y.-K. Lv, Chemosphere 286 (2022) 131646.
[184] G. Lin, H. Ding, R. Chen, Z. Peng, B. Wang, C. Wang, J. Am. Chem. Soc. 139 (2017) 8705–8709.
[185] Y.-N. Gong, W. Zhong, Y. Li, Y. Qiu, L. Zheng, J. Jiang, H.-L. Jiang, J. Am. Chem. Soc. 142 (2020) 16723–16731.
[186] M. Lu, J. Liu, Q. Li, M. Zhang, M. Liu, J.-L. Wang, D.-Q. Yuan, Y.-Q. Lan, Angew. Chem. Int. Ed. 58 (2019) 12392–12397.
[187] N. Singh, D. Yadav, S.V. Mulay, J.Y. Kim, N.-J. Park, J.-O. Baeg, ACS Appl. Mater. Interfaces 13 (2021) 14122–14131.
[188] C. Liu, Y. Xiao, Q. Yang, Y. Wang, R. Lu, Y. Chen, C. Wang, H. Yan, Appl. Surf. Sci. 537 (2021) 148082.
[189] L. Yin, Y. Zhao, Y. Xing, H. Tan, Z. Lang, W. Ho, Y. Wang, Y. Li, Chem. Eng. J. 419 (2021) 129984.
[190] S. Yang, W. Hu, X. Zhang, P. He, B. Pattengale, C. Liu, M. Cendejas, I. Hermans, X. Zhang, J. Zhang, J. Huang, J. Am. Chem. Soc. 140 (2018) 14614–14618.
[191] P. Dong, Y. Wang, A. Zhang, T. Cheng, X. Xi, J. Zhang, ACS Catal. 11 (2021) 13266–13279.
[192] S. Ghosh, A. Nakada, M.A. Springer, T. Kawaguchi, K. Suzuki, H. Kaji, I. Baburin, A. Kuc, T. Heine, H. Suzuki, R. Abe, S. Seki, J. Am. Chem. Soc. 142 (2020) 9752–9762.
[193] M. Zhang, M. Lu, Z.-L. Lang, J. Liu, M. Liu, J.-N. Chang, L.-Y. Li, L.-J. Shang, M. Wang, S.-L. Li, Y.-Q. Lan, Angew. Chem. Int. Ed. 59 (2020) 6500–6506.
[194] Y.-J. Yuan, Z.-T. Yu, D.-Q. Chen, Z.-G. Zou, Chem. Soc. Rev. 46 (2017) 603–631.
[195] J. Qi, W. Zhang, R. Cao, Adv. Energy Mater. 8 (2018) 1701620.
[196] Q. Wang, K. Domen, Chem. Rev. 120 (2020) 919–985.
[197] Y. Shi, A.-F. Yang, C.-S. Cao, B. Zhao, Coord. Chem. Rev. 390 (2019) 50–75.
[198] S. Wei, F. Zhang, W. Zhang, P. Qiang, K. Yu, X. Fu, D. Wu, S. Bi, F. Zhang, J. Am. Chem. Soc. 141 (2019) 14272–14279.
[199] J. Yang, A. Acharjya, M.-Y. Ye, J. Rabeah, S. Li, Z. Kochovski, S. Youk, J. Roeser, J. Grgneberg, C. Penschke, M. Schwarze, T. Wang, Y. Lu, R. Krol, M. Oschatz, R. Schom-cker, P. Saalfrank, A. Thomas, Angew. Chem. Int. Ed. 60 (2021) 19797–19803.
[200] P. Pachfule, A. Acharjya, J. Roeser, T. Langenhahn, M. Schwarze, R. Schomäcker, A. Thomas, J. Schmidt, J. Am. Chem. Soc. 140 (2018) 1423–1427.
[201] K. Wang, Z. Jia, Y. Bai, X. Wang, S.E. Hodgkiss, L. Chen, S.Y. Chong, X. Wang, H. Yang, Y. Xu, F. Feng, J.W. Ward, A.I. Cooper, J. Am. Chem. Soc. 142 (2020) 11131–11138.
[202] Y. Wan, L. Wang, H. Xu, X. Wu, J. Yang, J. Am. Chem. Soc. 142 (2020) 4508–4516.
[203] Z. Mi, T. Zhou, W. Weng, J. Unruangsri, K. Hu, W. Yang, C. Wang, K.A.I. Zhang, J. Guo, Angew. Chem. Int. Ed. 60 (2021) 9642–9649.
[204] J. Xu, C. Yang, S. Bi, W. Wang, Y. He, D. Wu, Q. Liang, X. Wang, F. Zhang, Angew. Chem. Int. Ed. 59 (2020) 23845–23853.

[205] J. Chen, X. Tao, C. Li, Y. Ma, L. Tao, D. Zheng, J. Zhu, H. Li, R. Li, Q. Yang, Appl. Catal. B Environ. 262 (2020) 118271.
[206] L. Wang, L. Zhang, B. Lin, Y. Zheng, J. Chen, Y. Zheng, B. Gao, J. Long, Y. Chen, L. Wang, L. Zhang, B. Lin, Y. Zheng, J. Chen, Y. Zheng, B. Gao, J. Long, Y. Chen, Small 17 (2021) 2101017.
[207] S. Li, M.-F. Wu, T. Guo, L.-L. Zheng, D. Wang, Y. Mu, Q.-J. Xing, J.-P. Zou, Appl. Catal. B Environ. 272 (2020) 118989.
[208] G.-B. Wang, F.-C. Zhu, Q.-Q. Lin, J.-L. Kan, K.-H. Xie, S. Li, Y. Geng, Y.-B. Dong, Chem. Commun. 57 (2021) 4464–4467.
[209] W. Li, X. Huang, T. Zeng, Y.A. Liu, W. Hu, H. Yang, Y.-B. Zhang, K. Wen, Angew. Chem. Int. Ed. 60 (2021) 1869–1874.
[210] R. Chen, Y. Wang, Y. Ma, A. Ma, X.-Y. Gao, L. Gao, L. Qiao, X.-B. Li, L.-Z. Wu, C. Wang, Nat. Commun. 12 (2021) 1354.
[211] L. Guo, Y. Niu, H. Xu, Q. Li, S. Razzaque, Q. Huang, S. Jin, B. Tan, J. Mater. Chem. A 6 (2018) 19775–19781.
[212] C. Li, J. Liu, H. Li, K. Wu, J. Wang, Q. Yang, Nat. Commun. 13 (2022) 2357.
[213] J.-L. Sheng, H. Dong, X.-B. Meng, H.-L. Tang, Y.-H. Yao, D.Q. Liu, L.-L. Bai, F.-M. Zhang, J.-Z. Wei, X.-J. Sun, ChemCatChem 11 (2019) 2313–2319.
[214] C. Lin, X. Liu, B. Yu, C. Han, L. Gong, C. Wang, Y. Gao, Y. Bian, J. Jiang, ACS Appl. Mater. Interfaces 13 (2021) 27041–27048.
[215] C. Mo, M. Yang, F. Sun, J. Jian, L. Zhong, Z. Fang, J. Feng, D. Yu, Adv. Sci. 7 (2020) 1902988.
[216] H. Wang, C. Qian, J. Liu, Y. Zeng, D. Wang, W. Zhou, L. Gu, H. Wu, G. Liu, Y. Zhao, J. Am. Chem. Soc. 142 (2020) 4862–4871.
[217] C. Wang, H. Zhang, W. Luo, T. Sun, Y. Xu, Angew. Chem. Int. Ed. 60 (2021) 25381–25390.
[218] Z. Fan, K. Nomura, M. Zhu, X. Li, J. Xue, T. Majima, Y. Osakada, Commun. Chem. 2 (2019) 55.
[219] Y. Zang, R. Wang, P.-P. Shao, X. Feng, S. Wang, S.-Q. Zang, T.C.W. Mak, J. Mater. Chem. A 8 (2020) 25094–25100.
[220] G. Liu, G. Pan, Q. Dang, R. Li, L. Li, C. Yang, Y. Yu, ChemCatChem 14 (2022) e202101800.
[221] Y. Li, M. Karimi, Y.-N. Gong, N. Dai, V. Safarifard, H.-L. Jiang, Matter 4 (2021) 2230–2265.
[222] T. Zhou, L. Wang, X. Huang, J. Unruangsri, H. Zhang, R. Wang, Q. Song, Q. Yang, W. Li, C. Wang, K. Takahashi, H. Xu, J. Guo, Nat. Commun. 12 (2021) 3934.
[223] X. Ren, C. Li, W. Kang, H. Li, N. Ta, S. Ye, L. Hu, X. Wang, C. Li, Q. Yang, CCS Chem. 3 (2021) 2453–2463.
[224] F. Li, D. Wang, Q.-J. Xing, G. Zhou, S.-S. Liu, Y. Li, L.-L. Zheng, P. Ye, J.-P. Zou, Appl. Catal. B Environ. 243 (2019) 621–628.
[225] C.-C. Li, M.-Y. Gao, X.-J. Sun, H.-L. Tang, H. Dong, F.-M. Zhang, Appl. Catal. B Environ. 266 (2020) 118565.
[226] D. Shang, D. Li, B. Chen, B. Luo, Y. Huang, W. Shi, ACS Sustainable Chem. Eng. 9 (2021) 14238–14248.
[227] F.-M. Zhang, J.-L. Sheng, Z.-D. Yang, X.-J. Sun, H.-L. Tang, M. Lu, H. Dong, F.-C. Shen, J. Liu, Y.-Q. Lan, Angew. Chem. Int. Ed. 57 (2018) 12106–12110.
[228] C.-X. Chen, Y.-Y. Xiong, X. Zhong, P.C. Lan, Z.-W. Wei, H. Pan, P.-Y. Su, Y. Song, Y.-F. Chen, A. Nafady, S. Uddin, S. Ma, Angew. Chem. Int. Ed. 61 (2022) e202114071.
[229] C. Lin, C. Han, L. Gong, X. Chen, J. Deng, D. Qi, Y. Bian, K. Wang, J. Jiang, Catal. Sci. Technol. 11 (2021) 2616–2621.
[230] N. Xu, Y. Liu, W. Yang, J. Tang, B. Cai, Q. Li, J. Sun, K. Wang, B. Xu, Q. Zhang, Y. Fan, ACS Appl. Energy Mater. 3 (2020) (1946) 11939–111931.
[231] C.L. Quéré, G.P. Peters, P. Friedlingstein, R.M. Andrew, J.G. Canadell, S.J. Davis, R.B. Jackson, M.W. Jones, Nat. Clim. Change 11 (2021) 197–199.
[232] K.R. Gurney, Y. Song, J. Liang, G. Roest, Environ. Sci. Technol. 54 (2020) 9896–9907.
[233] T. Kong, Y. Jiang, Y. Xiong, Chem. Soc. Rev. 49 (2020) 6579–6591.
[234] C.I. Ezugwu, S. Liu, C. Li, S. Zhuiykov, S. Roy, F. Verpoort, Coord. Chem. Rev. 450 (2022) 214245.
[235] J. Ran, M. Jaroniec, S.-Z. Qiao, Adv. Mater. 30 (2018) 1704649.
[236] Z. Jiang, X. Xu, Y. Ma, H.S. Cho, D. Ding, C. Wang, J. Wu, P. Oleynikov, M. Jia, J. Cheng, Y. Zhou, O. Terasaki, T. Peng, L. Zan, H. Deng, Nature 586 (2020) 549–554.
[237] Y. Fu, X. Zhu, L. Huang, X. Zhang, F. Zhang, W. Zhu, Appl. Catal. B Environ. 239 (2018) 46–51.
[238] L. Peng, S. Chang, Z. Liu, Y. Fu, R. Ma, X. Lu, F. Zhang, W. Zhu, L. Kong, M. Fan, Catal. Sci. Technol. 11 (2021) 1717–1724.
[239] W. Zhong, R. Sa, L. Li, Y. He, L. Li, J. Bi, Z. Zhuang, Y. Yu, Z. Zou, J. Am. Chem. Soc. 141 (2019) 7615–7621.
[240] S.-Y. Li, S. Meng, X. Zou, M. El-Roz, I. Telegeev, O. Thili, T.X. Liu, G. Zhu, Micropor. Mesopor. Mat. 285 (2019) 195–201.
[241] M. Lu, Q. Li, J. Liu, F.-M. Zhang, L. Zhang, J.-L. Wang, Z.-H. Kang, Y.-Q. Lan, Appl. Catal. B Environ. 254 (2019) 624–633.
[242] X. Wang, Z. Fu, L. Zheng, C. Zhao, X. Wang, S.Y. Chong, F. McBride, R. Raval, M. Bilton, L. Liu, X. Wu, L. Chen, R.S. Sprick, A.I. Cooper, Chem. Mater. 32 (2020) 9107–9114.
[243] M. Lu, M. Zhang, J. Liu, T.Y. Yu, J.N. Chang, L.J. Shang, S.L. Li, Y.Q. Lan, J. Am. Chem. Soc. 144 (2022) 1861–1871.
[244] H. Zhong, R. Sa, H. Lv, S. Yang, D. Yuan, X. Wang, R. Wang, Adv. Funct. Mater. 30 (2020) 2002654.
[245] K. Guo, X. Zhu, L. Peng, Y. Fu, R. Ma, X. Lu, F. Zhang, W. Zhu, M. Fan, Chem. Eng. J. 405 (2021) 127011.
[246] P. Sarkara, S. Riyajuddinb, A. Dasa, A.H. Chowdhurya, K. Ghoshb, S.M. Islam, Mol. Catal. 484 (2020) 110730.
[247] L. Wang, G. Huang, L. Zhang, R. Lian, J. Huang, H. She, C. Liu, Q. Wang, J. Energy Chem. 64 (2022) 85–92.
[248] M. Zhang, J.-N. Chang, Y. Chen, M. Lu, T.-Y. Yu, C. Jiang, S.-L. Li, Y.-P. Cai, Y.-Q. Lan, Adv. Mater. 33 (2021) 2105002.
[249] X. Lang, X. Chen, J. Zhao, Chem. Soc. Rev. 43 (2014) 473–486.
[250] S.P. Pitre, C.D.M. Tiernan, J.C. Scaiano, ACS Omega 1 (2016) 66–76.
[251] S. Fukuzumi, K. Ohkubo, Org. Biomol. Chem. 12 (2014) 6059–6071.
[252] Z. Jia, K. Wang, B. Tan, Y. Gu, Adv. Synth. Catal. 359 (2017) 78–88.
[253] C.-M. Che, J.-S. Huang, Coord. Chem. Rev. 242 (2003) 97–113.
[254] Z.-Y. Xu, Y. Luo, D.-W. Zhang, H. Wang, X.-W. Sun, Z.-T. Li, Green Chem. 22 (2020) 136–143.
[255] W. Stroek, M. Keilwerth, D.M. Pividori, K. Meyer, M. Albrecht, J. Am. Chem. Soc. 143 (2021) 20157–20165.
[256] T. Kitanosono, T. Hisada, Y. Yamashita, S. Kobayashi, Angew. Chem. Int. Ed. 60 (2021) 3407–3411.
[257] Y. Meng, Y. Luo, J.-L. Shi, H. Ding, X. Lang, W. Chen, A. Zheng, J. Sun, C. Wang, Angew. Chem. Int. Ed. 59 (2020) 3624–3629.
[258] H. Hao, F. Zhang, X. Dong, X. Lang, Appl. Catal. B Environ. 299 (2021) 120691.
[259] E. Jin, S. Fu, H. Hanayama, M.A. Addicoat, W. Wei, Q. Chen, R. Graf, K. Landfester, M. Bonn, K.A.I. Zhang, H.I. Wang, K. Müllen, A. Narita, Angew. Chem. Int. Ed. 61 (2022) e202114059.
[260] Y. Zhi, Z. Li, X. Feng, H. Xia, Y. Zhang, Z. Shi, Y. Mu, X. Liu, J. Mater. Chem. A 5 (2017) 22933–22938.
[261] S. Li, L. Li, Y. Li, L. Dai, C. Liu, Y. Liu, J. Li, J. Lv, P. Li, B. Wang, ACS Catal. 10 (2020) 8717–8726.
[262] L. Liu, B. Zhang, X. Tan, D. Tan, X. Cheng, B. Han, J. Zhang, Chem. Commun. 56 (2020) 4567–4570.
[263] Y. Yang, H. Niu, L. Xu, H. Zhang, Y. Cai, Appl. Catal. B Environ. 269 (2020) 118799.
[264] X. Wang, S. Zhang, X. Li, Z. Zhan, B. Tan, X. Lang, S. Jin, J. Mater. Chem. A 9 (2021) 16405–16410.
[265] J.-L. Shi, R. Chen, H. Hao, C. Wang, X. Lang, Angew. Chem. Int. Ed. 59 (2020) 9088–9093.
[266] W. Huang, J. Byun, I. Rçrich, C. Ramanan, P.W.M. Blom, H. Lu, D. Wang, L.C. Silva, R. Li, L. Wang, K. Landfester, K.A.I. Zhang, Angew. Chem. Int. Ed. 57 (2018) 8316–8320.
[267] R. Paul, S.C. Shit, H. Mandal, J. Rabeah, S.S. Kashyap, Y. Nailwal, D. Balaji Shinde, Z. Lai, J. Mondal, ACS Appl. Nano Mater. 4 (2021) 11732–11742.
[268] Z. Li, S. Han, C. Li, P. Shao, H. Xia, H. Li, X. Chen, X. Feng, X. Liu, J. Mater. Chem. A 8 (2020) 8706–8715.
[269] M. Liu, J. Liu, K. Zhou, J. Chen, Q. Sun, Z. Bao, Q. Yang, Y. Yang, Q. Ren, Z. Zhang, Adv. Sci. 8 (2021) 2100631.
[270] S. Bi, P. Thiruvengadam, S. Wei, W. Zhang, F. Zhang, L. Gao, J. Xu, D. Wu, J.-S. Chen, F. Zhang, J. Am. Chem. Soc. 142 (2020) (1900) 11893–111891.
[271] Q. Li, X. Lan, G. An, L. Ricardez-Sandoval, Z. Wang, G. Bai, ACS Catal. 10 (2020) 6664–6675.
[272] Y. Qian, D. Li, Y. Han, H.-L. Jiang, J. Am. Chem. Soc. 142 (2020) 20763–20771.
[273] H. He, X. Fang, D. Zhai, W. Zhou, Y. Li, W. Zhao, C. Liu, Z. Li, W. Deng, Chem. Eur. J. 27 (2021) 14390–14395.
[274] R. Chen, J.-L. Shi, Y. Ma, G. Lin, X. Lang, C. Wang, Angew. Chem. Int. Ed. 58 (2019) 6430–6434.
[275] H. Liu, C. Li, H. Li, Y. Ren, J. Chen, J. Tang, Q. Yang, ACS Appl. Mater. Interfaces 12 (2020) 20354–20365.
[276] H.-S. Lu, W.-K. Han, X. Yan, C.-J. Chen, T. Niu, Z.G. Gu, Angew. Chem. Int. Ed. 60 (2021) 17881–17886.
[277] K. Wang, X. Kang, C. Yuan, X. Han, Y. Liu, Y. Cui, Angew. Chem. Int. Ed. 60 (2021) 19466–19476.
[278] M. Bhadra, S. Kandambeth, M.K. Sahoo, M. Addicoat, E. Balaraman, R. Banerjee, J. Am. Chem. Soc. 141 (2019) 6152–6156.
[279] W. Dong, Y. Yang, Y. Xiang, S. Wang, P. Wang, J. Hu, L. Rao, H. Chen, Green Chem. 23 (2021) 5797–5805.
[280] Z. Almansaf, J. Hu, F. Zanca, H.R. Shahsavari, B. Kampmeyer, M. Tsuji, K. Maity, V. Lomonte, Y. Ha, P. Mastrorilli, S. Todisco, M. Benamara, R. Oktavian, A. Mirjafari, P.Z. Moghadam, A.R. Khosropour, H. Beyzavi, ACS Appl. Mater. Interfaces 13 (2021) 6349–6358.
[281] A. Jati, K. Dey, M. Nurhuda, M.A. Addicoat, R. Banerjee, B. Maji, J. Am. Chem. Soc. 144 (2022) 7822–7833.
[282] K. Zhang, G. Lu, Z. Xi, Y. Li, Q. Luan, X. Huang, Chinese Chem. Lett. 32 (2021) 2207–2211.
[283] G. Lu, X. Huang, Y. Li, G. Zhao, G. Pang, G. Wang, J. Energy Chem. 43 (2020) 8–15.
[284] Q. Gao, J. Xu, X.-H. Bu, Coord. Chem. Rev. 378 (2019) 17–31.
[285] S. Xie, S. Wu, S. Bao, Y. Wang, Y. Zheng, D. Deng, L. Huang, L. Zhang, M. Lee, Z. Huang, Adv. Mater. 30 (2018) 1800683.
[286] S. Bolisetty, M. Peydayesh, R. Mezzenga, Chem. Soc. Rev. 48 (2019) 463–487.
[287] Z. Li, J. Chen, H. Guo, X. Fan, Z. Wen, M.-H. Yeh, C. Yu, X. Cao, Z.L. Wang, Adv. Mater. 28 (2016) 2983–2991.
[288] Y. Fan, W. Ma, D. Han, S. Gan, X. Dong, L. Niu, Adv. Mater. 27 (2015) 3767–3773.
[289] V. Kumar, V. Singh, K.-H. Kim, E.E. Kwon, S.A. Younis, Coord. Chem. Rev. 447 (2021) 214148.
[290] Y. Lin, C. Yang, S. Wu, X. Li, Y. Chen, W.L. Yang, Adv. Funct. Mater. 30 (2020) 2002918.
[291] H. Lv, X. Zhao, H. Niu, S. He, Z. Tang, F. Wu, J.P. Giesy, H. Lv, X. Zhao, H. Niu, S. He, Z. Tang, F. Wu, J.P. Giesy, J. Hazard. Mater. 369 (2019) 494–502.

[292] L. Zhang, G.-P. Yang, S.-J. Xiao, Q.-G. Tan, Q.-Q. Zheng, R.-P. Liang, J.-D. Qiu, Small 17 (2021) 2102944.
[293] F. Liu, Q. Dong, C. Nie, Z. Li, B. Zhang, P. Han, W. Yang, M. Tong, Chem. Eng. J. 430 (2022) 132833.
[294] J. Pan, L. Guo, S. Zhang, N. Wang, S. Jin, B. Tan, Chem-Asian J. 13 (2018) 1674–1677.
[295] A. Jiménez-Almarza, A. López-Magano, R. Cano, B. Ortín-Rubio, D. Díaz-García, S. Gomez-Ruiz, I. Imaz, D. Maspoch, R. Mas-Ballesté, J. Alemán, Mater. Today Chem. 22 (2021) 100548.
[296] Z. Dong, L. Zhang, J. Gong, Q. Zhao, Chem. Eng. J. 403 (2021) 126383.
[297] L. Niu, X. Zhao, F. Wu, H. Lv, Z. Tang, W. Liang, X. Wang, J. Giesy, Chem. Eng. J. 414 (2021) 128619.
[298] X.-R. Chen, W.-R. Cui, R.-P. Liang, C.-R. Zhang, R.-H. Xu, W. Jiang, J.-D. Qiu, A.C. S. Appl, Bio Mater. 4 (2021) 6502–6511.
[299] W. Chen, Z. Yang, Z. Xie, Y. Li, X. Yu, F. Lu, L. Chen, J. Mater. Chem. A 7 (2019) 998–1004.
[300] Y. Deng, Z. Zhang, P. Du, X. Ning, Y. Wang, D. Zhang, J. Liu, S. Zhang, X. Lu, Angew. Chem. Int. Ed. 59 (2020) 6082–6089.
[301] F. Liu, C. Nie, Q. Dong, Z. Ma, W. Liu, M. Tong, J. Hazard. Mater. 398 (2020) 122865.
[302] H. Xue, Z. Bi, J. Cheng, S. Xiong, Y. Wang, Ind. Eng. Chem. Res. 60 (2021) 8687–8695.
[303] Y. Zhang, Y. Hu, J. Zhao, E. Park, Y. Jin, Q. Liu, W. Zhang, J. Mater. Chem. A 7 (2019) 16364–16371.
[304] G. Li, J. Ye, Y. Shen, Q. Fang, F. Liu, Chem. Eng. J. 421 (2021) 127784.
[305] X. Zhong, Y. Liu, S. Wang, Y. Zhu, B. Hu, Sep. Purif. Technol. 279 (2021) 119627.
[306] C.-R. Zhang, W.-R. Cui, C.-P. Niu, S.-M. Yi, R.-P. Liang, J.-X. Qi, X.-J. Chen, W. Jiang, L. Zhang, J.-D. Qiu, Chem. Eng. J. 428 (2022) 131178.
[307] D. Lin, P. Duan, W. Yang, X. Huang, Y. Zhao, C. Wang, Q. Pan, Chem. Eng. J. 430 (2022) 132817.
[308] K.K. Khaing, D. Yin, Y. Ouyang, S. Xiao, B. Liu, L. Deng, L. Li, X. Guo, J. Wang, J. Liu, Y. Zhang, Inorg. Chem. 59 (2020) 6942–6952.
[309] Y. Hou, C.-X. Cui, E. Zhang, J.-C. Wang, Y. Li, Y. Zhang, Y. Zhang, Q. Wang, J. Jiang, Dalton Trans. 48 (2019) 14989–14995.
[310] X. Guo, D. Yin, K.K. Khaing, J. Wang, Z. Luo, Y. Zhang, Inorg. Chem. 60 (2021) 15557–15568.
[311] Y. Yang, W. Zhao, H. Niu, Y. Cai, ACS Appl. Mater. Interfaces 13 (2021) 42035–42043.
[312] M. Zheng, C. Yao, Y. Xu, ACS Appl. Nano Mater. 3 (2020) 11307–11314.
[313] A.E. ElMetwally, E. Zeynaloo, D. Shukla, B. Surnar, S. Dhar, J.L. Cohn, M.R. Knecht, L.G. Bachas, ACS Appl. Nano Mater. 4 (2021) 2795–2805.